

**Deanship of Graduate Studies  
Al-Quds University**



**Spectroscopic Study of the Interaction of Human Serum  
Albumin with Steroid Hormones:  
Progesterone and its parent compound Cholesterol.**

**Jafar Hamed Taha Ghithan**

**M.Sc. Thesis**

**Jerusalem – Palestine**

**1431/ 2010**

Spectroscopic Study of the Interaction of Human Serum  
Albumin with Steroid Hormones: Progesterone and its  
parent compound Cholesterol.

Prepared by:

Jafar Hamed Taha Ghithan

B.Sc. Physics, Birzeit University, Palestine

Supervisor: Dr. Musa Abu Teir.

Co-supervisor: Prof. Mahmoud Abu hadid.

“A thesis Submitted to the Faculty of Science and Technology, Al-  
Quds University in Partial Fulfillment of the Requirements for the  
Degree of Master of Science in Physics”

1431 / 2010

**Al-Quds University**  
**Deanship of Graduate Studies**  
**Physics Department**

**Thesis Approval**

Spectroscopic Study of the Interaction of Human Serum Albumin with Steroid Hormones: Progesterone and its parent compound Cholesterol.

Prepared by: Jafar Hamed Taha Ghithan.  
Registration No.: 20714279

Supervisor: Dr. Musa Abu Teir  
Co-supervisor: Prof. Mahmoud Abu hadid

Master Thesis submitted and accepted, Date:     /     /2010  
The names and signatures of the examining committee members are as follows:

1-Head of Committee: ..... Signature .....

2-Internal Examiner: ..... Signature.....

3-External Examiner: ..... Signature .....

4-Committee member: ..... Signature.....

**Jerusalem – Palestine**

**1431 / 2010**

## **Dedication:**

I dedicate this thesis to the brightness of hearts, watercress's and remedy of chests, mister prophet Mohammad "peace and blessings of Allah be upon him". To my parents, Hamed and Najla thank you for every prayer, and bean of perspiration ripple from your brows, fatigued for me. My wife Dalal my soul mate and confidant, for always being there for me. Thank you for your continual love, support, and patience as I went through this journey. I could not have made it through without you by my side. My brothers and sisters; Taha, Yousef, Belal, Asma', Assem, Yasser, and Maysa' for their love and support throughout the years, thank you for the laughing, the fighting, and everything in between. To my Future daughter ... "Baby Daddy desirous to enfold you".

*Jafar Hamed Taha Ghithan*

**Declaration:**

I certify that this thesis submitted for the degree of Master is the result of my own research, except where otherwise acknowledged, and that this thesis (or any part of the same) has not been submitted for a higher degree to any other university or institution.

Signed: \_\_\_\_\_

Jafar Hamed Taha Ghithan

Date: / / 2010

## **Acknowledgements**

*After my Great commendation and Thanks to Allah.*

*This thesis arose in part out of months of research that has been done since I came to Al-Quds University. By that time, I have worked with a great number of people without whom this thesis might not have been written, and to whom I am greatly indebted.*

*First for providing the inspiration to embark on my master candidature my deepest thanks go to my supervisor who shepherded me through the bulk of the work, Dr.Musa Abu Teir, his kindly but rigorous oversight of this thesis constantly gave me the motivation to perform my maximum ability. I was very fortunate to have been able to work with him and hearing his jokes. I must also thank my co supervisor prof. Mahmoud Abu hadid, his detailed and constructive comments were vital to the development of this thesis, his advice and patience is appreciated.*

*Special thanks to whom spotlight my way in his glowing science Dr. Saqer Darwish who has made invaluable comments about the thesis.*

*A special thanks also goes to Sawsan Abu Sharhk who greatly enriched my knowledge with her experience in bio physics lab.*

*I would also like to thank the staff at Nano-Technology lab in Al-Quds University for their tireless efforts.*

*My parents who have supported me all the way since the beginning of my studies. And my beloved wife who has been a great source of motivation and inspiration. Thank you for your tremendous encouragement.*

*My friend Said Qshoua', for helping me preparing for my defense and printing my thesis, thank you for all what you have done for me.*

## ABSTRACT

---

It was found that the distribution and metabolism of many biologically active compounds in the body whether drugs or natural products are correlated with their affinities toward serum albumin. Thus, the study on the interaction of such molecules with albumin is of imperative and fundamental importance. Extensive studies on different aspects of drug-HSA interactions are still in progress because of the clinical significance of the processes.

In this study the interaction of steroid hormones (progesterone and its parent compound cholesterol) with human serum albumin at physiological pH have been studied using UV-VIS spectrophotometer, fluorescence spectrophotometer, and FT-IR spectroscopy.

The results showed that UV absorption intensity spectra were increased with the increase of progesterone or cholesterol molar ratios in fixed amount of HSA. From UV spectra the binding constants were obtained and equals ( $6.354 \times 10^2 \text{M}^{-1}$ ) for progesterone and ( $0.2641 \times 10^4 \text{M}^{-1}$ ) for cholesterol.

Beside that the results that have been obtained from analysis of fluorescence spectra indicated that progesterone and cholesterol have an ability to quench the intrinsic fluorescence of HSA through a static quenching procedure. The values of Stern-Volmer constant were determined to be ( $6.26 \times 10^2 \text{L mol}^{-1}$ ) for progesterone- HSA complexes and ( $6.21 \times 10^2 \text{L mol}^{-1}$ ) for cholesterol- HSA complexes. Also the quenching rate constant

values obtained were ( $6.20 \times 10^{10} \text{ L mol}^{-1} \text{ s}^{-1}$ ) for progesterone, and ( $6.21 \times 10^{10} \text{ L mol}^{-1} \text{ s}^{-1}$ ) for cholesterol.

The binding constants from fluorescence spectrum for progesterone- HSA complexes was found to be ( $6.56 \times 10^2 \text{ M}^{-1}$ ), and for cholesterol- HSA complexes was found to be ( $0.214 \times 10^4 \text{ M}^{-1}$ ). It was obviously noted that the obtained values agrees well with the values obtained using UV-VIS spectrophotometer, and that cholesterol binding constant is larger than progesterone binding constant, this refer to the structure of the two compounds which is consistent with that have been reported.

FT-IR spectroscopy with Fourier self-deconvolution and second derivative, as well as curve fitting procedures were used in the analysis of amide I, amide II, and amide III regions of HSA to determine protein secondary structure and hormone binding mechanism. It was observed that the intensity of absorption bands decreased as progesterone or cholesterol molar ratios increased. Also all peak positions of the three amide regions were assigned at different progesterone or cholesterol ratios.

In addition FT-IR spectra evidence showed that HSA secondary structure has been changed as progesterone or cholesterol molar ratios increased, which was observed in the reduction of  $\alpha$ -helices absorption band relative to  $\beta$ -sheets absorption band. The variation in the intensity is related indirectly to the formation of H-bonding in the complex molecules, which accorded for the different intrinsic propensities of  $\alpha$ -helix and  $\beta$ -sheets.

## Table of contents.

Abstract.....	iii
List of Tables.....	viii
List of Figures.....	ix
List of Abbreviations.....	xiv
List of Symbols.....	xv
<b>Chapter one: Introduction.....</b>	<b>1</b>
<b>Chapter two: Theoretical Background.....</b>	<b>5</b>
2.1 Fourier Transform Infrared (FT-IR) development.....	6
2.2 Electromagnetic (EM) Radiation.....	7
2.3 Molecular Vibrations.....	9
2.3.1 Normal modes of vibrations.....	11
2.3.2 Quantum mechanical treatment of vibrations.....	12
I. The harmonic approximation.....	12
II. Anharmonicity.....	12
2.3.3 Vibrational modes of polyatomic molecules.....	13
2.4 FT-IR Spectroscopy.....	15
2.4.1 Infrared (IR) spectroscopy.....	15
2.4.1.1 IR-region.....	15
2.4.1.2 IR Spectrum presentation.....	16
2.4.1.3 Principle of IR absorption.....	17
2.4.2 Theory of FT-IR spectrometer.....	18
2.4.3 The working principle of an FT-IR spectrometer.....	21
2.5 Ultraviolet-Visible (UV-VIS) spectrophotometer.....	21
2.6 Fluorescence spectrophotometer.....	23
2.7 Proteins.....	25
2.7.1 Protein structure.....	26
2.7.2 Human Serum Albumin.....	28
<b>Chapter Three: Experimental Part.....</b>	<b>31</b>
3.1 Samples and materials.....	32
3.1.1 Preparation of HSA stock solution.....	32
3.1.2 Preparation of Progesterone stock solution.....	33
3.1.3 Preparation of Cholesterol stock solution.....	33
3.1.4 HSA-Progesterone solutions.....	33
3.1.4 HSA-Cholesterol solutions.....	33
3.1.5 Thin film preparations.....	33
3.2 Instruments.....	34
3.2.1 FT-IR Spectrometer.....	34
3.2.2 UV-VIS spectrophotometer (NanoDrop ND-1000).....	34

3.2.3 Fluorospectrometer (NanoDrop 3300).....	34
3.3 Experimental procedures.....	35
3.3.1 UV-VIS Spectrophotometer Experimental Procedures.....	35
Operation .....	35
Basic Use .....	36
3.3.2 Fluorospectrometer Experimental Procedures.....	36
Operation .....	37
Basic Use .....	37
3.3.3 FT-IR Spectrophotometer Experimental Procedures.....	38
3.3.4 FT-IR data processing.....	38
3.3.4.1 Baseline correction.....	39
3.3.4.2 Peak picking.....	39
3.3.4.3 Second Derivative.....	39
3.3.4.4 Fourier self-deconvolution.....	39
3.3.4.5 Spectral subtraction.....	40
3.3.4.6 Curve fitting.....	40
<b>Chapter Four: Results and discussion.</b> .....	<b>41</b>
4.1 UV-VIS spectrophotometer .....	42
4.1.1 Binding constants of progesterone or cholesterol and HSA complexes using UV-VIS Spectrophotometer.....	45
4.2 Fluorescence spectrophotometer .....	48
4.2.1 Stern-Volmer quenching constants ( $K_{sv}$ ) and the quenching rate constant of the biomolecule ( $K_q$ ).....	51
4.2.2 Determination of binding constant using fluorescence spectrophotometer.....	54
4.3 FT-IR Spectroscopy.....	57
<b>Chapter five: Conclusions and future work.</b> .....	<b>82</b>
References.....	85
Arabic Abstract .....	93

## List of Tables

<b>Table No.</b>	<b>Table Caption</b>	<b>Page</b>
<b>Table 2.1</b>	Degrees of freedom for polyatomic molecules.	11
<b>Table 4.1</b>	Band assignment in the absorbance spectra of HSA with different progesterone molecular ratios for amide I, amide II, and amide III regions	62
<b>Table 4.2</b>	Band assignment in the absorbance spectra of HSA with different cholesterol molecular ratios for amide I, amide II, and amide III regions	63
<b>Table 4.3</b>	Secondary structure determination for Amide I, amide II, and amide III regions in HSA and its Progesterone complexes	73
<b>Table 4.4</b>	Secondary structure determination for Amide I, amide II, and amide III regions in HSA and its Cholesterol complexes	74

## List of figures

Figure No.	Figure Caption	Page
Figure 1.1	Chemical structure of progesterone	2
Figure 1.2	Chemical structure of cholesterol	3
Figure 2.1	Representation of an electromagnetic wave	8
Figure 2.2	Electromagnetic spectrum	8
Figure 2.3	Diatomic model a) relaxed b) stretched	10
Figure 2.4	Carbon dioxide and water molecules	11
Figure 2.5	Potential energy of a diatomic molecule as a function of the atomic displacement during vibration for a harmonic oscillator (dashed line) and an anharmonic oscillator (solid line)	13
Figure 2.6	Regions of IR spectrum	16
Figure 2.7	Optical arrangement of Michelson interferometer. M1 and M2 are a fixed and a moving mirror, respectively. B is the half-transparent surface of the beam splitter J, and K is a compensator plate. The beamsplitter and the compensator plate have the same thickness $l$ and the same refractive index	18
Figure 2.8	A wide-band continuous spectrum $E(\nu)$ and an infinitesimal monochromatic section of the width $d\nu$	20
Figure 2.9	An interference record $F(x)$	20
Figure 2.10	a) Basic components of FT-IR spectroscopy. b) Simplified layout of an FT-IR spectrometer	21
Figure 2.11	Electronic energy levels	22
Figure 2.12	Electronic energy transitions	22

<b>Figure 2.13</b>	One form of a Jablonski diagram	23
<b>Figure 2.14</b>	Structure of the intrinsic fluorophores amongst amino acids	25
<b>Figure 2.15</b>	General structure of amino acids	26
<b>Figure 2.16</b>	The $\alpha$ -helix. The main chain carboxyl group of amino acid j is hydrogen bonded to the NH group of amino acid j+4	27
<b>Figure 2.17</b>	Parallel (top) and antiparallel (bottom) $\beta$ -sheets	28
<b>Figure 2.18</b>	Chemical structure of human serum albumin	29
<b>Figure 3.1</b>	Main steps for using the sample UV-VIS Spectrophotometer (NanoDrop 1000).	36
<b>Figure 3.2</b>	Main steps for using the sample Fluorospectrophotometer (NanoDrop 3300).	37
<b>Figure 4.1</b>	UV-Absorbance spectra of HSA with different molar ratios of progesterone (a=0:10, b=2:10, c=6:10, d=10:10, e=14:10, f=18:10).	43
<b>Figure 4.2</b>	UV-Absorbance spectra of HSA with different molar ratios of cholesterol (a=0:10, b=2:10, c=6:10, d=10:10, e=14:10, f=18:10)	44
<b>Figure 4.3</b>	The plot of $1/(A-A_0)$ vs $1/L$ for HSA with different concentrations of progesterone	46
<b>Figure 4.4</b>	The plot of $1/(A-A_0)$ vs $1/L$ for HSA with different concentrations of cholesterol	47
<b>Figure 4.5</b>	Fluorescence emission spectra of HSA in the absence and presence of progesterone in these ratios ( Prog:HSA a=0:10, b=2:10, c=6:10, d=10:10, e=14:10, f=18:10, g=free progesterone)	49

<b>Figure 4.6</b>	Fluorescence emission spectra of HSA in the absence and presence of cholesterol in these ratios ( Chol:HSA a=0:10, b=2:10, c=6:10, d=10:10, e=14:10, f=18:10, g=free cholesterol)	50
<b>Figure 4.7</b>	The Stern-Volmer plot for progesterone- HSA complexes	52
<b>Figure 4.8</b>	The Stern-Volmer plot for cholesterol- HSA complexes	53
<b>Figure 4.9</b>	The plot of $1/(F_0-F)$ vs $(1/L) \times 10^4$ for progesterone-HSA complexes	55
<b>Figure 4.10</b>	The plot of $1/(F_0-F)$ vs $(1/L) \times 10^4$ for cholesterol-HSA complexes	56
<b>Figure 4.11</b>	Sample spectrum showing the three relevant regions for determination of protein secondary structure. Amide I ( $1700-1600 \text{ cm}^{-1}$ ), amide II ( $1600-1480 \text{ cm}^{-1}$ ) and amide III ( $1330-1220 \text{ cm}^{-1}$ )	57
<b>Figure 4.12</b>	A: The spectra of HSA free (second derivative) And B: (a, b, c, d, e, f) Progesterone-HSA with ratios (0:10, 2:10, 6:10, 10:10, 14:10, 18:10)	59
<b>Figure 4.13</b>	A: The spectra of HSA free (second derivative) And B: (a, b, c, d, e, f) Cholesterol-HSA with ratios (0:10, 2:10, 6:10, 10:10, 14:10, 18:10)	60
<b>Figure 4.14</b>	FT-IR spectra (top two curves) and difference spectra of HSA and its complexes with different progesterone concentrations in the region $1800-1500 \text{ cm}^{-1}$	66
<b>Figure 4.15</b>	FT-IR spectra (top two curves) and difference spectra of HSA and its complexes with different progesterone concentrations in the region of $1330-1220 \text{ cm}^{-1}$	67

<b>Figure 4.16</b>	FT-IR spectra (top two curves) and difference spectra of HSA and its complexes with different cholesterol concentrations in the region 1800-1500 $\text{cm}^{-1}$	68
<b>Figure 4.17</b>	FT-IR spectra (top two curves) and difference spectra of HSA and its complexes with different cholesterol concentrations in the region of 1330-1220 $\text{cm}^{-1}$	69
<b>Figure 4.18</b>	Second-derivative enhancement and curve-fitted Amide I region (1610-1700 $\text{cm}^{-1}$ ) and secondary structure determination of the free human serum albumin ( A and B) and it progesterone complexes ( C and D) with 18:10 progesterone: HSA ratios	75
<b>Figure 4.19</b>	Second-derivative resolution enhancement and curve fitted amide II region (1600-1480 $\text{cm}^{-1}$ ) and secondary structure determination of the free human serum albumin (A,B) and its progesterone complexes (C,D) with 18:10 hormone: protein ratio	76
<b>Figure 4.20</b>	Second-derivative resolution enhancement and curve fitted amide III region (1330-1220 $\text{cm}^{-1}$ ) and secondary structure determination of the free human serum albumin (A,B) and its progesterone complexes (C,D) with 18:10 hormone: protein ratio	77
<b>Figure 4.21</b>	Second-derivative enhancement and curve-fitted Amide I region (1610-1700 $\text{cm}^{-1}$ ) and secondary structure determination of the free human serum albumin ( A and B) and it cholesterol complexes ( C and D) with 18:10 cholesterol: HSA ratios	78
<b>Figure 4.22</b>	Second-derivative enhancement and curve-fitted Amide II region (1600-1480 $\text{cm}^{-1}$ ) and secondary structure determination of the free human serum albumin ( A and B) and it cholesterol complexes ( C and D) with 18:10 cholesterol: HSA ratios	79

**Figure 4.23** Second-derivative resolution enhancement and curve fitted amide III region ( $1330\text{-}1220\text{ cm}^{-1}$ ) and secondary structure determination of the free human serum albumin (A,B) and its cholesterol complexes (C,D) with 18:10 cholesterol: protein ratio

80

## List of abbreviations

Symbol	Abbreviation representation
HSA	Human Serum Albumin
UV-VIS spectrophotometer	Ultraviolet Visible spectrophotometer
FT-IR	Fourier Transform Infrared
$\alpha$ -helix	Alpha helix
$\beta$ -sheets	Beta sheets
CAT	Computer Assisted Tomography
MIR	Magnetic Imaging Resonance
CD	Circular Dichroism.
FSD	Fourier Self Deconvolution
EM	Electromagnetic
ZPE	Zero Point Energy
HOMO	Highest Occupied Molecular Orbitals
LUMO	Lowest Unoccupied Molecular Orbitals
kDa	Kilodalton
Prog.	Progesterone
Chole.	Cholesterol
MCT	Mercury Cadmium Telluride
LED's	Light Emitting Diodes
nm	Nanometer
OPUS	Optical User Software
ICT	Intramolecular Charge Transfer
CCD	Charge Coupled Device

## List of symbols.

Symbol	description
$h$	Planck's constant
$\nu$	Frequency
$E_{\text{total}}$	Total energy
$E_{\text{ele}}$	Electronic energy
$E_{\text{vib}}$	Vibrational energy
$E_{\text{rot}}$	Rotational energy
$K$	Binding constant
$r_0$	Equilibrium position
$\Delta x$	Displacement
$F_x$	Restoring force
$N$	Number of molecules
$n_i$	Vibrational quantum numbers
$V_{\text{iv}}$	Potential energy of a harmonic oscillator
$r$	Distance between the atoms
$x_i$	The anharmonicity constant
$Q_i$	Normal modes of vibrations
$V(Q)$	Potential energy of polyatomic
$V_e$	Minimum potential energy
$\lambda_i$	The force constant $i$
$n_i$	Energy state
$x_{ij}$	Anharmonicity term introduces coupling between normal modes
$1^{\text{st}}, 2^{\text{nd}}$	First, Second
$T$	Transmittance
$I$	Radiant power transmitted by the sample
$I_0$	Radiation power incident on the sample
$A$	Absorbance
$C, L$	Concentration
$a$	Absorptivity
$b$	Pathlength
$E(\nu)$	Spectrum of the two beams in Michelson interference
$x$	Optical path difference
$d\nu$	Infinitesimal spectral signal
$dF(x, \nu)$	Interference signal
$F(x)$	The interference record
$S_0, S_1, S_2$	First, second, third electronic states
$K_{\text{sv}}$	Stern volmer quenching constant
$K_q$	Biomolecular quenching constant
$\tau_0$	Unquenched lifetime
$F_0$	Fluorescence intensities without quencher
$F$	Fluorescence intensities with quencher
$A_0$	Initial absorption of protein
$A_\infty$	Final absorption of the ligated-protein

*Chapter One:*

# **Introduction**

## Chapter one

---

### Introduction.

This thesis is an experimental investigations of the effects of the interaction of steroid hormones (progesterone and its parent compound; cholesterol) with HSA by means of UV-VIS spectrophotometer, fluorescence spectrophotometer, and FT-IR spectroscopy.

Hormones are the most familiar compound to the general public, because of the medications use and abuse of steroid hormones for diverse purposes, such as contraception and body building (Hardie, 1991).

Hormones have many physiological effects on human body; the disorders of hormones may cause many abnormalities in it (Korkmaz et al., 2005; Andr'e et al., 2003). Progesterone, is one of the steroid hormones, and is synthesized from cholesterol (Hardie, 1991), and is secreted naturally by the corpus luteum. Progesterone is a C-21 steroid hormone; its chemical structure is shown in Fig.(1.1) (Korkmaz et al., 2005).

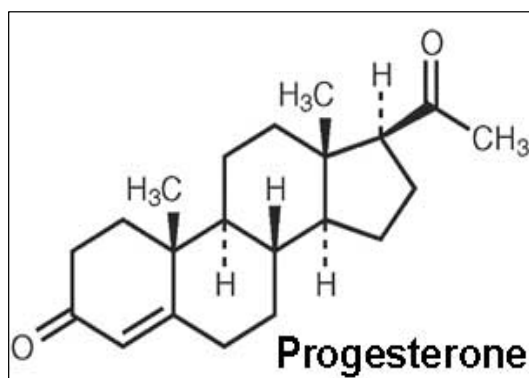


**Figure 1.1:** Chemical structure of progesterone.

Cholesterol is an extremely important biological molecule being a major component of cell membrane as well as a precursor for the synthesis of a number of essential vitamins, steroid hormones and bile acids (Pani et al., 2003), its chemical structure is shown in Fig.(1.2).

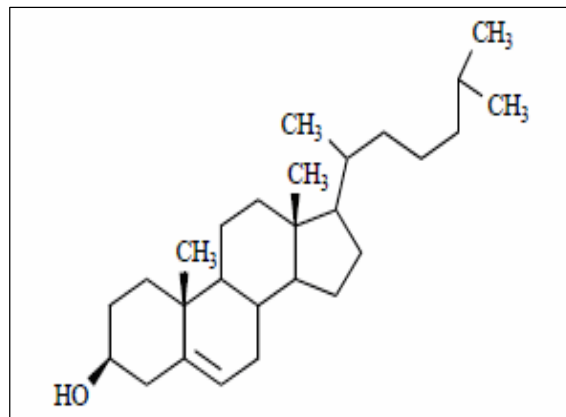


**Figure 1.2:** Chemical structure of cholesterol.

Human serum albumin (HSA) is the most abundant plasma carrier protein in human body with a high affinity for a wide range of metabolites and drugs. The most important physiological role of HSA, is to transport such solutes in the blood stream and then deliver them to the target organs, as well as to maintain the pH and osmotic pressure of plasma (Maiti et al., 2008), its structure and function will be discussed briefly in chapter two.

The molecular interactions between HSA and some compounds have been investigated successfully (Jürgens et al., 2002; Ouameur et al., 2004; Ha et al., 2006). It has recently been proved that serum albumin plays a decisive role in the transport and disposition of a variety of endogenous and exogenous compound such as free fatty acids, hormones, bilirubin, drugs... (Tang et al., 2006).

The distribution and metabolism of many biologically active compounds in the body whether drugs or natural products are correlated with their affinities toward serum albumin. Thus, the study on the interaction of such molecules with albumin is of imperative and fundamental importance (Maiti et al., 2008). Extensive studies on different aspects of drug–HSA interactions are still in progress because of the clinical significance of the processes (Andr´e et al., 2003).

In recent years, many investigations on drugs and natural products binding to protein were carried out. Progesterone and cholesterol, as a possible ligands, was not studied in detail on its binding reaction with HSA. It has been reported that progesterone and cholesterol binds to HSA (Morley, 1997; Peng et al., 2008). So far, none of the investigations determine in

details the progesterone-HSA, and cholesterol-HSA binding constants and the effects of progesterone or cholesterol complexation on the protein structure.

In this thesis, the interaction of progesterone and its parent compound cholesterol with HSA will be investigated by means of FT-IR, UV-VIS, and fluorescence spectrophotometers.

Infrared spectroscopy provides measurements of molecular vibrations due to the specific absorption of infrared radiation by chemical bonds. It is known that the form and frequency of the Amide I band, which is assigned to the C=O stretching vibration within the peptide bonds is very characteristic for the structure of the studied protein. From the band secondary structure, components peaks ( $\alpha$ -helix,  $\beta$ -sheets) can be derived and the analysis of this single band allows elucidation of conformational changes with high sensitivity (Darwish et al., 2010).

This work will be limited to the mid-range infrared, which covers the frequency range from 4000 to 400  $\text{cm}^{-1}$ . This wavenumber region includes bands that arise from three conformational sensitive vibrations within the peptide backbone (Amides I, II & III). Amide I is the most widely used and can provide information on secondary structure composition and structural stability. However, it has been reported that amide II and amide III bands have high information content and could be used for prediction of proteins secondary structure (Cui et al., 2008; Kang et al., 2004; Rondeau et al., 2007).

Other spectroscopic techniques are usually used in studying drugs interaction with proteins, such as fluorescence and UV-VIS spectrophotometers which are commonly used because of their high sensitivity, rapidity and ease of implementation (Wybranowski et al., 2008; Li et al., 2008; Li et al., 2006).

This thesis includes five chapters; chapter two will discuss the theoretical aspects to guide readers to the important ideas of this study. Chapter three includes details of the experimental, procedures, and instruments used. In chapter four the results obtained are presented and discussed. Final chapter contains the conclusions and future work.

*Chapter Two:*

# **Theoretical Background**

## **Chapter two**

---

### **Theoretical background.**

The emphasis on biophysics research has gradually changed over the years, in the early part of the 20<sup>th</sup> century, the research concentrated on issues related to medicine such as monitoring of heart and brain functions.

In recent years more influence on biophysics research has been emphasized; this is due to ascending development in spectroscopic instrumentations, such as; (X-ray diffractions, electron microscope, computer assisted tomography scanning (CAT), magnetic resonance imaging (MIR), Fourier transform (FT-IR), Circular dichroism (CD), UV-VIS, and fluorescence spectrophotometers.

Spectrophotometers are powerful tools for studying biological samples such as proteins. This chapter will cover theoretical aspects on this research, the first two sections will include a short historical background on the development of FT-IR spectroscopy and Electromagnetic spectrum, next section will cover briefly molecular vibrations, the following three sections discuss the spectroscopic approaches used in this work; FT-IR, UV-VIS, and fluorescence spectrophotometers. Final section will include protein structure and the protein model that have been used in this work which is "Human Serum Albumin (HSA)".

### **2.1 Fourier Transform Infrared (FT-IR) development.**

A wealth of information about structure and local microenvironment of biological materials; such as proteins, can be deduced from the spectral parameters: band position, band width and absorption; this standing due to the sensitivity and stability of spectrophotometers; which are valuable tools for the investigation of protein folding unfolding, and other protein structural changes during molecular interactions. IR

spectroscopy is one of the classical methods used for structure determination in biological systems, due to the high information content in an IR spectrum and its sensitivity to the chemical composition of molecules (Uversky, 2007).

The discovery of IR spectroscopy goes back to the year 1800, when William Herschel discovered the IR portion of electromagnetic spectrum (Coblentz, 1951). However, Gruenwedel et al, 1984; mentioned that it was not until 1892 that Julius made the observation that the type of atoms present and their structural arrangement in the molecule determined the character of IR absorption. Since that time, spectacular advances have been made in the instrumentation from single beam to double beam dispersive spectrometers, and the development of Fourier transform IR spectrometer in 1960 that are operable over the entire IR range (Gruenwedel. et al., 1987).

Quoting Jackson et al, 1995; the first use of infrared spectroscopy for determining the conformational structure of proteins and polypeptides was in 1950 by Elliot and Ambrose, who showed that an empirical correlation existed between the frequency of the so-called amide I and amide II absorptions of a protein and the predominant secondary structural motif within the protein as determined by X-ray diffraction studies (Jackson et al., 1995).

As was reported by Lakowicz, 2006; a number of mathematical techniques, such as Fourier self deconvolution (FSD) and derivative, have been developed to study proteins, also a number of tools such as fluorospectrophotometer became a widely used scientific tool in biophysics and material science after the pioneering works of Kasha, Vavilov, Perrin, Jabolonski, Weber, Stokes and Forster in 1951 (Lakowicz, 2006).

## **2.2 Electromagnetic (EM) radiation.**

Spectroscopy is the study of the interaction of electromagnetic radiation with matter (Coleman, 1993). Electromagnetic radiations are transverse waves that consisting of both electric and magnetic fields which are oscillating in a perpendicular fashion to each other and to the direction of the propagation see Fig.(2.1) (Hollas, 2004).

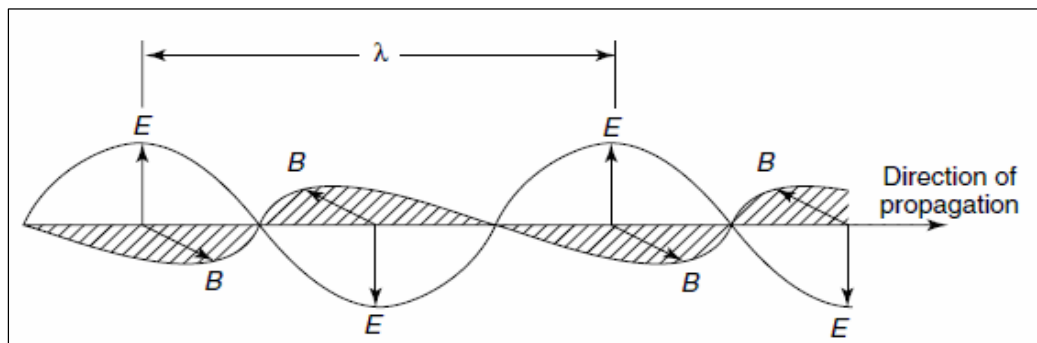


**Figure2.1:** Representation of an electromagnetic wave.

Electromagnetic radiation can be divided into different regions of energy that correspond to different spectroscopic techniques. The extent of the electromagnetic spectrum from low-energy Radio wave to high-energy  $\gamma$ -ray radiation is illustrated in Fig.(2.2) (Coleman, 1993). The region from 4000 to 400  $\text{cm}^{-1}$  is considered the mid-infrared region where vibrational and rotational bands are observed, and the region from 10 to 800 nm is the UV-VIS region where the work of this thesis lies.

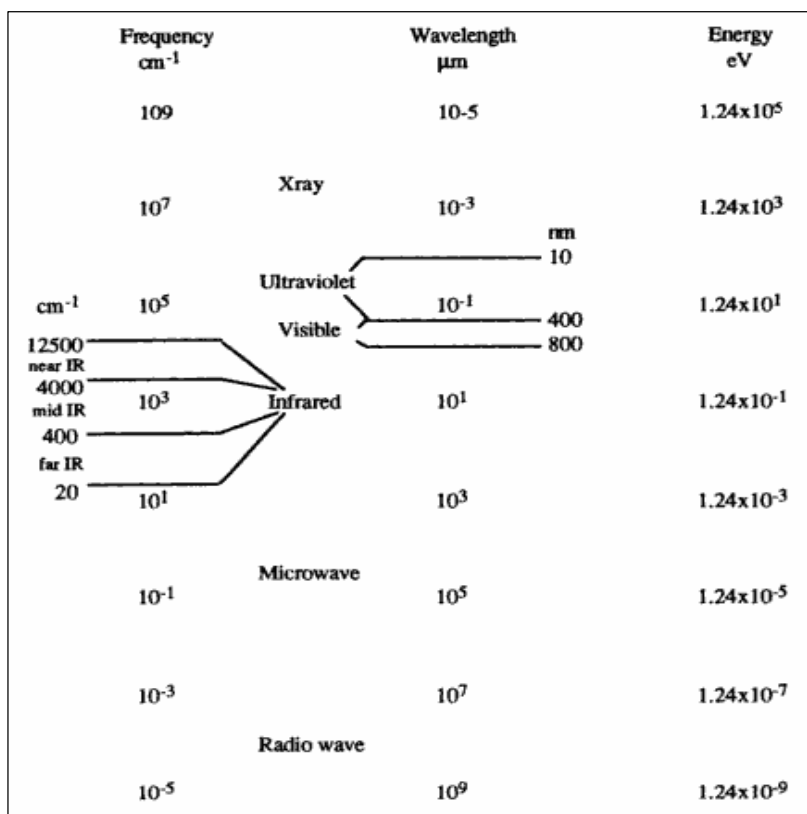


**Figure 2.2:** Electromagnetic spectrum.

In general, the spectrum gives information about the energy levels of the molecule, which helps to determine the structure of the molecule. In some types of spectroscopy there are only a few, well-separated energy levels. In these cases, only a very narrow range of wavelengths is absorbed by the molecule which is excited from its lowest energy state to some higher energy state, to give for each transition an absorption line. In many cases, each energy state has a number of energy sublevels, then a number of closely spaced wavelengths are absorbed. The lines are so close together, therefore they can't be resolved and the absorption appears as a band or a broad peak (Britlain et al., 1970).

If molecules are exposed to EM radiation the radiation can be absorbed, transmitted, reflected, scattered or undergo photoluminescence\*. According to quantum mechanical theory electromagnetic radiation and absorption can only occur at discrete energy levels. The discrete energy equals to  $h\nu$  where  $h$  is Planck's constant,  $\nu$  is the frequency. The absorbed EM radiation by a molecule can change its electronic state causing electron transitions, or changes in the internuclear distance of two or more atoms, or changes in the molecule rotation as it rotates around its center of mass. (OPUS Bruker manual, 2004) So the total energy of a molecule is due to electronic, vibrational, and rotational contributions as described in the equation below:

$$E_{\text{total}} = E_{\text{ele}} + E_{\text{vib}} + E_{\text{rot}} \quad (1)$$

Where  $E_{\text{total}}$ ,  $E_{\text{ele}}$ ,  $E_{\text{vib}}$ , and  $E_{\text{rot}}$  stands for total, electronic, vibrational, and rotational energy, respectively (Coleman, 1993; Hollas, 2004).

## 2.3 Molecular Vibrations.

IR spectroscopy is a technique based on the vibrations of the atoms of a molecule. An IR spectrum is commonly obtained by passing IR radiation through a sample and determining what fraction of the incident radiation is absorbed at a particular energy. The energy at which peak in absorption spectrum appears corresponds to a frequency of vibration of a part of a sample molecule.

As the starting point for introducing the concept of molecular vibrations, it is instructive to consider molecules as an array of point masses that are connected with each other by massless springs representing the intramolecular interactions between the atoms. The simplest case is given by two masses,  $m_1$  and  $m_2$ , corresponding to a diatomic molecule  $m_1$ - $m_2$ . Upon displacement of the spheres along the x-axis from the equilibrium position  $r_0$  by  $\Delta x$ ,

a restoring force ( $F_x$ ) acts on the spheres, which according to Hooke's law, is given by equation (1):

$$F_x = -K \Delta x \quad (2)$$

Here  $K$  is the spring or force constant, which is a measure of the rigidity of the spring, that is, the strength of the bond. (Siebert et al., 2008) An illustration of this model is shown in Fig.(2.3). When this spring is stretched or compressed beyond the equilibrium distance of the bond, the potential energy of the system increases. When a bond vibrates, as for any harmonic oscillator, its energy of vibration is continuously and periodically changing from kinetic to potential energy. The total energy of the bond is proportional to the frequency of the vibration, as follows:

$$E_{osc} \propto \nu_{osc} \quad (3)$$

This total energy for a harmonic oscillator is determined by the force constant of the spring ( $K$ ), and the masses ( $m_1$  and  $m_2$ ) of the two bonded atoms. The natural wavenumber ( $\bar{\nu}$ ) of vibration of a bond is given by the equation, which is derived from Hooke's Law for vibrating springs.

$$\bar{\nu} = \frac{1}{2\pi c} \sqrt{\frac{K}{\mu}} \quad (4)$$

Where  $\mu$  is the reduced mass of the system, is given by:

$$\mu = \frac{m_1 m_2}{m_1 + m_2} \quad (5)$$

The force constant  $K$  varies from one bond to another (Bellamy, 1975).

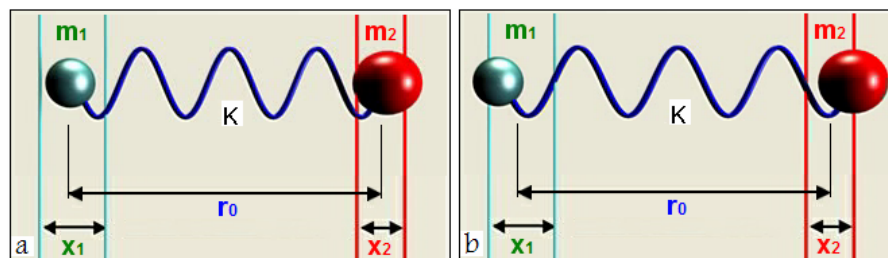


**Figure 2.3:** Diatomic model a) relaxed b) stretched.

---

\* It's a term used to designate a number of effects including phosphorescence and Raman scattering.

### 2.3.1 Normal modes of vibrations.

In the Cartesian coordinate system, each atom can be displaced in the x-, y-, and z-directions, corresponding to three degrees of freedom. Thus, a molecule of N nonlinear atoms has total  $3N$  degrees of freedom, but not all of them correspond to vibrational degrees of freedom (Siebert et al., 2008). Three of which represent translational motion in mutually perpendicular directions (the x-, y- and z-axes) and three represent rotational motion about the x-, y- and z-axes. The remaining  $3N - 6$  degrees of freedom give the number of ways that the atoms in the molecule can vibrate, i.e. the number of *vibrational modes* (Chalmers et al., 2002). The degrees of freedom for polyatomic molecules, i.e linear or non linear (see Fig.(2.4)) are summarized in Table (2.1).

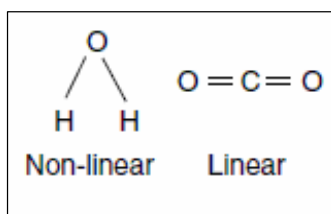


**Figure 2.4:** Water and Carbon dioxide molecules.

**Table 2.1:** Degrees of freedom for polyatomic molecules, (Stuart, 2004)

Type of degrees of freedom	Linear	Non-linear
Translational	3	3
Rotational	2	3
Vibrational	$3N - 5$	$3N - 6$
Total	$3N$	$3N$

The normal mode of vibration is defined as a molecular motion in which all the atoms move in phase and with the same frequency (Banwell, 1972). Two types of molecular vibrations correspond to the normal mode of the molecule: stretching and bending. Stretching is rhythmical movement along the bond axis and can be symmetric or antisymmetric. Bending vibrations arise from a change in bond angle between two atoms or movement of a group of atoms, relative to the remainder of the molecule.

For many vibrational modes, only a few atoms have large displacements and the rest of the molecule is almost stationary. The frequency of such modes is characteristic of the specific functional group in which the motion is centered and is minimally affected by the nature of the other atoms in the molecule. Thus the observation of spectral features in a certain region of the spectrum is often indicative of a specific chemical functional group in the molecule. For example, if a series of compounds which all contain an –OH group are examined, the infrared spectra universally show bands near 3500 and 1650  $\text{cm}^{-1}$  corresponding to the –OH stretching and bending modes, respectively. Even though most other atoms in the molecule also vibrate, their effect on the –OH constituent is relatively small (Mirabeela,1998).

### 2.3.2 Quantum mechanical treatment of vibrations.

#### *I. The harmonic approximation.*

According to classical mechanics, a harmonic oscillator may vibrate with any amplitude, which means that it can possess any amount of energy, large or small. Quantum mechanics, however, shows that molecules can only exist in definite energy states. In the case of harmonic potentials, these states are equidistant,

$$V_{iv} = hv_i(n_i + \frac{1}{2}) \quad (6)$$

where  $n_i$  is the vibrational quantum number, which can take only positive integer values including zero,  $h$  is Planck's constant (Schrader, 1995). The potential energy,  $V_{iv}$ , of a harmonic oscillator is shown by the dashed line in Fig.(2.5) as a function of the distance between the atoms,  $r$  (Griffiths et al., 2007).

#### *II. Anharmonicity.*

The bonds in actual molecules, however, are not obeying Hooke's law exactly, the actual variation of the potential energy as a function of the displacement of the atoms from their equilibrium positions is shown as the solid line in Fig.(2.5).

From this curve it can be seen that equation (5) is only valid for low values of the vibrational quantum number, and is not valid when  $v_i$  is large. In practice,  $V_{iv}$  must be described using an *anharmonic* (Morse-type) potential function. This behavior is shown on Fig.(2.5) as the solid line, and the vibrational energy becomes:

$$V_{iv} = hv_i \left( n_i + \frac{1}{2} \right) + hv_i x_i \left( n_i + \frac{1}{2} \right) \quad (7)$$

Where  $x_i$  is the *anharmonicity constant*.  $x_i$  is dimensionless and typically has values between 0.001 and 0.02 depending on the mode. If all vibrational modes were strictly harmonic, no transitions involving changes in  $n_i$  by more than  $\pm 1$  would be allowed. The effect of anharmonicity is to relax this selection rule, i.e. to allow bands caused by  $|\Delta n_i| > 1$  to become allowed (Chalmers et al., 2002).

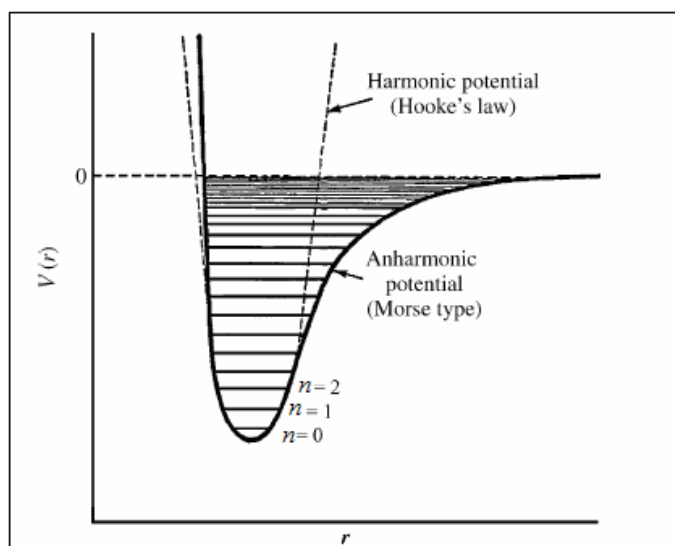


**Figure 2.5:** potential energy of a diatomic molecule as a function of the atomic displacement during vibration for a harmonic oscillator (dashed line) and an anharmonic oscillator (solid line) (Griffiths et al., 2007).

### 2.3.3 Vibrational modes of polyatomic molecules.

As discussed by Schermann, 2008; in a polyatomic molecule containing  $N$  atoms,  $3N$  degrees of freedom describe the whole molecule (3 per atom). After removal of the centre of mass motion and rotation of the whole molecule,  $3N-6$  vibrational degrees of freedom must be considered. In a given normal mode of vibration  $Q_i$ , all nuclei undergo harmonic

motion and move in phase with different amplitudes. All nuclei have the same frequency of oscillation. The potential energy is then given by:

$$V(Q) = V_e + \frac{1}{2} \sum_i \lambda_i Q_i^2 \quad (8)$$

$V_e$  is the energy minimum usually taken as the origin ( $V_e=0$ ) and the  $\lambda_i$  are the force constants. In a first approximation, the vibrational motion of a polyatomic molecule can then be considered as the sum of  $3N-6$  harmonic motions and the vibrational energy is then:

$$E_{\text{vib}} = \sum_{i=1}^{3N-6} (n_i + \frac{1}{2}) h\nu_i \quad (9)$$

In the lowest energy state,  $n_1=0, n_2=0\dots$  and the vibrational energy is equal to the zero-point energy

$$ZPE = \sum_i^{3N-6} \frac{1}{2} h\nu_i \quad (10)$$

In general, normal modes of vibrations involve the movement of all atoms of a molecule but, in some cases, the movement is more or less localized on a single bond of the molecule as in a diatomic molecule, the potential energy of a polyatomic molecule is not a simple sum of harmonic energies but anharmonic terms must be considered:

$$V(Q) = V_e + \frac{1}{2} \sum_i \lambda_i Q_i^2 + \frac{1}{6} \sum_{rst} Q_r Q_s Q_t + \dots \quad (11)$$

The vibrational energy becomes:

$$E_{\text{vib}} = \sum_{i=1}^{3N-6} (n_i + \frac{1}{2}) h\nu_i + \sum_{i<j}^{3N-6} x_{ij} (n_i + \frac{1}{2})(n_j + \frac{1}{2}) + \dots \quad (12)$$

The existence of the anharmonicity terms  $x_{ij}$  introduces coupling between normal modes. The selection rules are no longer  $\Delta n_i = 1$  but overtones ( $\Delta n_i = 2$ ) and intercombination bands with frequencies  $n_i n_i + n_j n_j$  appear. This has several consequences. From the lowest vibrational energy state  $n_1 = n_2 = \dots = n_i = 0$ , the frequency of an absorbed photon is equal to one of the fundamental vibrational frequencies  $n_i$  or one of its harmonics  $n_i \nu_i$ . When the internal energy of a molecule increases due to vibrational excitation, either by absorption of photons or following collisions, the density of vibrational states (number of vibrational energy levels per frequency unit) increases extremely rapidly. The vibrational levels can no longer be considered as discrete but rather as forming a quasi-continuum. Nearly any photon energy can then be absorbed (Schermann, 2008).

## **2.4 FT-IR Spectroscopy.**

Since the development of the first spectrophotometers in the beginning of the 20<sup>th</sup> century a rapid technological development has taken place. The first generation spectrometers were all dispersive. Initially, the dispersive elements were prisms, and later, they changed over the gratings (OPUS Bruker manual, 2004).

In the mid 1960s IR spectroscopy witnessed a revival due to the advent of spectrometers that utilized the Fourier transform. These second generation spectrometers, with an integrated Michelson interferometer, provided some significant advantages compared to dispersive spectrometers (OPUS Bruker manual, 2004). The most important advantage of FT-IR spectroscopy for biological studies is that spectra of almost any biological system can be obtained in a wide variety of environments (Li et al., 2007).

### **2.4.1 Infrared (IR) spectroscopy.**

IR spectroscopy is certainly one of the most important analytical techniques available to today's scientists. One of the great advantages of IR spectroscopy is that virtually any sample in virtually any state may be studied; liquids, solutions, pastes, powders, films, fibers, gases and surface can all be examined with a judicious choice of sampling technique (Stuart, 2004).

#### **2.4.1.1 IR-region.**

Infrared radiation spans a section of the electromagnetic spectrum adjacent to the visible spectral region and extends from wavelength, roughly 0.78 $\mu\text{m}$  to about 1000 $\mu\text{m}$ . IR spectroscopists do not usually use the wavelength to plot their spectra but rather the inverse of the wavelength; the wavenumber. This quantity has the advantage of being proportional to vibrational frequency and the vibrational energy (Uversky, 2007). So the wavenumber range of IR radiation is from about 12800 to 10  $\text{cm}^{-1}$ . IR spectrum is conveniently divided into three regions due to their location relative to visible spectrum near-, mid-, and far-IR regions; the rough limits of each are shown in Fig.(2.6) (Serdyuk et al., 2007).

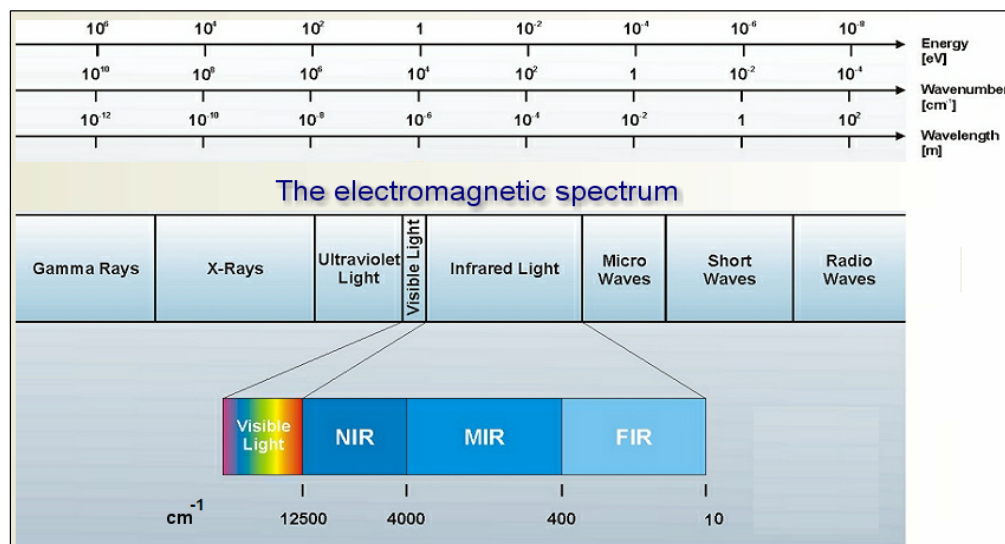


**Figure 2.6 :** Regions of IR spectrum.

### 2.4.1.2 IR Spectrum presentation.

In IR spectroscopy the horizontal coordinate of the spectrum runs from high wavenumbers to low wavenumbers according to a recommendation of the international union of pure and applied chemistry this is equivalent to running from small wavelength to large wavelength (Uversky, 2007).

IR absorption is generally presented in the form of a spectrum showing wavelength or wavenumber versus transmittance or absorption intensity. The Transmittance (T), is the ratio of radiant power transmitted by the sample (I) to the radiant power incident on the sample (I<sub>0</sub>). Absorbance (A) is the logarithm to the base 10 of the reciprocal of the transmittance (T) as shown in equation (9),

$$A = \log_{10} \left( \frac{1}{T} \right) = -\log_{10} T = -\log_{10} \frac{I}{I_0} \quad (13)$$

The transmittance spectra provide better contrast between intensities of strong and weak bands, because transmittance ranges from 0 to 100%; whereas absorbance ranges from infinity to zero (Settle, 1997).

### 2.4.1.3 Principle of IR absorption.

As with other types of energy absorption, molecules are excited to a higher energy state when they absorb infrared radiation. The absorption of infrared radiation is, like other absorption processes; a quantized process. A molecule absorbs only selected frequencies (energies) of infrared radiation. The absorption of infrared radiation corresponds to energy changes on the order of 8 to 40 kJ/mole. Radiation in this energy range corresponds to the range encompassing the stretching and bending vibrational frequencies of the bonds in most covalent molecules. In the absorption process, those frequencies of infrared radiation that match the natural vibrational frequencies of the molecule in question are absorbed, and the energy absorbed serves to increase the amplitude of the vibrational motions of the bonds in the molecule. However, not all bonds in a molecule are capable of absorbing infrared energy, even if the frequency of the radiation exactly matches that of the bond motion. Only those bonds that have a dipole moment that changes as a function of time are capable of absorbing infrared radiation (Pavia et al., 2009).

Almost all molecules absorb infrared light, and each type of molecule absorbs infrared light at certain frequencies only. This property provides a unique characteristic for each molecule. It provides a way to identify the molecule type (Qualitative analysis) and the amount or quantity of this molecule in the sample (Quantitative analysis). Since each type of molecule only absorbs at certain frequencies, it provides a unique absorption spectral pattern or fingerprint through the entire infrared light spectrum. In this way, the more molecules of the same type in the sample, the more infrared light is absorbed at those specific frequencies at which those molecules absorb infrared light.

The height of the peaks are defined by the Beer-Lambert relationship (or Beer's law). Beer's law states that the concentration  $C$  is directly proportional to the absorbance  $A$ .

That is:

$$A=abC \tag{14}$$

Where  $a$  is the absorptivity of the molecule and  $b$  is the path length or distance that the light travels through the sample (Workman, 1998).

## 2.4.2 Theory of FT-IR spectroscopy.

FT-IR is an infrared spectroscopy which has the design of the optical pathway produces interference signals, which contain infrared spectral information called interferogram (Pavia et al., 2009).

FT-IR Spectroscopy bases its functionality on the principle that almost all molecules absorb IR radiation (Banwell, 1972). The heart of an FT-IR spectrometer is an interferometer. Like the Michelson interferometer shown in Fig.(2.7) it has a fixed and a movable mirror. The latter generates a variable optical path difference between two beams and thus a detector signal that contains the spectral information.

When the two beams recombine they interfere and there will be redistribution of energy interference depending on the optical path difference  $d$ . The instrument measures the light intensity relative to the position of the movable mirror and this is called an interferogram. It turns out that the interferogram is the fourier transform of the spectrum (Uversky, 2007).

The interferogram is Fourier transformed with the help of computer to convert the space domain into the wave number domain (Vij, 2006).

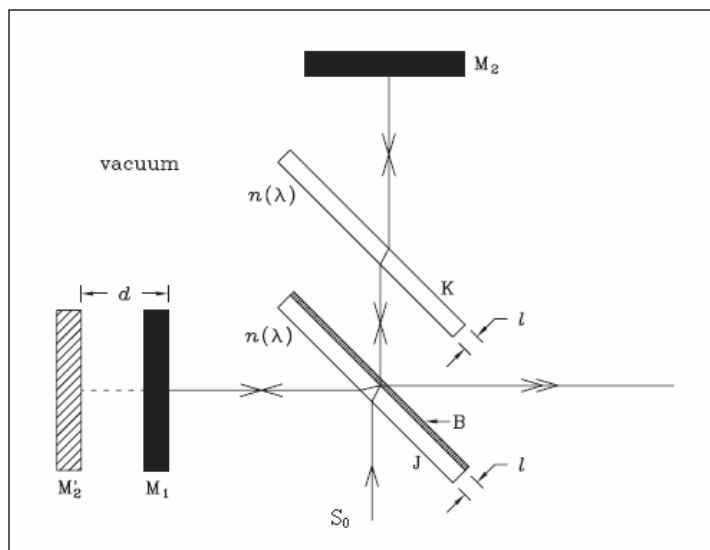


**Figure 2.7:** Optical arrangement of Michelson interferometer.  $M_1$  and  $M_2$  are a fixed and a moving mirror, respectively. B is the half-transparent surface of the beam splitter J, and K is a compensator plate. The beamsplitter and the compensator plate have the same thickness  $l$  and the same refractive index (Kauppinen et al., 2001).

The basic integral equation used in FT-IR spectroscopy can be obtained from the definition of Fourier integral theorem. The basic equation used in the case of the Michelson interferometer can be derived mathematically as reported by J. Kauppinen et al., 2001; as follows:

Let us assume that the spectrum of the light source  $S_0$  is continuous and consists of a wide band of wavenumbers, so that the spectrum of the beams in both branches of the interferometer is  $E(\nu)$ , shown in Fig.(2.8). We shall assume that the source is still a point source. At a given optical path difference  $x$ , the interference signal from the infinitesimal spectral element between  $\nu$  and  $\nu + d\nu$  is,

$$dF(x, \nu) = 2E(\nu)[1 + \cos(2\pi\nu x)]d\nu \quad (15)$$

Consequently, the total signal from the whole spectral band is

$$F(x) = 2 \int_0^{\infty} E(\nu)[1 + \cos(2\pi\nu x)]d\nu \quad (16)$$

$F(x)$  is called an *interference record*. An interference record is the total interference signal of the whole spectral band, measured as the function of the optical path difference  $x$ . A typical interference record is shown in Fig.(2.9).

If we subtract the constant term

$$\frac{1}{2}F(0) = 2 \int_0^{\infty} E(\nu)d\nu \quad (17)$$

from the interference record  $F(x)$ , we obtain

$$I(x) = F(x) - \frac{1}{2}F(0) = 2 \int_0^{\infty} E(\nu) \cos(2\pi\nu x) d\nu \quad (18)$$

$I(x)$  is called an *interferogram*, and looks like as shown in Fig.(2.9).

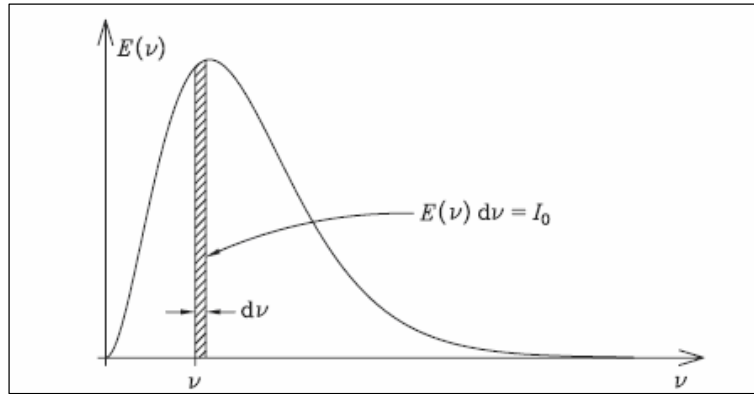


**Figure 2.8:** A wide-band continuous spectrum  $E(\nu)$  and an infinitesimal monochromatic section of the width  $d\nu$  (Kauppinen, 2001).

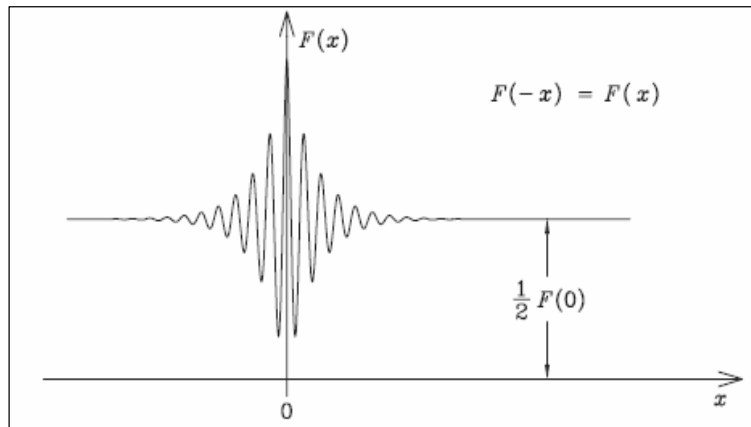


**Figure 2.9:** An interference record  $F(x)$  (Kauppinen, 2001).

If we define  $E(-\nu) = E(\nu)$ , the computation is simplified, and we obtain

$$I(x) = \int_{-\infty}^{\infty} E(\nu) \cos(2\pi\nu x) d\nu = \int_{-\infty}^{\infty} E(\nu) e^{i2\pi\nu x} d\nu = \mathcal{F}\{E(\nu)\} \quad (19)$$

Where  $\mathcal{F}$  is the Fourier transform. Hence,  $I(x)$  and  $E(\nu)$  form a Fourier transform pair, and they can be written as (Kauppinen, 2001):

$$\begin{aligned} I(x) &= \int_{-\infty}^{\infty} E(\nu) e^{i2\pi\nu x} d\nu = \mathcal{F}\{E(\nu)\}, \\ E(\nu) &= \int_{-\infty}^{\infty} I(x) e^{-i2\pi\nu x} dx = \mathcal{F}^{-1}\{I(x)\} \end{aligned} \quad (20)$$

### 2.4.3 The working principle of an FT-IR spectrometer.

The basic components of an FT-IR spectrometer are shown schematically in Fig.(2.10.a) (Stuart, 2004). The working principle of an FT-IR spectrometer is as follows; a steady illumination from a broad-band IR source is modulated by a Michelson interferometer, i.e. a beam splitter that divides the collimated light along different paths to two mirrors. The light reflected from the fixed and moving mirrors is recombined at the beam splitter and is directed through the sample and into the IR detector. The path length difference between the light reflected from the fixed mirror and the light reflected from the moving mirror is measured very precisely. Next a computer stores the digitized interferogram and converts it via Fourier transformation to an IR spectrum. As illustrated in Fig.(2.10.b) (Serdyuk et al., 2007).

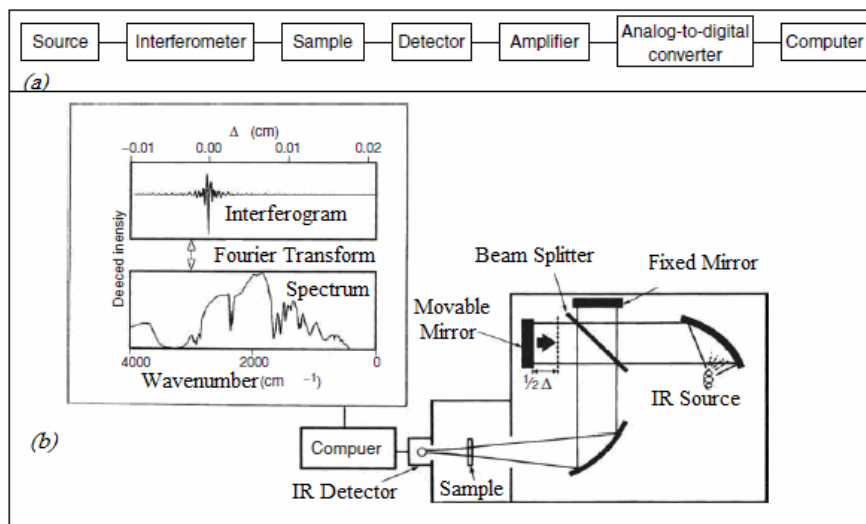


**Figure 2.10:** a) Basic components of FT-IR spectrometer. b) Simplified layout of an FT-IR spectrometer (Serdyuk et al., 2007).

### 2.5 Ultraviolet-Visible (UV-VIS) spectrophotometer.

When continuous radiation passes through a transparent material, a portion of the radiation may be absorbed. In the case of UV-VIS spectrophotometer, the transitions that result in the absorption of electromagnetic radiation in this region of the spectrum are transitions between electronic energy levels. As a molecule absorbs energy, an electron is promoted from an occupied orbital to an unoccupied orbital of greater potential energy.

For most molecules, the lowest-energy occupied molecular orbitals are the  $\sigma$  orbitals, which correspond to  $\sigma$  bonds. The  $\pi$  orbitals lie at somewhat higher energy levels, and orbitals that hold unshared pairs, the nonbonding ( $n$ ) orbitals, lie at even higher energies. The unoccupied, or antibonding orbitals ( $\pi^*$  and  $\sigma^*$ ), are the orbitals of highest energy. Fig.(2.11), shows a typical progression of electronic energy levels (Pavia et al., 2009).

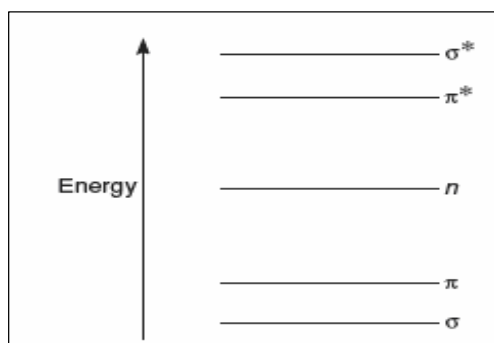


**Figure 2.11:** Electronic energy levels.

In all compounds, the electrons may undergo several possible transitions of different energies Fig.(2.12) illustrates these transitions (Pavia et al., 2009).

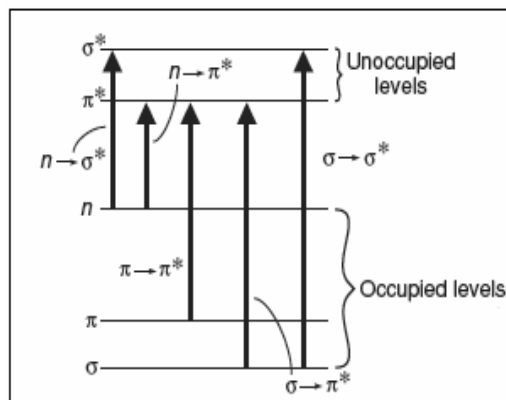


**Figure 2.12:** Electronic energy transitions (Pavia et al., 2009).

A *spectrophotometer* is an instrument that measures the intensity of a light beam as a function of wavelength. Spectrophotometers for the measurement of absorbance in the UV-VIS range come in a variety of configurations. The most common routine laboratory instruments are single- or double-beam devices made up of a light source, monochromator, sample compartment, detector, data processor and display (Alan Cooper, 2004).

The absorption of UV light by proteins has been analyzed in detail and proposed as a structural probe from the very early days of molecular biology. The absorption of proteins in the UV arises mainly from electronic bands in the aromatic amino acid side-chains (tryptophan, tyrosine, phenylalanine) and, to a lesser extent, cysteine residues, close to 280 nm (Serdyuk et al., 2007; Alan Cooper, 2004).

## 2.6 Fluorescence spectrophotometer.

Fluorescence spectrophotometer is one of the most widely used spectroscopic techniques in the fields of biochemistry and molecular biophysics today (Cui et al., 2008; Royer, 1995). Fluorescence is a particular case of luminescence, the other case is phosphorescence. Luminescence is an emission of ultraviolet, visible or infrared photons from an electronically excited species. (Valeur, 2002) Fluorescence is a phenomenon whereby a material absorbs light at one wavelength and then emits it at a longer wavelength (lower energy) (Jue, 2009).

The processes that occur between the absorption and emission of light are usually illustrated by the Jablonski diagram, a typical Jablonski diagram is shown in Fig.(2.13) (Lakowicz, 2006). Quoting Lakowicz, 2006; The singlet ground, first, and second electronic states are depicted by  $S_0$ ,  $S_1$ , and  $S_2$ , respectively. At each of these electronic energy levels the fluorophores can exist in a number of vibrational energy levels, depicted by 0, 1, 2,...etc. The transitions between states are depicted as vertical lines to illustrate the instantaneous nature of light absorption.

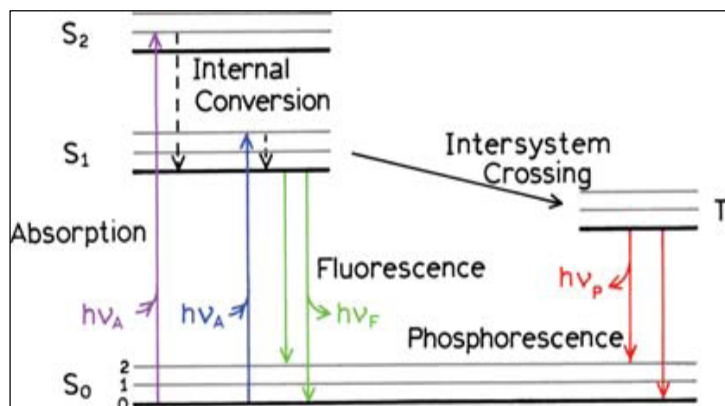


**Figure 2.13** : One form of a Jablonski diagram (Lakowicz, 2006).

The fluorescence lifetime and quantum yield are the most important characteristics of a fluorophore. Quantum yield is the number of emitted photons relative to the number of absorbed photons. The lifetime is determined by the time available for the fluorophore to interact with or diffuse in its environment, and hence the information available from its emission (Lakowicz, 2006).

It is clear that fluorescence is the result of an energy process that occurs in a molecule called fluorophore. The wavelength in manometer is determined by the spectral properties of the fluorophores. Fluorophores are divided into two main classes: (1) Intrinsic fluorophores are those that occur naturally, such as aromatic amino acids. (2) Extrinsic fluorophore are added to the sample to provide fluorescence when none exists, or to change the spectral properties of the sample (Lakowicz, 2006).

Following light absorption, several processes usually occur. A fluorophore is usually excited to some higher vibrational level of either  $S_1$  or  $S_2$ . An interesting consequence of emission to higher vibrational ground states is that the emission spectrum is typically a mirror image of the absorption spectrum of the  $S_0 \rightarrow S_1$  transition. This similarity occurs because electronic excitation does not greatly alter the nuclear geometry. Hence the spacing of the vibrational energy levels of the excited states is similar to that of the ground state. As a result, the vibrational structures seen in the absorption and the emission spectra are similar.

Upon excitation into higher electronic and vibrational levels, the excess energy is quickly dissipated, leaving the fluorophore in the lowest vibrational level of  $S_1$ . This relaxation occurs in about  $10^{-12}$  s, and is presumably a result of a strong overlap among numerous states of nearly equal energy. Because of this rapid relaxation, emission spectra are usually independent of the excitation wavelength.

The intensity of fluorescence can be decreased by a wide variety of processes. Such decreases in intensity are called quenching. Quenching can occur by different mechanisms: Collisional quenching occurs when the excited-state fluorophore is deactivated upon contact with some other molecule in solution, which is called the quencher, and static quenching resulting from the formation of a ground state complex between the fluorophore and the quencher.

For collisional quenching the decrease in intensity is described by the well-known Stern-Volmer equation (Lakowicz, 2006):

$$\frac{F_0}{F} = 1 + K_q \tau_0(L) = 1 + K_{sv}(L) \quad (21)$$

In this expression  $F$  and  $F_0$  are the fluorescence intensities with and without quencher,  $K_{sv}$  is the Stern-Volmer quenching constant,  $K_q$  is the bimolecular quenching constant,  $\tau_0$  is the unquenched lifetime, and  $(L)$  is the quencher concentration. The Stern-Volmer quenching constant  $K_{sv}$  indicates the sensitivity of the fluorophore to a quencher.

In proteins, Tryptophan, Phenylalanine, and Tyrosine; are the amino-acid residues mostly responsible for the absorbing and the emitting of energy. Fig.(2.14) shows the molecular schematics of the three residues. Tryptophan is known to be the most efficient intrinsic amino acid emitter residue (Jue, 2009). Due to a very low quantum yield of Phenylalanine, and the fluorescence of Tyrosine is almost completely quenched if that Tyrosine is ionized, near an amino group, a carboxyl group, or a Tryptophan (Zhang et al., 2008).



**Figure 2.14:** Structure of the intrinsic fluorophores amongst amino acids.

## 2.7 Proteins.

Proteins are one of the important molecules of our life and the major target of many types of medication in the body (Zhang et al., 2008). Proteins are a particular type of biological molecules that can be found in every single living being on Earth. Proteins are polymers made up of specific sequences of amino acids linked together by covalent peptide (amide) bonds. Amino acids are chosen from a basic set of 20 building blocks differing in their side-chain. Amino acids have the general formula  $H_2NCHRCOOH$ , where  $R$  is an organic

substituent (Fig.(2.15)). The number of amino acids units contained in the protein, the identity, and sequential order of the amino acids are used to distinguish proteins from one another (Cooper, 2004).

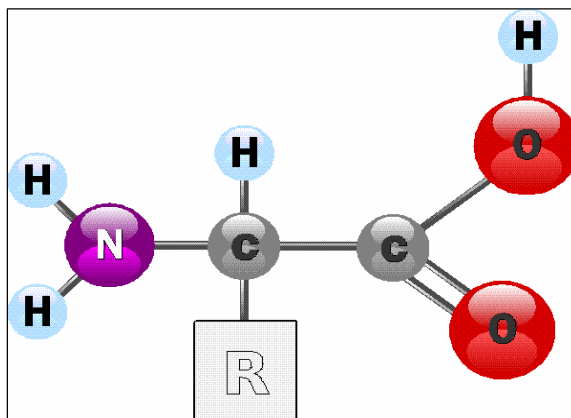


**Figure 2.15:** General structure of amino acids.

### 2.7.1 Protein structure.

Protein chemical structure and molecular conformation are commonly described in terms of four levels of structure: Primary, Secondary, Tertiary, and Quaternary structure. Primary structure is the sequence of amino acids in the polypeptide chain which is unique to each protein (Cooper, 2004).

The secondary structures imply the hierarchy by providing repeating sets of interactions between functional groups along the polypeptide backbone chain that creates, in turn, irregularly shaped surfaces of projecting amino acid side chains. The secondary structures in proteins arise from repeating patterns of similar peptide dihedral angles, for successive residues.

Most protein structures are built up from combinations of  $\alpha$ -helices and  $\beta$ -sheets, which form stable hydrophobic core, the remaining portions of protein structures are made up of well-ordered but nonrepetitive conformations referred to as coils.

The C=O bond is parallel to the helical axis and the linear hydrogen bond formed between the C=O and N—H in the  $\alpha$ -helix is the most stable geometrical arrangement. Fig.(2.16).

The polypeptide chains that form the  $\beta$ -structure are called  $\beta$ -strands. The  $\beta$ -strands are aligned adjacent to each other such that hydrogen bonds can form between N—H groups of one  $\beta$ -strand and C=O groups of an adjacent strand and vice versa alternatively to the left and to the right. Therefore the basic unit of  $\beta$ -sheet is not the individual  $\beta$ -strand but the  $\beta$ -strand pair, which form hydrogen bonds between them. The  $\beta$ -structure that forms from several such  $\beta$ -strands is pleated, termed  $\beta$ -pleated sheet ( $\beta$ -sheet), with  $C\alpha$  atoms successively sticking slightly above and below the plane of the  $\beta$ -sheet. The  $\beta$ -strands in the  $\beta$ -sheet interact in two ways, i.e. parallel in which all amino acids in the aligned  $\beta$ -strands run in the same direction, or antiparallel in which the amino acids in successive strands run in opposite directions (Tsai, 2007).

Hydrogen bond networks that hold  $\beta$ -strands are different in parallel and antiparallel sheets. The parallel  $\beta$ -sheets have evenly spaced hydrogen bonds that angle across between the  $\beta$ -strands, whereas antiparallel  $\beta$ -sheets have parallel narrowly spaced hydrogen bonds that alternate with widely-spaced pairs. Fig.(2.17) (Tsai, 2007).

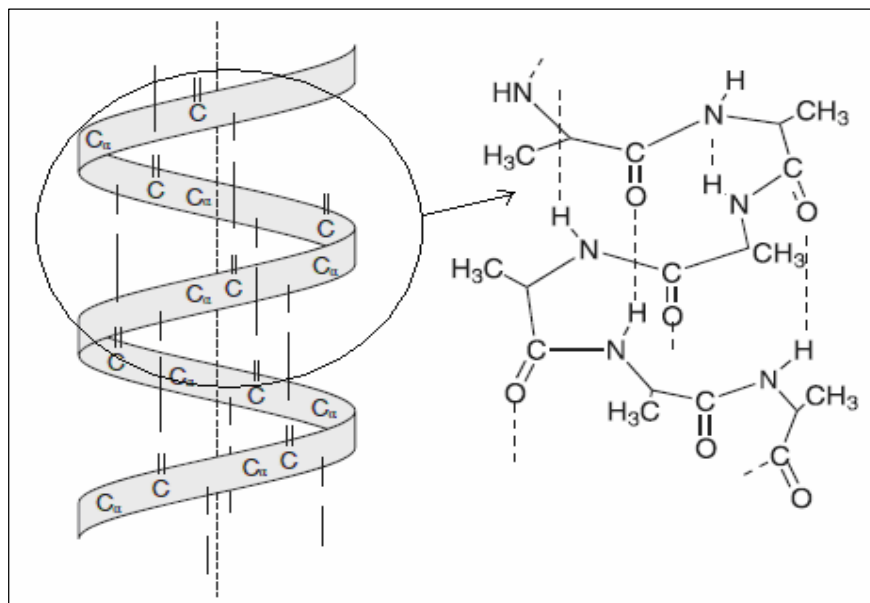


**Figure 2.16:** The  $\alpha$ -helix. The main chain carboxyl group of amino acid  $j$  is hydrogen bonded to the NH group of amino acid  $j+4$  (Serdyuk et al., 2007).

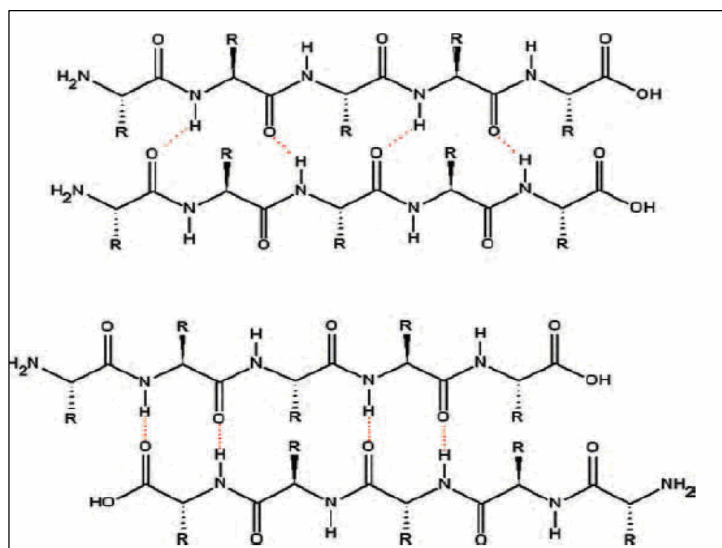


**Figure 2.17:** Parallel (top) and antiparallel (bottom)  $\beta$ -sheets (Serdyuk et al., 2007).

Tertiary structure describes the way in which the elements of protein secondary structure are arranged in space and Quaternary structure describes how several polypeptide chains come together to form a single functional protein (Cooper, 2004).

### 2.7.2 Human Serum Albumin (HSA).

HSA is the most abundant protein in human plasma, which is synthesized in the liver (Fengling et al., 2006), and is able to bind and thereby transport, various compounds such as fatty acids, hormones, bilirubin, tryptophan, steroids, metal ions, therapeutic agents and a large number of drugs. HSA serves as the major soluble protein constituent of the circulatory system, it contributes to colloid osmotic blood pressure, it can bind and carry drugs which are mainly poorly soluble in water (Peters, 1985). HSA accounts for approximately 60% of the total plasma protein corresponding to a concentration of 40mg/ml in the blood ( $\sim 0.6\text{mM}$ ) (Tang et al., 2006).

The three dimensional structure of HSA was determined through x-ray crystallographic measurements (He et al., 1992). This globular protein consists of a single polypeptide chain of 585 amino acids (Purcell et al., 2000), which have a molecular weight of 66 kDa (Bian et al., 2004).

This protein composed of three structurally similar domains (labeled as I, II, III). Each containing two sub domains ( A & B) having six and four  $\alpha$ -helices, respectively (Curry et al., 1999), and stabilized by 17 disulphide bridges, that assemble to form a heart shaped molecule, see Fig.(2.18) (He et al., 1992; Bian et al., 2004).

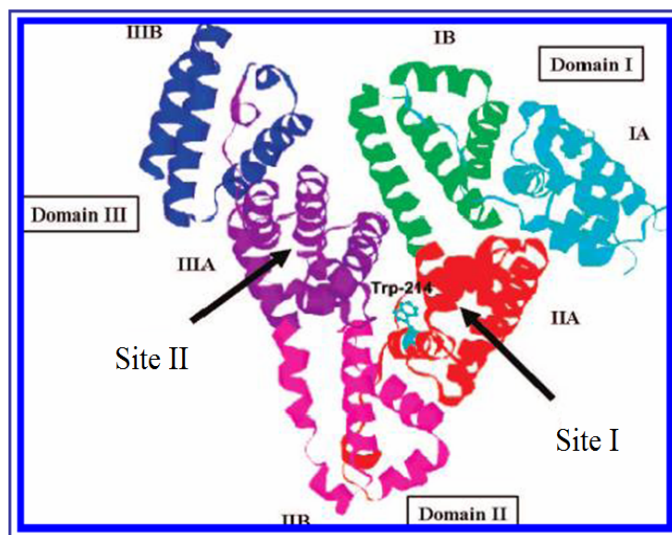


**Figure 2.18:** Chemical structure of human serum albumin (Abou-Zied, 2009).

It has been shown that distribution, free concentration, and the metabolism of various drugs can be significantly altered as a result of their binding to HSA (Artali et al., 2004; Kang et al., 2004). The binding properties of albumin depend on the three dimensional structure of the binding sites, which are distributed all over the molecule. Strong binding can decrease the concentrations of free drugs in plasma, whereas weak binding can lead to a short lifetime or poor distribution or both. Its remarkable capacity to bind a variety of drugs results in its prevailing role in drug pharmacokinetics and pharmacodynamics (P.B. Kandagal, et al., 2007).

Multiple drug binding sites have been reported for HSA by several researchers (Bhattacharya, et al., 2000; Simard et al., 2006; Ulrich et al., 2006). The principal regions of ligand binding sites of HSA are located in hydrophobic cavities in sub domains IIA and IIIA, which are corresponding to site I and site II, respectively. Site I is dominated by strong hydrophobic interaction with most neutral, bulky, heterocyclic compounds, while site II mainly by dipole–dipole, van der Waals, and/or hydrogen-bonding interactions with many aromatic carboxylic acids. HSA contained a single tryptophan residue (Trp 214) in

domain IIA and its intrinsic fluorescence is sensitive to the ligands bounded nearby (Krishnakumar, et al., 2002; Il'ichev, et al., 2002). Therefore, it is often used as a probe to investigate the binding properties of drugs with HSA.

*Chapter Three:*

# **Experimental Part**

## **Chapter Three**

---

### **Experimental part.**

This chapter consists of three sections; section one contains information about samples, and film preparation. The next section includes a descriptions of the spectrometers used in this work, which are Bruker IFS 66/S FT-IR spectrophotometer, UV-VIS spectrophotometer (NanoDrop ND-1000), and Fluorospectrometer (NanoDrop 3300). The final section presents the experimental procedure in full details.

### **3.1 Samples and materials.**

HSA (fatty acid free), progesterone, and cholesterol in powder form were purchased from Sigma Aldrich chemical company and used without further purifications.

The data were collected using samples in the form of thin films for FT-IR measurements and liquid form for UV-VIS and fluorescence measurements.

Preparations of the thin film samples required several stock solutions as described below:

#### **3.1.1 Preparation of HSA stock solution.**

HSA was dissolved in phosphate buffer saline, at physiological pH 7.4, to a concentration of (80mg/ml), to get a final concentration of (40 mg/ml) in the final hormone- HSA solution.

### **3.1.2 Preparation of progesterone stock solution.**

Progesterone with molecular weight of (314.47 g/mol) was dissolved in phosphate buffer saline (0.7622 mg/ml), the solution was placed in ultrasonic water bath (SIBATA AU-3T) for six hours to ensure that all the amount of progesterone was completely dissolved.

### **3.1.3 Preparation of cholesterol stock solution.**

Cholesterol with molecular weight (386.66g/mol), was dissolve in phosphate buffer saline (0.9373 mg/ml), the solution was placed in ultrasonic water bath (SIBATA AU-3T) for six hours to ensure that all the amount of cholesterol was completely dissolved.

### **3.1.4 HSA-Progesterone solutions.**

The final concentrations of HSA-hormone solutions were prepared by mixing equal volume of HSA and hormone. HSA concentration in all samples kept at 40mg/ml. However, the concentration of hormone in the final protein hormone solutions was reduced such that the molecular ratios (HSA:hormone) are 10:18, 10:14, 10:10, 10:6, and 10:2.

### **3.1.4 HSA-Cholesterol solutions.**

The final concentrations of HSA-cholesterol solutions were prepared by mixing equal volume of HSA and cholesterol. HSA concentration in all samples kept at 40mg/ml. However, the concentration of colesterol in the final protein cholesterol solutions was reduced such that the molecular ratios (HSA:cholesterol) are 10:18, 10:14, 10:10, 10:6, and 10:2.

### **3.1.5 Thin film preparations.**

Silicon windows (NICODOM Ltd) were used as spectroscopic cell windows. The optical transmission is high with little or no distortion of the transmitted signal. The 100% line of a NICODOM silicon window shows that the silicon bands in the mid- IR region do not

exhibit total absorption and can be easily subtracted. 50 $\mu$ l of each sample of HSA-progesterone was spread on a silicon window and an incubator was used to evaporate the solvent, to obtain a transparent thin film on the silicon window. All solutions were prepared at the same time at room temperature.

The same procedure was followed for HSA-cholesterol films preparation.

## **3.2 Instruments.**

Many instruments can be used in studying the interaction of HSA with drugs. In this work the following instruments have been used in taking the measurements.

### **3.2.1 FT-IR Spectrometer.**

The FT-IR measurements were obtained on a Bruker IFS 66/S spectrophotometer equipped with a liquid nitrogen-cooled MCT detector and a KBr beam splitter. The spectrometer was continuously purged with dry air during the measurements.

### **3.2.2 UV-VIS spectrophotometer (NanoDrop ND-1000).**

The absorption spectra were obtained by the use of a NanoDrop ND-1000 spectrophotometer. It is used to measure the absorption spectrum of the samples in the range between 220-750nm, with high accuracy and reproducibility.

### **3.2.3 Fluorospectrometer (NanoDrop 3300).**

The fluorescence measurements were performed by a NanoDrop ND-3300 Fluorospectrophotometer at 25 °C. The excitation source comes from one of three solid-state light emitting diodes (LED's). The excitation source options include: UV LED with maximum excitation 365 nm, Blue LED with excitation 470 nm, and white LED from 500 to 650nm excitation. A 2048-element CCD array detector covering 400–750 nm, is connected by an optical fiber to the optical measurement surface. The excitation is done at the wavelength of 360 nm and the maximum emission wavelength is at 439 nm. Other

equipment such as Digital balance, pH meter, Vortex, Plate stir ... and Micropipettes were used (NanoDrop 3300 Fluorospectrometer V2.7 User's Manual, 2008).

### **3.3 Experimental procedures.**

#### **3.3.1 UV-VIS Spectrophotometer experimental procedures.**

Procedure of UV-VIS spectrophotometer was followed as described in NanoDrop 1000 Spectrophotometer V3.7, 2008, User's Manual (NanoDrop 1000 Spectrophotometer V3.7, User's Manual, 2008). Which is as follows:

##### **Operation**

A 1  $\mu$ l sample of progesterone or cholesterol is pipetted into the end of a fiber optic cable (the receiving fiber). A second fiber optic cable (the source fiber) is then brought into contact with the liquid sample causing the liquid to bridge the gap between the fiber optic ends. The gap is controlled to both 1mm and 0.2 mm paths. A pulsed xenon flash lamp provides the light source and a spectrophotometer utilizing a linear CCD array is used to analyze the light after passing through the sample. The instrument is controlled by PC based software, and the data is logged in an archive file on the PC.

Before taking the absorbance of samples the NanoDrop 1000 Spectrophotometer is "blanked". When the NanoDrop 1000 Spectrophotometer is "blanked", a spectrum is taken of a reference material (blank) and stored in memory as an array of light intensities by wavelength. When a measurement of a sample is taken, the intensity of light that has transmitted through the sample is recorded. The sample intensities along with the blank intensities are used to calculate the sample absorbance according to the following equation:

$$\text{Absorbance} = -\log \left( \frac{\text{Intensity}_{\text{sample}}}{\text{Intensity}_{\text{blank}}} \right)$$

Thus, the measured light intensity of both the sample and of the blank are required to calculate the absorbance at a given wavelength, and Beer-Lambert equation is used to correlate the calculated absorbance with concentration.

**Basic Use:** The main steps for using the sample retention system are listed below:

1. With the sampling arm open, pipette the sample onto the lower measurement pedestal see photo one of Fig.(3.1).
2. Close the sampling arm and initiate a spectral measurement using the operating software on the PC. The sample column is automatically drawn between the upper and lower measurement pedestals and the spectral measurement made see photo two of Fig.(3.1).
3. When the measurement is complete, open the sampling arm and wipe the sample from both the upper and lower pedestals using a soft laboratory wipe. Simple wiping prevents sample carryover in successive measurements for samples varying by more than 1000 fold in concentration see photo three of Fig.(3.1).

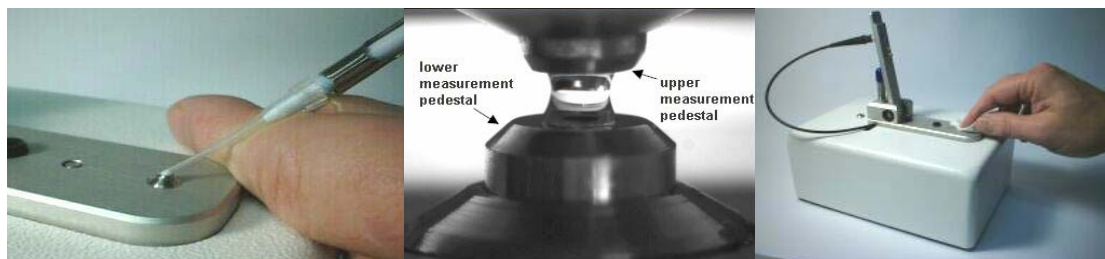


**Figure 3.1:** Main steps for using the sample UV-VIS Spectrophotometer (NanoDrop1000).

### 3.3.2 Fluorospectrophotometer experimental procedures.

Procedure of Fluorospectrophotometer was followed as described in NanoDrop 3300 Fluorospectrometer V2.7, 2008 User's Manual, (NanoDrop 3300 Fluorospectrometer V2.7 User's Manual, 2008), which is as follows:

Before taking the measurements of samples the NanoDrop 3300 Fluorospectrometer was "blanked".

## Operation

A 1-2  $\mu\text{l}$  sample of progesterone or cholesterol is pipetted onto the end of the lower measurement pedestal (the receiving fiber). A non-reflective “bushing” attached to the arm is then brought into contact with the liquid sample causing the liquid to bridge the gap between it and the receiving fiber. The gap, or pathlength, is controlled to 1mm. Following excitation with one of the three LEDs, emitted light from the sample passing through the receiving fiber is captured by the spectrophotometer. The NanoDrop 3300 is controlled by software run from a PC. All data is logged and archived in a folder at a user defined location.

**Basic Use:** The main steps for making a measurement are listed below:

1. With the sampling arm open, pipette the sample into the lower measurement pedestal see photo one of Fig.(3.2).
2. Close the sampling arm and initiate a measurement using the operating software on the PC. The sample column is automatically drawn between the upper bushing and the lower measurement pedestal and the measurement is made see photo two of Fig.(3.2) .
3. When the measurement is complete, open the sampling arm and wipe the sample from both the upper bushing and the lower pedestal using low lint laboratory wipe see photo three of Fig.(3.2).



**Figure 3.2:** Main steps for using the sample Fluorospectrophotometer (NanoDrop 3300).

### **3.3.3 FT-IR Spectrometer experimental procedures.**

The absorption spectra were obtained in the wave number range of 400–4000  $\text{cm}^{-1}$ . A spectrum was taken as an average of 60 scans to increase the signal to noise ratio, and the spectral resolution was at 4  $\text{cm}^{-1}$ . The aperture used in this study was 8 mm, since we found that this aperture gives best signal to noise ratio. Baseline correction, normalization and peak areas calculations were performed for all the spectra by OPUS software. The peak positions were determined using the second derivative of the spectra.

The infrared spectra of HSA, progesterone–HSA complexes, and cholesterol-HSA complexes, were obtained in the region of 1000–1800  $\text{cm}^{-1}$ . The FT-IR spectrum of free HSA was acquired by subtracting the absorption spectrum of the buffer solution from the spectrum of the protein solution. For the net interaction effect, the difference spectra {(protein and progesterone/ cholesterol solution) – (protein solution)} were generated using the featureless region of the protein solution 1800–2200  $\text{cm}^{-1}$  as an internal standard (Surewicz, et al, 1993).

### **3.3.4 FT-IR data processing.**

The analysis of IR spectra in terms of protein structure is not straightforward and presents serious conceptual and practical problems, despite the well-recognized conformational sensitivity of the IR-active bonds. Bands in amide I, amide II and amide III regions are broad, not resolved into individual components corresponding to different secondary structure elements.

Resolution enhancement or band-narrowing methods are applied to resolve broad overlapped bands into individual bands. FT-IR spectroscopy presents several advantages over conventional dispersive techniques for this type of analysis through the application of *second derivative, peak picking, spectral subtraction, baseline correction, smoothing, integration, curve fitting, and Fourier self-deconvolution.*

In the present study several data processing tasks were used, such as:

#### **3.3.4.1 Baseline correction.**

The baseline correction method applied here includes two steps. The first step is to recognize the baseline; this is done by selecting a point from spectral points on the spectrum. Then adding or subtracting a intensity value from the point or points to correct the baseline offset. Baseline correction task is used to bring the minimum point to zero. This is done automatically using Optic User Software (OPUS) and successfully removes most baseline offsets (Griffiths et al., 2007; OPUS Bruker manual , 2004).

#### **3.3.4.2 Peak picking.**

Automated peak picking involves two steps: (1) the recognition of peaks, and (2) the determination of the wavenumber values of maximum or minimum absorbance. A threshold absorbance value is usually set so that weak bands are not measured (Griffiths et al., 2007).

#### **3.3.4.3 Second derivative.**

Increased separation of the overlapping bands can be achieved by calculating the second derivative rate of change of slope of the absorption spectrum, second-derivative procedure have been successfully applied in the qualitative study of a large number of proteins (Haris et al., 1999).

#### **3.3.4.4 Fourier self-deconvolution.**

The Fourier deconvolution procedure, sometimes referred to as ‘resolution enhancement’ is the most widely used band narrowing technique in infrared spectroscopy of biological materials (Jackson et al., 1991). It involves narrowing the widths of infrared bands, allowing increased separation of the overlapping components present within the broad band envelope (Kauppinen, et al., 1981).

Both second-derivative and deconvolution procedures have been successfully applied in the qualitative study of a large number of protein. (Workman, 1998; Kauppinen et al, 1981). In addition to providing valuable information about their secondary structure, the method has been shown to be useful for detecting conformational changes arising as a result of ligand binding, pH, temperature, organic solvents, detergents, ... etc. In many cases results obtained using this approach has been later supported by studies using other

techniques such as X-ray diffraction and NMR. However, both derivative and deconvolution techniques should be applied with care since they amplify the noise significantly (Haris et al., 1999).

#### **3.3.4.5 Spectral subtraction.**

Difference spectroscopy is another approach that is very useful for investigating subtle differences in protein structure. The principle of difference spectroscopy involves the subtraction of a protein absorbance spectrum in state A from that of the protein in state B. The resultant difference spectrum only shows peaks that are associated with those groups involved in the conformational change (Goormaghtigh, et al., 2006; Haris et al., 1999).

The accuracy of this subtraction method is tested using several control samples with the same protein or drug concentrations, which resulted into a flat base line formation.

#### **3.3.4.6 Curve fitting.**

The Curve Fit command allows calculating single components in a system of overlapping bands. A model consisting of an estimated number of bands and a baseline should be generated before the fitting calculation is started. The model can be set up interactively on the display and is optimized during the calculation (OPUS Bruker manual, 2004).

*Chapter Four:*

# **Results and Discussion**

## Chapter Four

---

### **Results and discussion.**

This chapter includes the main results, analysis and discussions of our data. In the first section, UV-VIS spectrophotometer results are discussed and analyzed. The next section deals with fluorescence spectrophotometer results. In the final section, FT-IR graphs and data analysis are given.

#### **4.1 UV-VIS spectrophotometer.**

Many researchers have reported the effectiveness use of UV-VIS spectroscopy to investigate the interaction of drugs with HSA (Dukor, et al., 2001; Chirgadze. et al., 1975; Bi, et al., 2005). The absorption spectra of different ratios of progesterone or cholesterol with fixed amount of HSA are displayed in Fig.(4.1) and Fig.(4.2), respectively. The excitation has been done on 210 nm and the absorption is recorded at 278 nm. The figures show that the UV-VIS intensity of HSA increases with the increasing of progesterone or cholesterol percentages, and that the absorption peaks of these solutions showed moderate shifts indicating that with the addition of progesterone or cholesterol, the peptide strands of HSA molecules extended more and the hydrophobicity of progesterone and cholesterol was decreased (Peng et al., 2008). The results indicated that an interaction occurred between progesterone or cholesterol with HSA. Obviously, it was seen from the spectrum that pure hormone and its parent compound cholesterol have little or no UV absorption. This results support that the peaks are due to the interaction between progesterone or cholesterol with HSA. Repeated measurements were done for all the samples showing consistent results and no significant differences were observed.

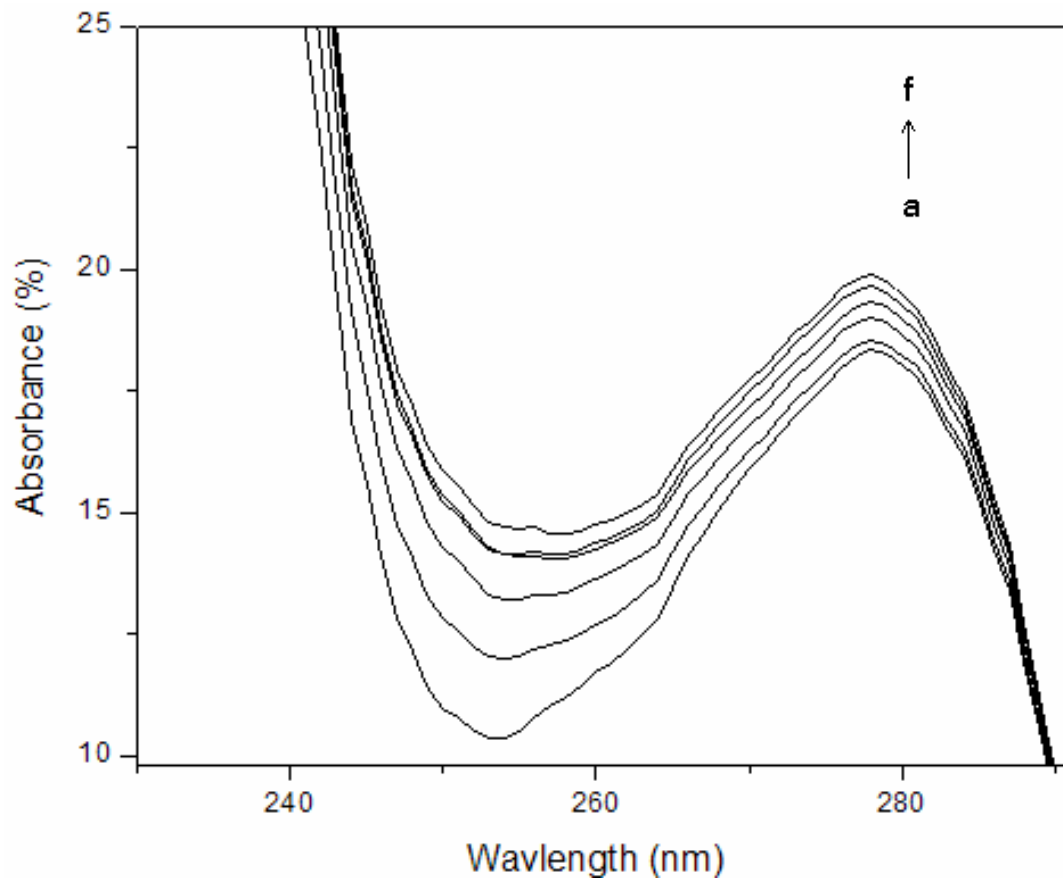


**Figure 4.1:** UV-Absorbance spectra of HSA with different molar ratios of progesterone (a=0:10, b=2:10, c=6:10, d=10:10, e=14:10, f=18:10).

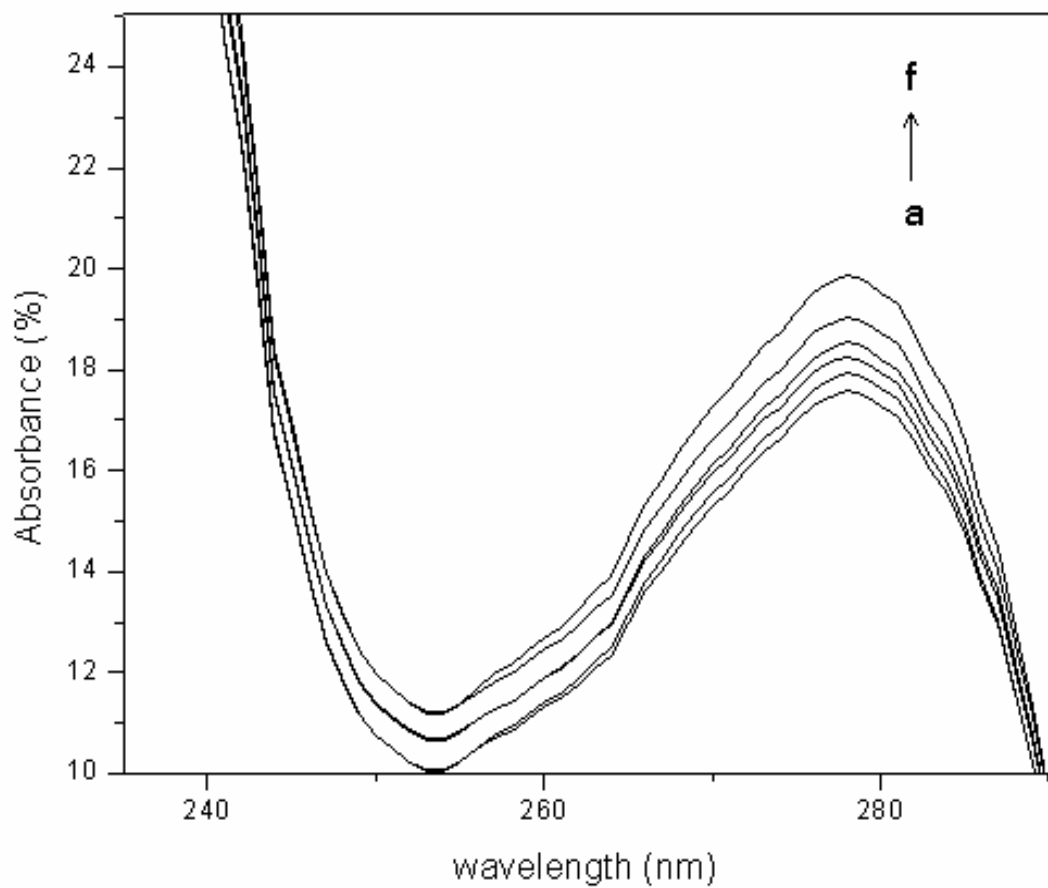
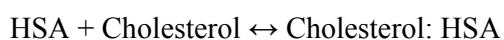


**Figure 4.2:** UV-Absorbance spectra of HSA with different molar ratios of cholesterol (a=0:10, b=2:10, c=6:10, d=10:10, e=14:10, f=18:10).

#### 4.1.1 Binding constants of progesterone or cholesterol and HSA complexes using UV-VIS Spectrophotometer.

The progesterone or cholesterol- HSA complexes binding constants were determined using UV-VIS spectrophotometer results according to published method (Stephanos, et al.,1996; Klotz, et al., 1971; Ouameur et al., 2004), by assuming that there is only one type of interaction between progesterone or cholesterol and HSA in aqueous solution, which leads to establish Equations. (1) and (2) as follows:



$$K = [\text{Progesterone:HSA}] / [\text{Progesterone}][\text{HSA}] \quad (2)$$

$$K = [\text{Cholesterol:HSA}] / [\text{Cholesterol}][\text{HSA}]$$

The absorption data were treated using linear double reciprocal plots based on the following equation (Lakowicz, 2006):

$$\frac{1}{A-A_0} = \frac{1}{A_\infty-A_0} + \frac{1}{K[A_\infty-A_0]} \times \frac{1}{L} \quad (3)$$

where  $A_0$  corresponds to the initial absorption of protein at 280 nm in the absence of ligand,  $A_\infty$  is the final absorption of the ligated protein, and  $A$  is the recorded absorption at different progesterone or cholesterol concentrations ( $L$ ). The double reciprocal plot of  $1/(A - A_0)$  vs.  $1/L$  is linear (Fig.(4.3) and (4.4)) and the binding constant ( $K$ ) can be estimated from the ratio of the intercept to the slope to be  $(6.354 \times 10^2 \text{M}^{-1})$  and  $(0.2641 \times 10^4 \text{M}^{-1})$  for progesterone- HSA and cholesterol- HSA complexes, respectively. The values obtained is indicative of a weak progesterone or cholesterol protein interaction with respect to the other drug-HSA complexes with binding constants in the range of  $10^5$  and  $10^6 \text{M}^{-1}$  (Kragh-Hanse, 1981). The reason for the low stability of the progesterone or cholesterol-HSA complexes can be attributed to the presence of mainly hydrogen bonding interaction between protein donor atoms and the progesterone or cholesterol polar groups or an indirect hormone- protein interaction through water molecules. Similar weak interactions were observed in *cis*-  $\text{Pt}(\text{NH}_3)_2$ -HSA and taxol-HSA complexes (Purcell et al., 2000; Neault, et al., 1998).

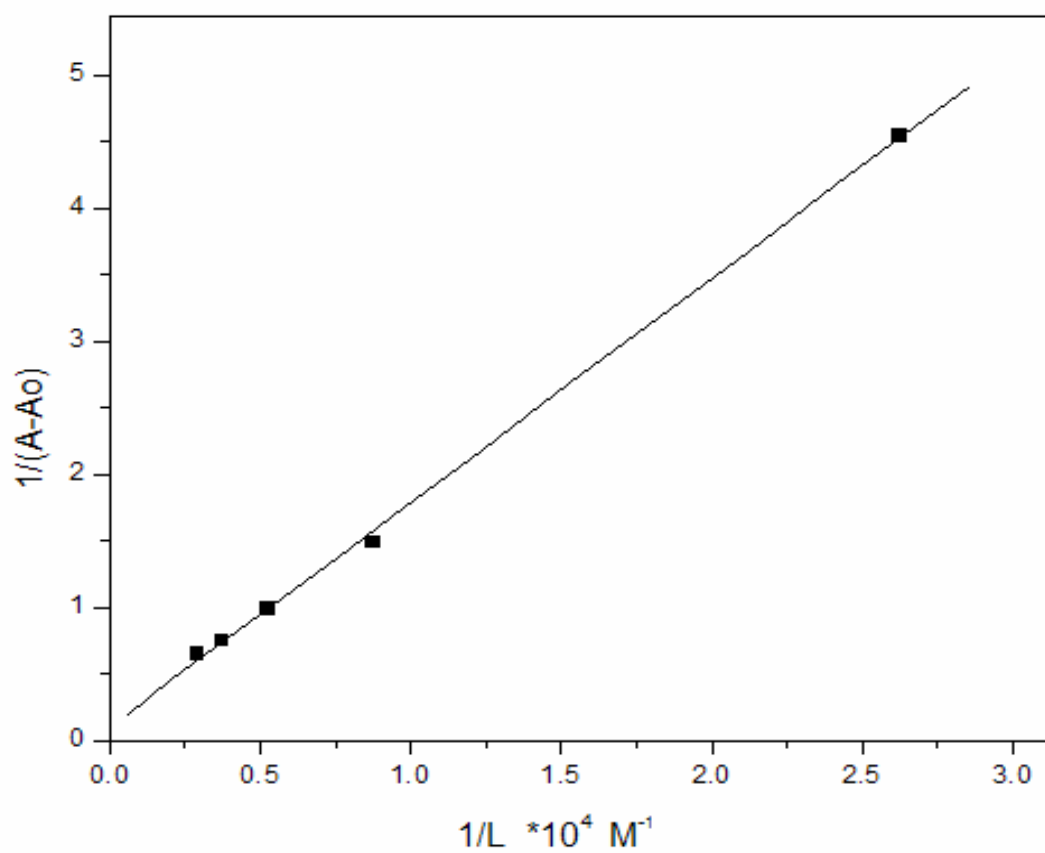


**Figure 4.3:** The plot of  $1/(A-A_0)$  vs  $1/L$  for HSA with different concentrations of progesterone.

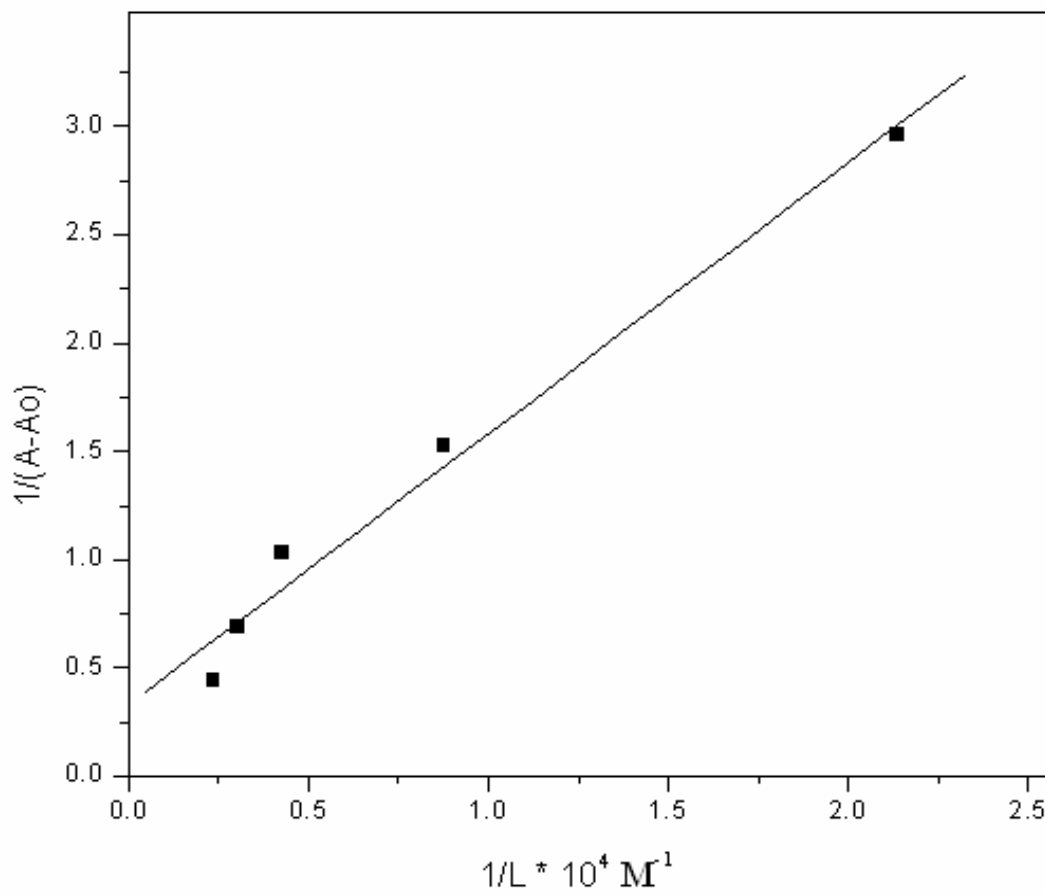


**Figure 4.4:** The plot of  $1/(A-A_0)$  vs  $1/L$  for HSA with different concentrations of cholesterol.

## **4.2 Fluorescence spectrophotometer.**

Fluorescence spectrophotometer is one of the most widely used spectroscopic techniques in the fields of biochemistry and molecular biophysics today (Royer, 1995). The auto fluorescence of HSA is attained mainly from the single tryptophan, tyrosine and phenylalanine residues. Actually, the intrinsic fluorescence of HSA is almost contributed by tryptophan alone, because phenylalanine has a very low quantum yield and the fluorescence of tyrosine is almost totally quenched if it is ionized or near an amino group, a carboxyl group or a tryptophan (Sulkowska, 2002).

In this work for both HSA-progesterone or cholesterol complexes excitation wavelength at 360nm was used, and the observed wavelength emission was at 439nm. The fluorescence sensor is based on intramolecular charge transfer (ICT), which is highly sensitive to the polarity of microenvironment. Therefore, it is expected to act as fluorescent probe for some biochemical systems like proteins (Tian et al., 2003).

The fluorescence quenching spectra of HSA at various percentage of progesterone or cholesterol are shown in Fig.(4.5) and Fig.(4.6), respectively. Obviously from the results, the fluorescence intensity of HSA gradually decreased while the peak position shows little or no change upon increasing the percentage of progesterone or cholesterol, indicating that both progesterone and cholesterol bind to HSA. Under the same condition, no fluorescence of progesterone or cholesterol was observed. Which indicates that both progesterone and cholesterol could quench the auto fluorescence of HSA, and that the interaction between both progesterone and cholesterol from one hand, and HSA from the other indeed exists, leading to a change in the microenvironment around the tryptophan residue and further exposure of tryptophan residue to the polar solvent (Petitpas et al., 2001; Wang. et al., 2007; Gerbanowski et al., 1999; Cui et al., 2008).

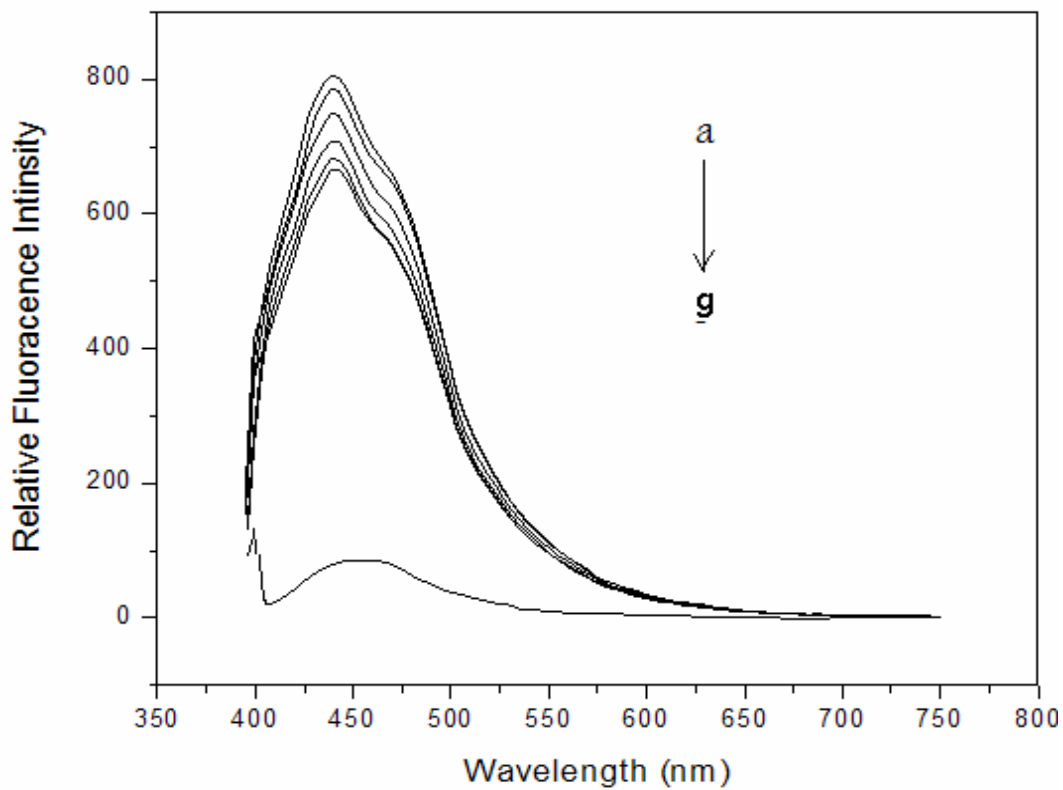


**Figure 4.5:** Fluorescence emission spectra of HSA in the absence and presence of progesterone in these ratios ( Prog:HSA a=0:10, b=2:10, c=6:10, d=10:10, e=14:10, f=18:10, g= free progesterone).

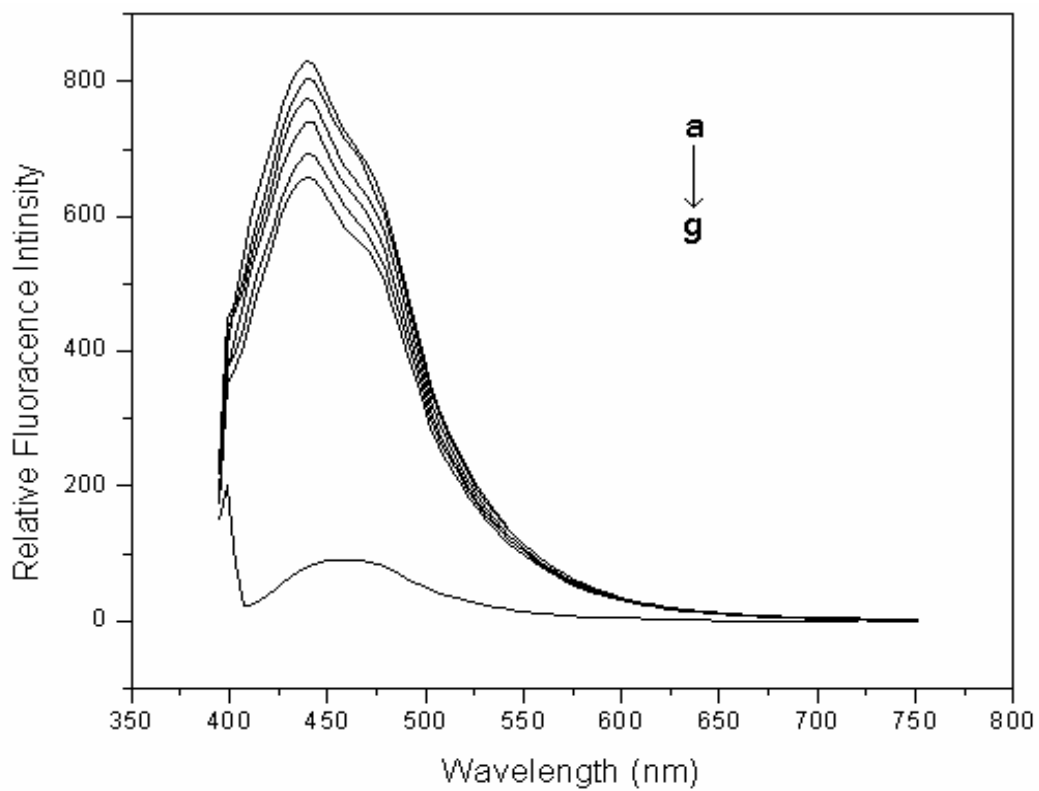


**Figure 4.6:** Fluorescence emission spectra of HSA in the absence and presence of cholesterol in these ratios ( chol:HSA a=0:10, b=2:10, c=6:10, d=10:10, e=14:10, f=18:10, g=free cholesterol)

#### 4.2.1 Stern-Volmer quenching constants ( $K_{sv}$ ) and the quenching rate constant of the biomolecule ( $K_q$ ).

Fluorescence quenching refers to any process, which decreases the fluorescence intensity of a sample (Lakowicz, 2006), a variety of molecular interactions can result in quenching, these include excited-state reactions, molecular rearrangements, energy transfer, ground-state complex formation, and collisional quenching (Peng et al., 2008). Fluorescence quenching can be induced by different mechanisms, usually classified into dynamic and static quenching (Cui et al., 2007).

As discussed in chapter two assuming dynamic quenching is dominating, then the decrease in intensity is described by the well-known Stern-Volmer equation:

$$\frac{F_0}{F} = 1 + K_q \tau_0 (L) = 1 + K_{sv} (L) \quad (4)$$

In this expression  $F$  and  $F_0$  are the fluorescence intensities with and without quencher,  $K_{sv}$  is the Stern-Volmer quenching constant,  $K_q$  is the bimolecular quenching constant,  $\tau_0$  is average lifetime of the biomolecule without quencher, and  $(L)$  is the quencher concentration. The Stern-Volmer quenching constant  $K_{sv}$  indicates the sensitivity of the fluorophore to a quencher.

Linear curves were plotted according to the Stern–Volmer equation as shown in Fig.(4.7) for progesterone- HSA complexes and Fig.(4.8) for cholesterol- HSA complexes. The Stern–Volmer quenching constant  $K_{sv}$  was obtained by the slope of the curves obtained in Fig. (4.7) and Fig.(4.8), and its value equals  $(6.26 \times 10^2 \text{ L mol}^{-1})$  for progesterone- HSA complexes and  $(6.21 \times 10^2 \text{ L mol}^{-1})$  for cholesterol- HSA complexes. Obviously from equation 4 the value of  $K_{sv} = K_q \tau_0$ , from which we can calculate the value of  $K_q$  using the fluorescence life time of  $10^{-8} \text{ s}$  for HSA (Cheng et al., 2006; Lakowica et al., 1973), to obtain  $K_q$  values of  $(6.20 \times 10^{10} \text{ L mol}^{-1} \text{ s}^{-1})$  for progesterone- HSA complexes and  $(6.21 \times 10^{10} \text{ L mol}^{-1} \text{ s}^{-1})$  for cholesterol- HSA complexes. Which is larger than the maximum dynamic quenching constant for various quenchers with biopolymer  $(2 \times 10^{10} \text{ L mol}^{-1} \text{ s}^{-1})$  (Lakowica et al., 1973; Eftink, 1991). Which implies that the quenching is not initiated by dynamic collision but from formation of a complex, so static quenching is dominant (Cui et al., 2007; Wang et al., 2008).

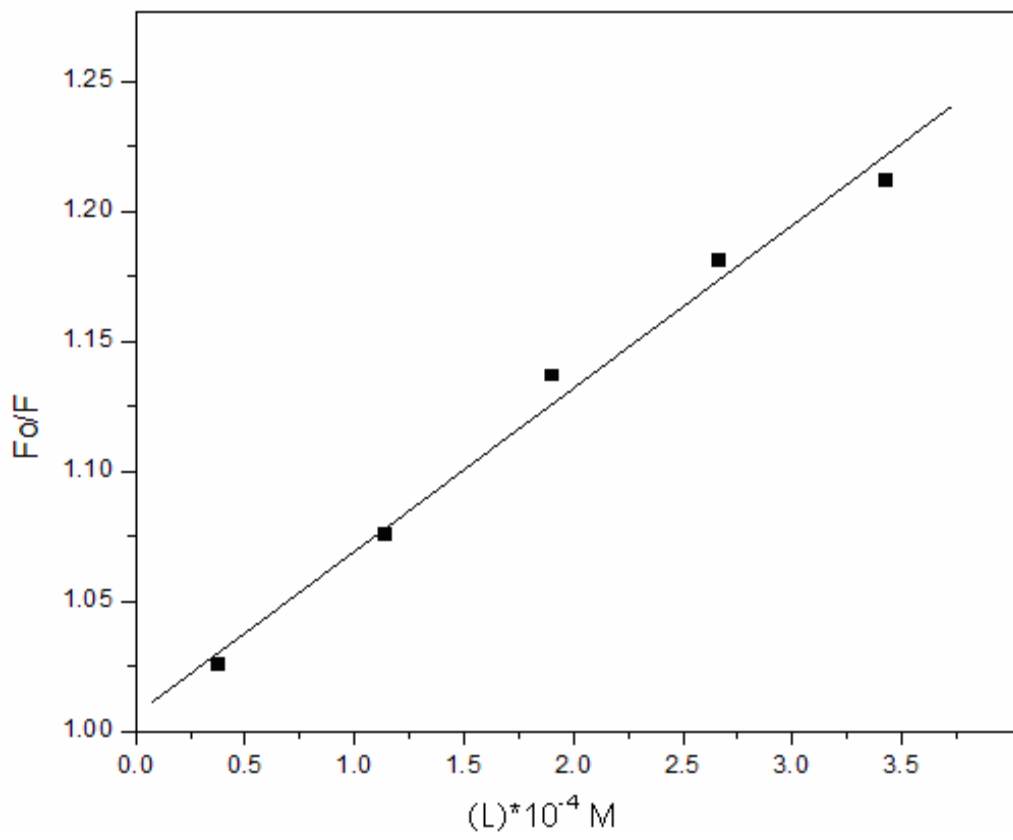


**Figure 4.7:** The Stern-Volmer plot for progesterone- HSA complexes.

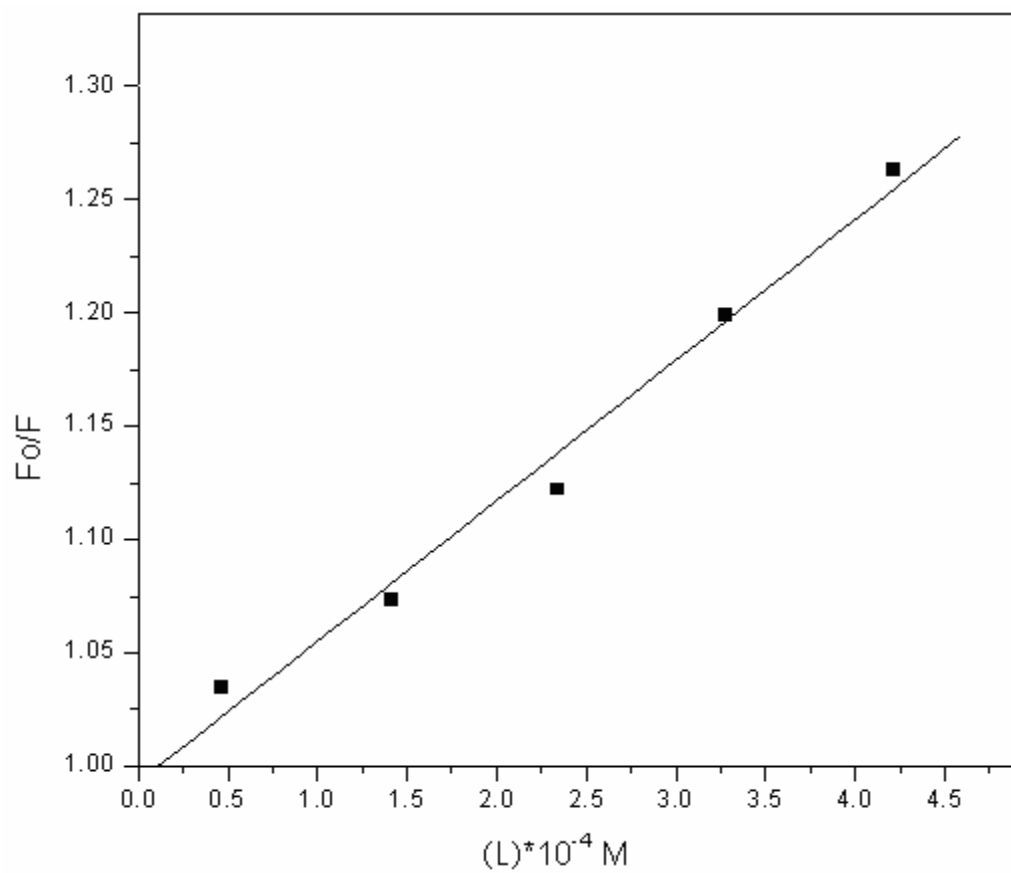


**Figure 4.8:** The Stern-Volmer plot for cholesterol- HSA complexes.

#### 4.2.2 Determination of the binding constant using fluorescence spectrophotometer.

When static quenching is dominant the modified Stern-Volmer equation could be used (Yang, et al., 1994):

$$\frac{1}{F_0 - F} = \frac{1}{F_0 K L} + \frac{1}{F_0} \quad (5)$$

Where K is the binding constant of progesterone or cholesterol with HSA, and can be calculated by plotting  $1/(F_0 - F)$  vs  $1/L$ , see Fig.(4.9) and Fig.(4.10). The value of K equals the ratio of the intercept to the slope. The obtained values of K equals  $(6.56 \times 10^2 \text{ M}^{-1})$  for progesterone- HSA complexes from Fig.(4.9), and  $(0.214 \times 10^4 \text{ M}^{-1})$  for cholesterol- HSA complexes from Fig.(4.10), which agrees well with the value obtained earlier by UV spectroscopy and supports the effective role of static quenching. The highly effective quenching constant in this case has led to a lower value of binding constant between the hormone or its parent compound and HSA, due to an effective hydrogen bonding between progesterone or cholesterol and HSA (Darwish et al., 2010).

The acting forces between a small molecule substance and macromolecule mainly include hydrogen bond, van der Waals force, electrostatic force and hydrophobic interaction force. It was more likely that hydrophobic and electrostatic interactions were involved in the binding process. However, progesterone or cholesterol might be largely unionized under the experimental conditions, as expected from its structure. Hence, electrostatic interaction could be precluded from the binding process. Thus, the binding of progesterone or cholesterol to HSA includes the hydrophobic interaction (Cui et al., 2008).

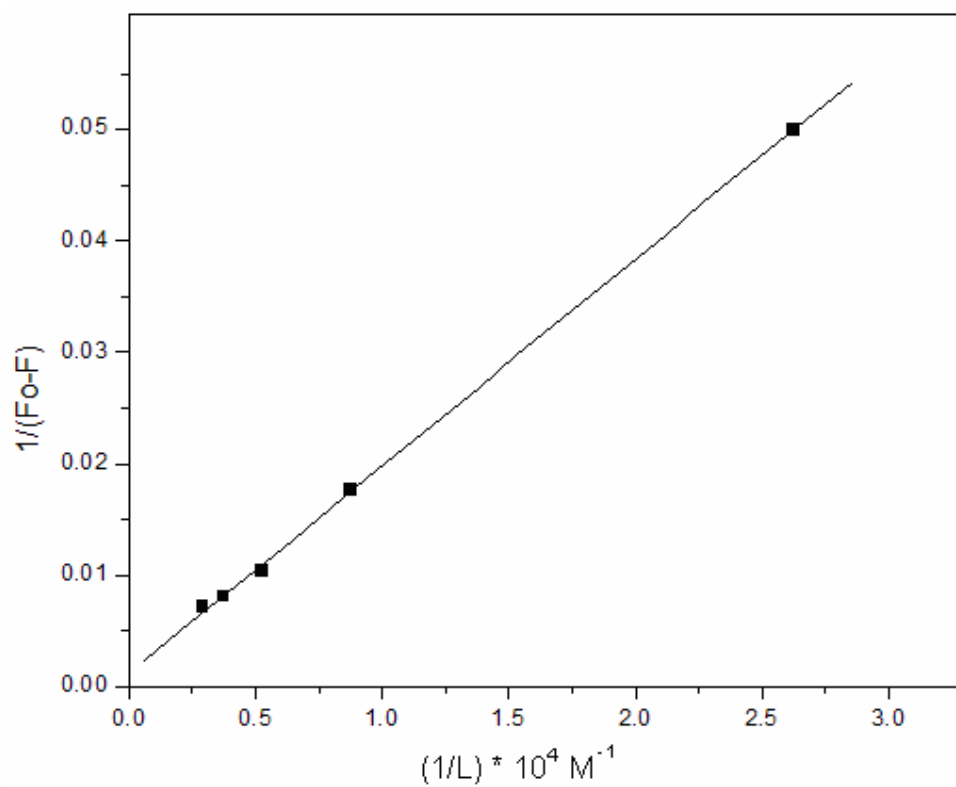


**Figure 4.9:** The plot of  $1/(F_o-F)$  vs  $(1/L) \times 10^4$  for progesterone- HSA complexes.

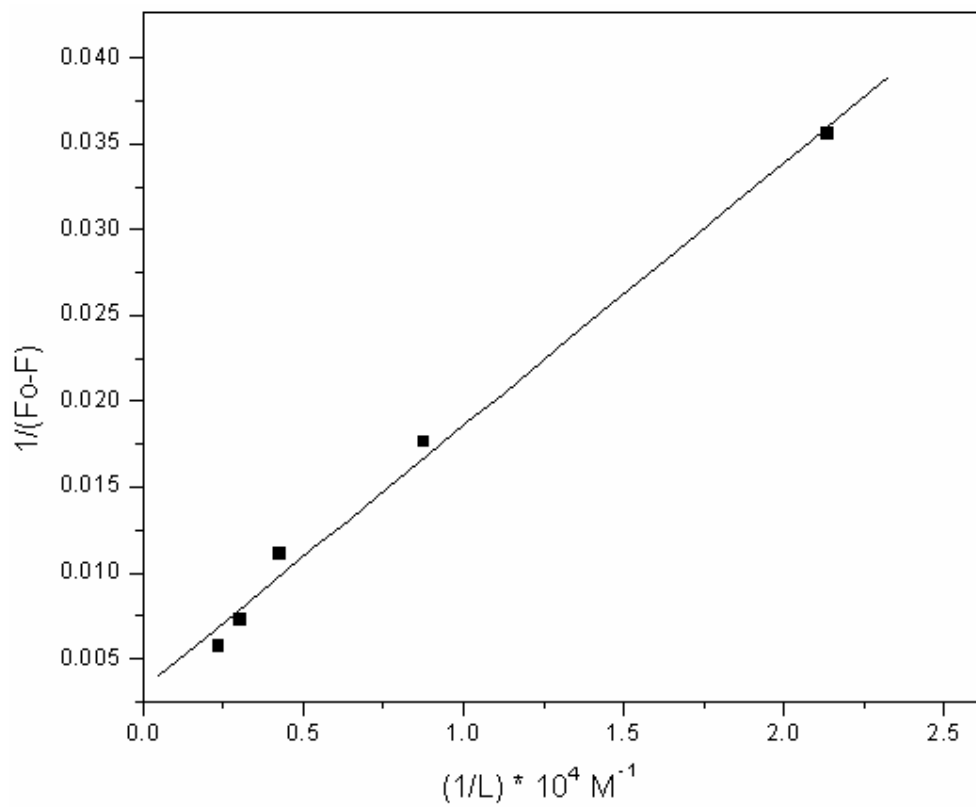


**Figure 4.10:** The plot of  $1/(F_0-F)$  vs  $(1/L) \times 10^4$  for cholesterol- HSA complexes.

### 4.3 FT-IR Spectroscopy.

FT-IR spectroscopy is a powerful technique for the study of hydrogen bonding (Li et al., 2006), and has been identified as one of the few techniques that is established in the determination of protein secondary structure at different physiological systems (Sirotkin, et al., 2001; Surewicz, et al., 1993; Arrondo, et al., 1993). The information on the secondary structure of proteins arises from the amide bands which is a result from the vibrations of the groups around the peptide bonds of proteins. When drugs bind to a globular protein like HSA, changes in hydrogen bonding which is involved in the peptide linkages would occur, resulting in changes in the vibrational frequency of the different amide modes (Ganim, et al., 2006; Haris et al., 1999).

The modes most widely used in protein structural studies are amide I, amide II and amide III. amide I band ranging from 1700 to 1600  $\text{cm}^{-1}$  and arises principally from the C=O stretching (Vandenbussche, et al., 1992), and has been widely accepted to be used (Workman, 1998). The amide II band is primarily N-H bending with a contribution from C-N stretching vibrations, amide II ranging from 1600 to 1480  $\text{cm}^{-1}$ . And amide III band ranging from 1330 to 1220  $\text{cm}^{-1}$  which is due to the C-N stretching mode coupled to the in-plane N - H bending mode. See Fig.(4.11) (Goormaghtigh, et al., 1990; Sirotkin, et al., 2001).

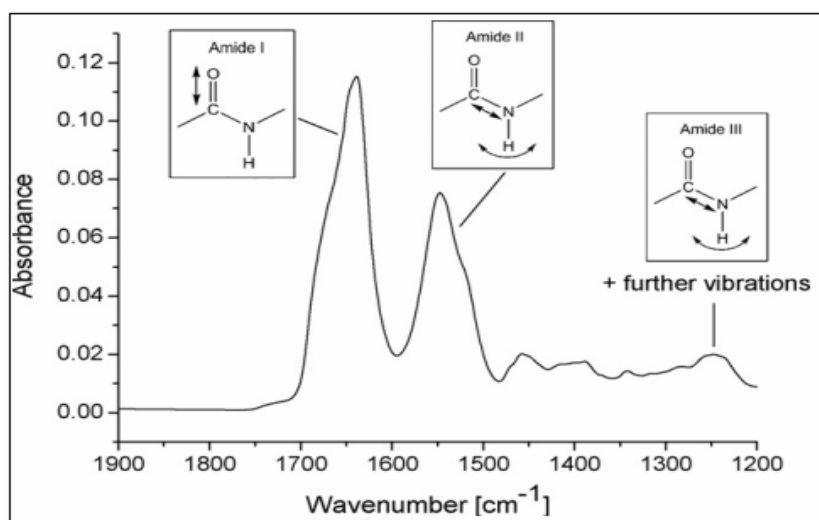


**Figure 4.11:** Sample spectrum showing the three relevant regions for determination of protein secondary structure. Amide I (1700-1600  $\text{cm}^{-1}$ ), amide II( 1600-1480  $\text{cm}^{-1}$ ) and amide III (1330-1220  $\text{cm}^{-1}$ ) (Vonhoff et al., 2010).

The second derivative of HSA free is shown in Fig.(4.12A) and Fig.(4.13A), where the spectra is dominated by absorbance bands of amide I and amide II at peak positions  $1656\text{cm}^{-1}$  and  $1543\text{cm}^{-1}$ , respectively. Fig.(4.12B), shows the spectrum of progesterone-HSA complexes with different percentages of progesterone, and Fig.(4.13B), shows the spectrum of cholesterol- HSA complexes with different percentages of cholesterol. It is obviously seen as progesterone or cholesterol ratios was increased the intensities of the amide I, amide II and amide III bands decreased further in the spectra of all progesterone-HSA and cholesterol- HSA complexes. The reduction in the intensity of the three amide bands is related to the progesterone- HSA and cholesterol- HSA interactions.

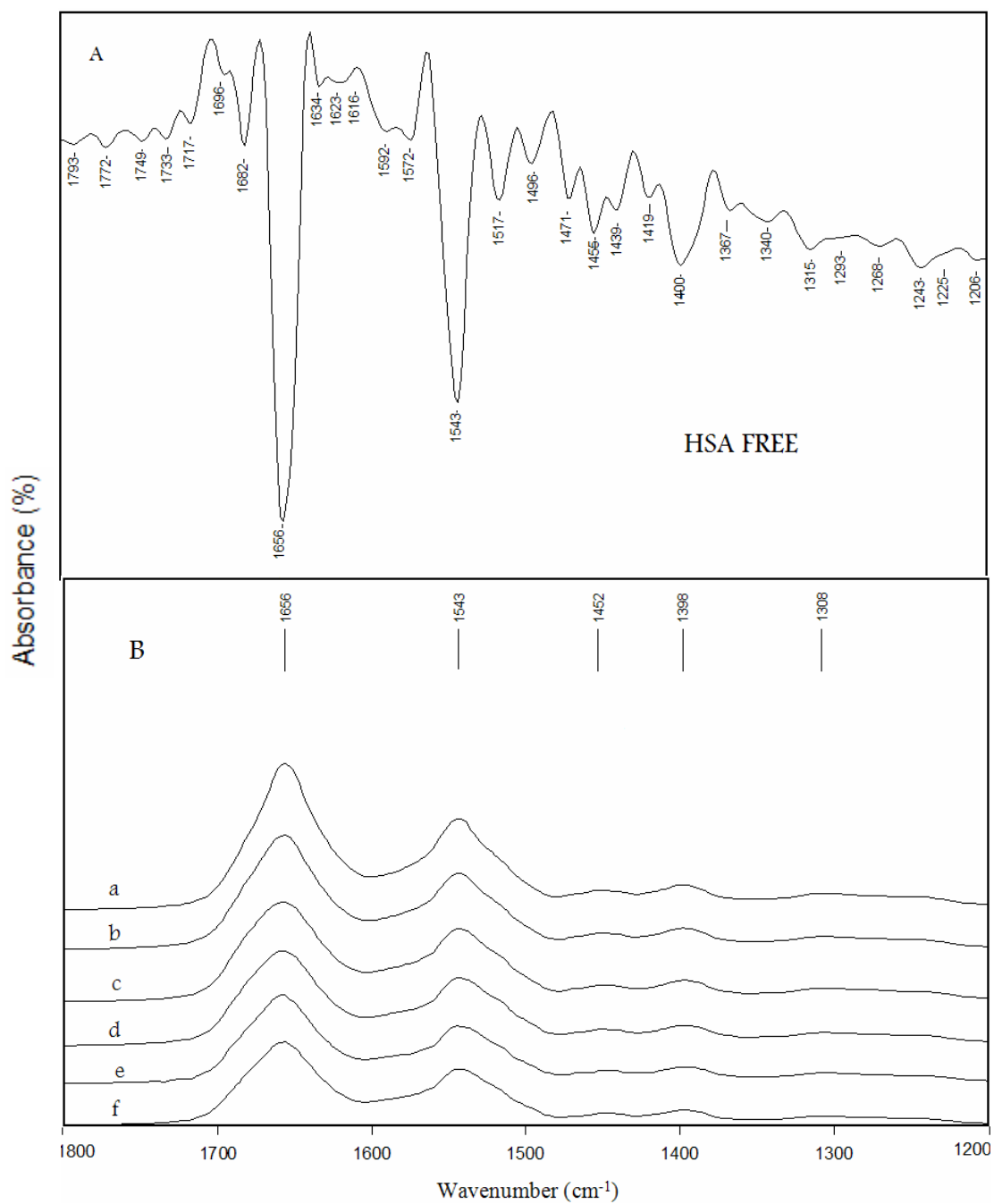


**Figure 4.12:** A: The spectra of HSA free (second derivative) And B: (a, b, c, d, e, f) Progesterone-HSA with ratios (0:10, 2:10, 6:10, 10:10, 14:10, 18:10), respectively.

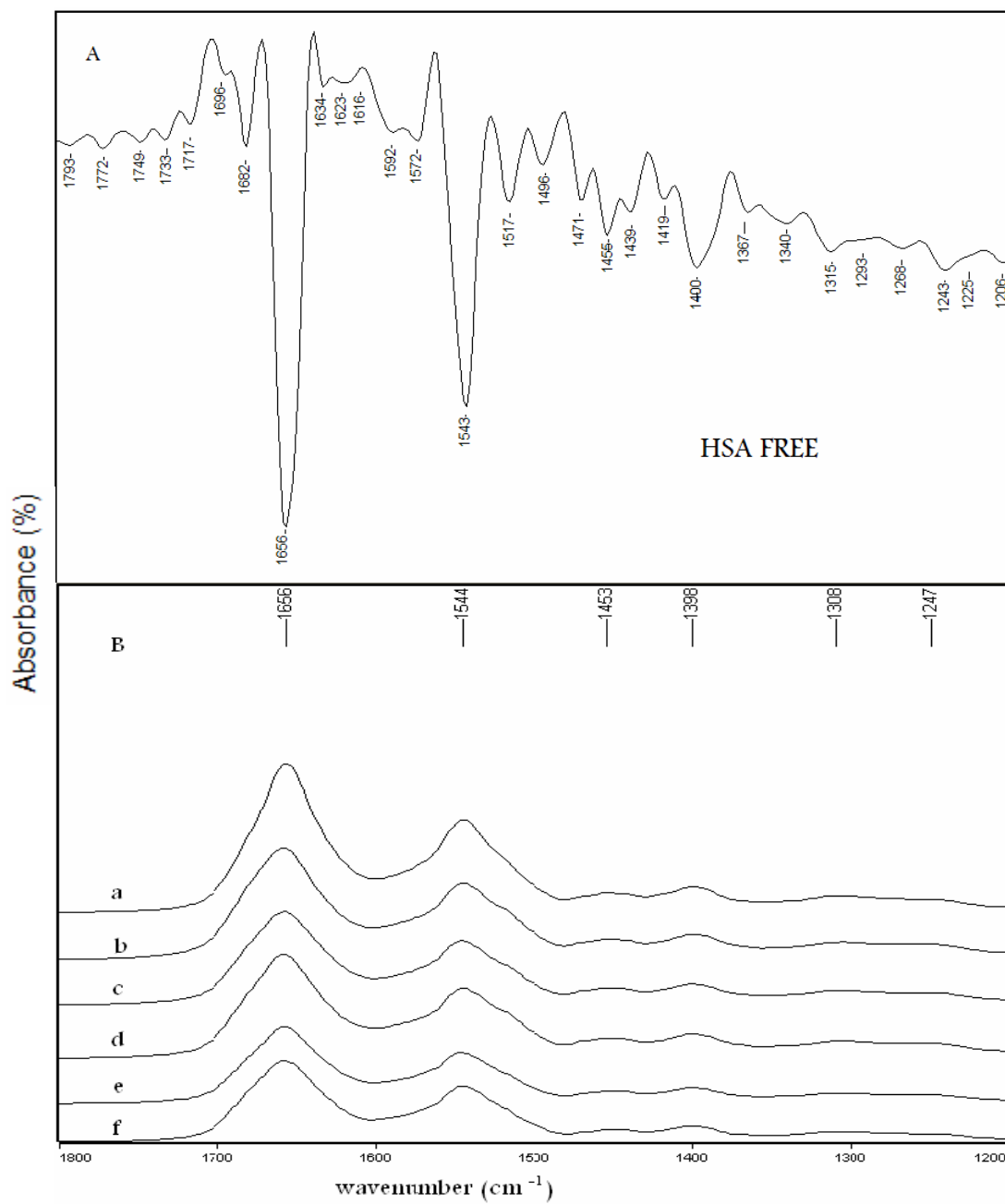


**Figure 4.13:** A: The spectra of HSA free (second derivative) And B: (a, b, c, d, e, f) Cholesterol-HSA with ratios (0:10, 2:10, 6:10, 10:10, 14:10, 18:10), respectively.

In Table (4.1) and Table (4.2) the peak positions of HSA with different ratios of progesterone or cholesterol are listed, respectively. For progesterone-HSA interaction the amide bands of HSA infrared spectrum shifted as listed in Table (4.1), for amide I band the peak positions have shifted as follows: 1616 to 1615 $\text{cm}^{-1}$ , 1634 to 1628 $\text{cm}^{-1}$ , 1656 to 1658 $\text{cm}^{-1}$ , 1682 to 1681 $\text{cm}^{-1}$ , and 1696 to 1692 $\text{cm}^{-1}$ . Also a peak at 1623 $\text{cm}^{-1}$  has disappeared after the interaction of progesterone with HSA. In amide II the peak positions have shifted as follows: 1496 to 1498 $\text{cm}^{-1}$ , 1517 to 1516 $\text{cm}^{-1}$ , 1543 to 1548 $\text{cm}^{-1}$ , 1572 to 1569 $\text{cm}^{-1}$ , and 1592 to 1596 $\text{cm}^{-1}$ . In addition a new peak at 1584 $\text{cm}^{-1}$  appeared after the interaction of progesterone with HSA. In amide III region the peak positions have also been shifted in the following order: 1225 to 1226 $\text{cm}^{-1}$ , 1243 to 1241 $\text{cm}^{-1}$ , 1268 to 1266 $\text{cm}^{-1}$ , and 1315 to 1311 $\text{cm}^{-1}$ . In addition a new peak has appeared at high molecular ratios of progesterone at 1276 $\text{cm}^{-1}$ , also a peak at 1293 $\text{cm}^{-1}$  has disappeared after the interaction of progesterone with HSA.

For cholesterol-HSA interaction the amide bands of HSA infrared spectrum shifted as listed in Table (4.2), for amide I band the peak positions have shifted as follows: 1616 to 1614 $\text{cm}^{-1}$ , 1623 to 1628 $\text{cm}^{-1}$ , 1656 to 1657 $\text{cm}^{-1}$ , 1682 to 1681 $\text{cm}^{-1}$ , and 1696 to 1692 $\text{cm}^{-1}$ . Also a peak at 1634 $\text{cm}^{-1}$  has disappeared after the interaction of cholesterol with HSA. In amide II the peak positions have shifted as follows: 1496 to 1497 $\text{cm}^{-1}$ , 1517 to 1515 $\text{cm}^{-1}$ , 1543 to 1549 $\text{cm}^{-1}$ , 1572 to 1569 $\text{cm}^{-1}$ , and 1592 to 1596 $\text{cm}^{-1}$ . In addition a new peak at 1584 $\text{cm}^{-1}$  appeared after the interaction of cholesterol with HSA. In amide III region the peak positions have also been shifted in the following order: 1268 to 1269 $\text{cm}^{-1}$ , 1293 to 1296 $\text{cm}^{-1}$ , and 1315 to 1313 $\text{cm}^{-1}$ . In addition a peak at 1225 $\text{cm}^{-1}$  has disappeared, and a peak at 1243 $\text{cm}^{-1}$  remains unchanged after the interaction of cholesterol with HSA.

The shifts in peak positions and shape of HSA amides after progesterone or cholesterol complexation with HSA come from the changes in protein secondary structure. The minor changes in peak positions can be attributed to the effect of the newly imposed H-bonding between the hormone and its parent compound (cholesterol) molecules with the protein. It is suggested that, the shift to a higher frequency for the major peak in amide I region (1656–1658 $\text{cm}^{-1}$ ) for progesterone- HSA complexes and (1656-1657 $\text{cm}^{-1}$ ) for cholesterol-HSA complexes came as a result of stabilization by hydrogen bonding by having the C–N bond assuming partial double bond character due to a flow of electrons from the C=O to the C–N bond (Jackson, et al., 1991).

**Table 4.1:** Band assignment in the absorbance spectra of HSA with different progesterone molecular ratios for amide I, amide II, and amide III regions

Bands	HSA free	Prog:HSA	Prog:HSA	Prog:HSA	Prog:HSA	Prog:HSA
		2:10	6:10	10:10	14:10	18:10
Amide I (1700-1600)	1616	1616	1615	1613	1612	1615
	1623					
	1634	1632	1630	1627	1627	1628
	1656	1654	1653	1658	1659	1658
	1682	1682	1682	1680	1679	1681
	1696	1692	1691	1691	1691	1692
Amide II (1600-1480)	1496	1497	1497	1498	1498	1498
	1517	1516	1515	1515	1515	1516
	1543	1546	1548	1548	1549	1548
	1572	1572	1570	1569	1567	1569
			1589	1586	1584	1584
	1592	1594	1595	1595	1596	1596
Amide III (1330-1220)	1225	1226	1226	1226	1226	1226
	1243	1243	1243	1242	1241	1241
	1268	1269	1269	1267	1266	1266
					1276	1276
	1293					
	1315	1314	1313	1312	1311	1311

**Table 4.2:** Band assignment in the absorbance spectra of HSA with different cholesterol molecular ratios for amide I, amide II, and amide III regions

<b>Bands</b>	HSA free	Chol:HSA	Chol:HSA	Chol:HSA	Chol:HSA	Chol:HSA
		2:10	6:10	10:10	14:10	18:10
Amide I (1700-1600)	1616	1613	1611	1612	1616	1614
	1623	1626	1626	1627	1627	1628
	1634					
	1656	1655	1657	1657	1658	1657
	1682	1682	1681	1681	1681	1681
	1696	1693	1692	1693	1693	1692
Amide II (1600-1480)	1496	1497	1497	1496	1497	1497
	1517	1515	1514	1514	1515	1515
	1543	1547	1548	1548	1549	1549
	1572	1571	1570	1570	1570	1569
		1582	1582	1582	1589	1584
	1592	1595	1595	1595	1595	1596
Amide III (1330-1220)	1225					
	1243	1243	1243	1243	1243	1243
	1268	1270	1269	1269	1268	1269
	1293	1298	1298	1297	1297	1296
	1315	1314	1313	1315	1314	1313

The difference spectra for [(HSA + progesterone or cholesterol) - (HSA)] were obtained in order to monitor the intensity variations of these vibrations; the results are shown in Figures 4.14, 4.15, 4.16, 4.17. The results for progesterone- HSA interactions are illustrated in Fig.(4.14) for FT-IR spectra (top two curves) and difference spectra of HSA and its complexes with different progesterone percentages in amide I and amide II regions, and Fig.(4.15) for FT-IR spectra (top two curves) and difference spectra of HSA and its complexes with different progesterone percentages in amide III region. In amide I region clearly there is a strong negative feature at  $1656\text{cm}^{-1}$ , and in amide II region one negative feature was also observed at  $1544\text{cm}^{-1}$ (Fig.(4.14)). For amide III region two negative feature was observed at  $1248\text{cm}^{-1}$  and at  $1310\text{cm}^{-1}$  with a little shift as progesterone ratios was increased, another two weak negative features was observed at  $1270\text{cm}^{-1}$  and  $1301\text{cm}^{-1}$  also with a little shift as the ratios of progesterone was increased (Fig.(4.15)).

For cholesterol-HSA interaction the results are illustrated in Fig.(4.16) for FT-IR spectra (top two curves) and difference spectra of HSA and its complexes with different cholesterol percentages in amide I and amide II regions, and Fig.(4.17) for FT-IR spectra (top two curves) and difference spectra of HSA and its complexes with different cholesterol percentages in amide III region. In amide I region clearly there is a strong negative feature at  $1654\text{cm}^{-1}$  with a little shift in its position, and in amide II region one negative feature was also observed at  $1543\text{cm}^{-1}$  also with a little shift in its position (Fig.(4.16)). For amide III region two negative feature was observed at  $1245\text{cm}^{-1}$  and at  $1311\text{cm}^{-1}$  with a little shift in their positions as cholesterol ratios was increased, another weak negative feature was observed at  $1287\text{cm}^{-1}$  at low cholesterol concentration and disappeared as the molecular ratio of cholesterol was increased (Fig.(4.17)).

It is clearly shown that the strong negative features in the difference spectra became stronger as percentages of progesterone or cholesterol were increased with a little shift in their positions, which are attributed to the intensity decrease in the amide I, II and III bands in the spectra of the progesterone- HSA and cholesterol- HSA complexes, that is due to the interaction (H bonding) of the progesterone or cholesterol with protein C=O and C-N groups, and the reduction of the proteins  $\alpha$ -helix structure upon progesterone or cholesterol-HSA interaction (Purcell, et al., 2000; Krimm, et al., 1986).

The band at  $1523\text{ cm}^{-1}$  of the free HSA, related to the tyrosine amino acid side-chain vibration (Fabian et al., 1994; Yamamoto et al., 1991; Matsuura, et al., 1986; Goormaghtigh, et al., 1990), exhibited no spectral changes upon progesterone or cholesterol complexation, which is indicative of no perturbation of the tyrosine residue in the progesterone or cholesterol–HSA complexes.

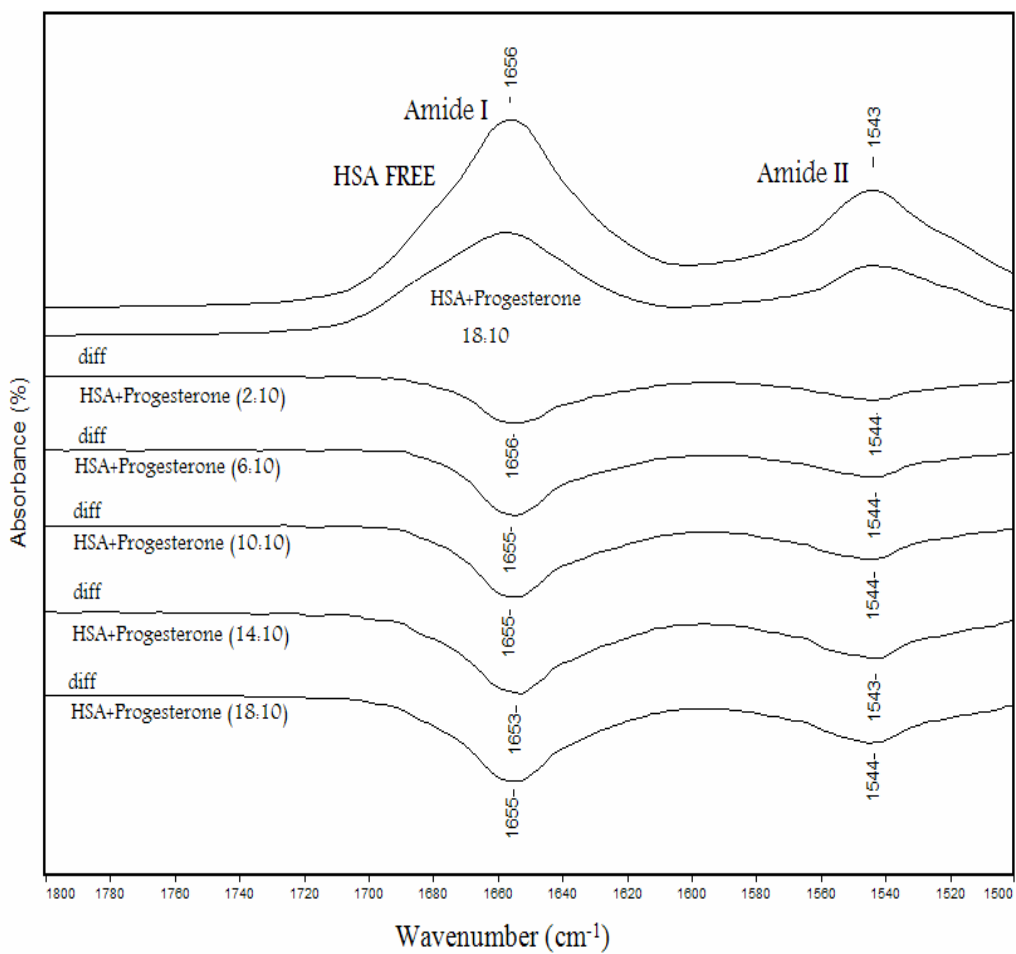


**Figure 4.14:** FT-IR spectra (top two curves) and difference spectra of HSA and its complexes with different progesterone concentrations in the region 1800-1500 cm<sup>-1</sup>

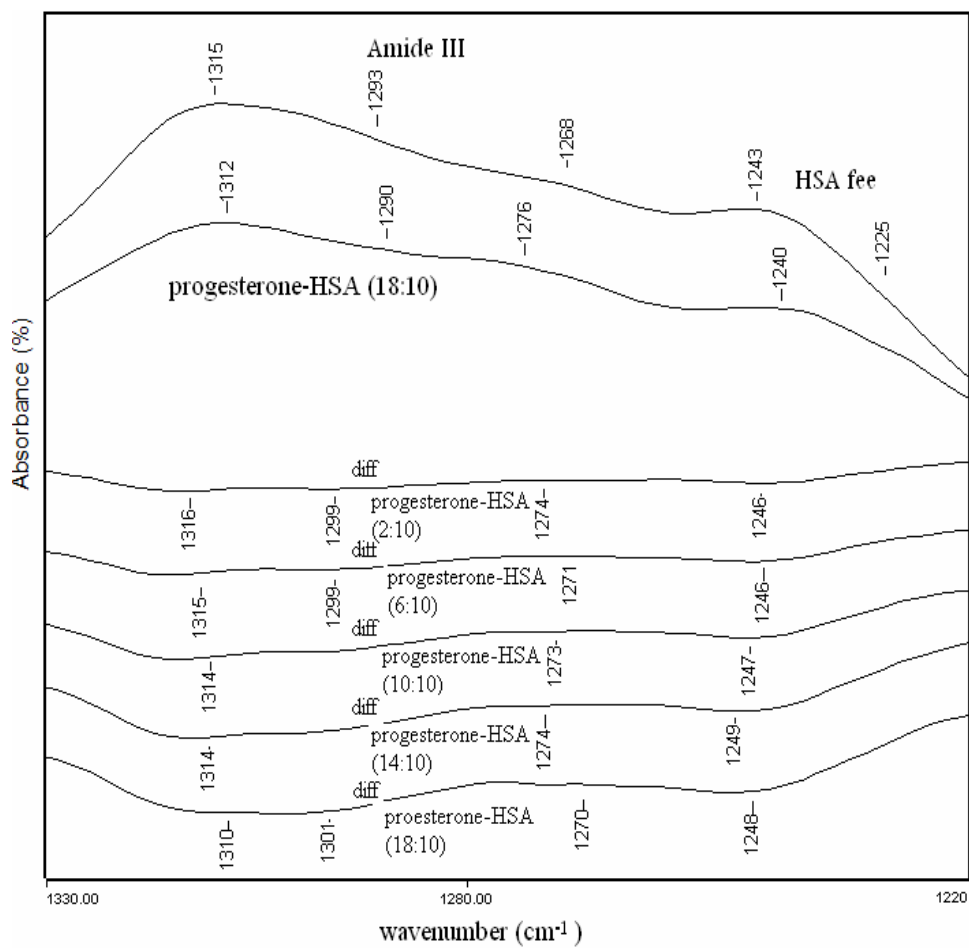


**Figure 4.15:** FT-IR spectra (top two curves) and difference spectra of HSA and its complexes with different progesterone concentrations in the region of 1330- 1220  $\text{cm}^{-1}$ .

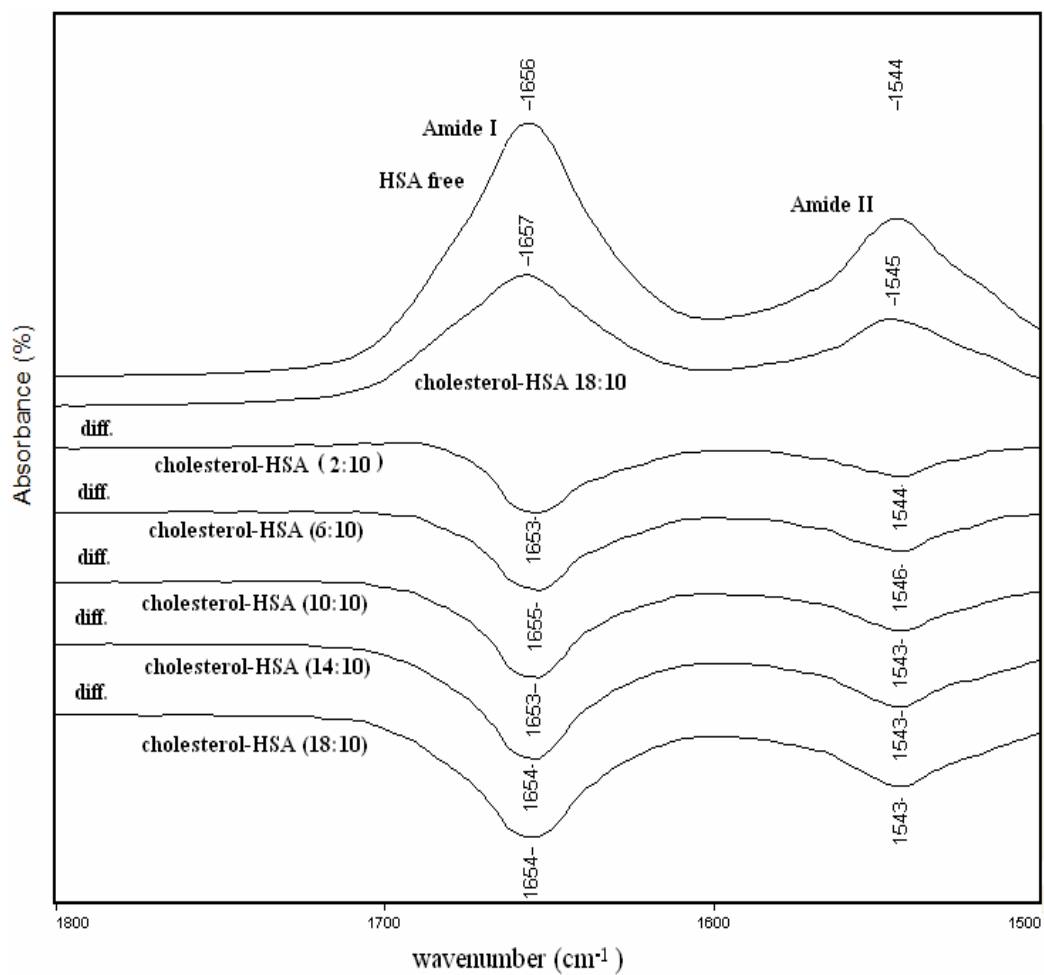


**Figure 4.16:** FT-IR spectra (top two curves) and difference spectra of HSA and its complexes with different cholesterol concentrations in the region 1800-1500  $\text{cm}^{-1}$ .

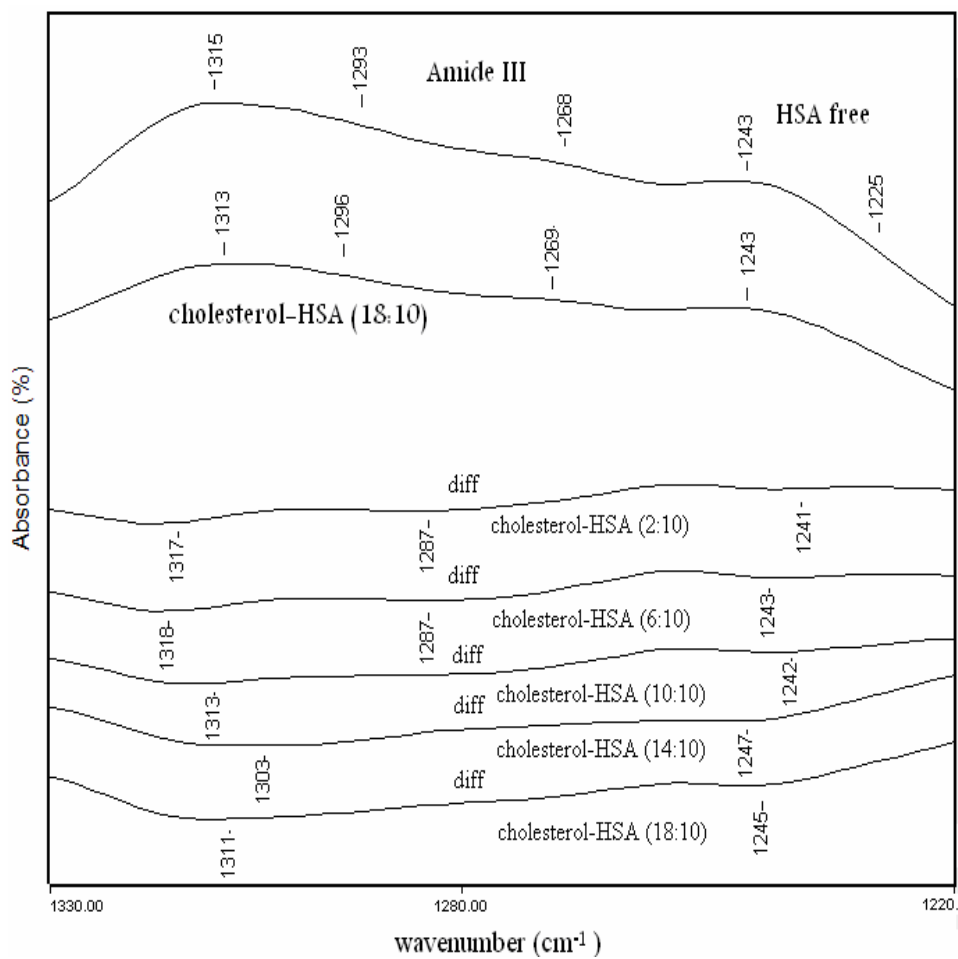


**Figure 4.17:** FT-IR spectra (top two curves) and difference spectra of HSA and its complexes with different cholesterol concentrations in the region of 1330- 1220 cm<sup>-1</sup>.

Determination of the secondary structure of HSA and its progesterone or cholesterol complexes was carried out on the basis of the procedure described by Byler and Susi (Byler, et al., 1986). In this work, a quantitative analysis of the protein secondary structure for the free HSA and progesterone or cholesterol– HSA complexes in dehydrated films is determined from the shape of Amide I, amide II and amide III bands. Infrared Fourier self-deconvolution with second derivative resolution and curve fitting procedures, were applied to increase spectral resolution and therefore to estimate the number, position and area of each component bands. The procedure was in general carried out considering only components detected by second derivatives and the half widths at half height (HWHH) for the component peaks are kept around  $5\text{cm}^{-1}$ , the above procedure was reported in a recent publication (Darwish et al., 2010).

The component bands of amide I, II, and III regions were assigned to a secondary structure according to the frequency of its maximum a raised after Fourier self deconvolution have been applied; for amide I band ranging from  $1610$  to  $1700\text{cm}^{-1}$  assigned as follows:  $1610$ – $1624\text{cm}^{-1}$  are generally represented to  $\beta$ -sheet,  $1625$ – $1640\text{cm}^{-1}$  to random coil,  $1646$ – $1671\text{cm}^{-1}$  to  $\alpha$ -helix,  $1672$ – $1787\text{cm}^{-1}$  to turn structure, and  $1689$ – $1700\text{cm}^{-1}$  to  $\beta$ -antiparallel. For amide II ranging from  $1480$  to  $1600\text{cm}^{-1}$ , the absorption band assigned in the following order:  $1488$ – $1504\text{cm}^{-1}$  to  $\beta$ -sheet,  $1508$ – $1523\text{cm}^{-1}$  to random coil,  $1528$ – $1560\text{cm}^{-1}$  to  $\alpha$ -helix,  $1562$ – $1585\text{cm}^{-1}$  to turn structure, and  $1585$ – $1598\text{cm}^{-1}$  to  $\beta$ -antiparallel. And for amide III ranging from  $1220$  to  $1330\text{cm}^{-1}$  have been assigned as follows:  $1220$ – $1256\text{cm}^{-1}$  to  $\beta$ -sheet,  $1257$ – $1285\text{cm}^{-1}$  to random coil,  $1287$ – $1301\text{cm}^{-1}$  to turn structure, and  $1302$ – $1329\text{cm}^{-1}$  to  $\alpha$ -helix. Most investigations have concentrated on Amide I band assuming higher sensitivity to the change of protein secondary structure (Vass, et al., 1997). However, it has been reported that amide II and amide III bands has high information content and could be used for prediction of proteins secondary structure (Oberg et al., 2004; Jiang et al., 2004; Xie et al., 2003; Liu, et al., 2003).

Based on the above assignments, the percentages of each secondary structure of HSA were calculated by integrated areas of the component bands in amide I, amide II and amide III then summed and divided by the total area. The obtained number is taken as the proportion of the polypeptide chain in that conformation.

The Secondary structure determination for the free HSA and its progesterone or cholesterol complexes, are given in (Table (4.3), and Table (4.4)). The second derivative resolution enhancement and curve – fitted Amide I, Amide II, and Amide III regions and secondary structure determinations of the free human serum albumin (A, B) and its progesterone or cholesterol complexes (C, D) with the highest percentage of progesterone or cholesterol in dehydrated films are shown in (Fig. (4.18), Fig.(4.19), Fig.(4.20), Fig.(4.21), Fig.(4.22), and Fig.(4.23)).

Table (4.3) and Table (4.4) shows the content of each secondary structure of HSA before and after the interaction with progesterone or cholesterol at different ratios, respectively. It is obviously seen that  $\alpha$ -helix percentage decrease with the increase of progesterone or cholesterol ratios in the calculations, and this trend is consistent in the three Amide regions.

For progesterone- HSA interaction: in amide I region HSA free consists of (17%)  $\beta$ -sheet, (8%) random coil, (57%)  $\alpha$ -helical structure, and (18%) turn structure. After progesterone-HSA complexation, see Fig.(4.18) and Table (4.3),  $\alpha$ -helical structure reduced from 57% to 49%,  $\beta$ -sheet increased from 17% to 34%, turn structure reduced from 18% to 15%, and the random coil reduced from 8% to 2%. In amide II region HSA free consists of (25%)  $\beta$ -Sheet, (7%) random coil, (53%)  $\alpha$ -helical structure, and (15%) turn structure. After progesterone- HSA interaction, see Fig.(4.19) and Table (4.3),  $\alpha$ -helical structure reduced from 53% to 43%,  $\beta$ -sheet increased from 25% to 33%, turn structure reduced from 15% to 14%, and the random coil increased from 7% to 10%. And in amide III region HSA free consists of (40%)  $\beta$ -Sheet, (8%) random coil, (46%)  $\alpha$ -helical structure, and (6%) turn structure. After progesterone- HSA interaction, see Fig.(4.20) and Table (4.3),  $\alpha$ -helical structure reduced from 46% to 41%,  $\beta$ -sheet increased from 40% to 45%, turn structure reduced from 6% to 4%, and the random coil increased from 8% to 10%.

For cholesterol- HSA interaction: in amide I region HSA free consists of (17%)  $\beta$ -sheet, (8%) random coil, (57%)  $\alpha$ -helical structure, and (18%) turn structure. After cholesterol-HSA complexation, see Fig.(4.21) and Table (4.4),  $\alpha$ -helical structure reduced from 57% to 53%,  $\beta$ -sheet increased from 17% to 29%, turn structure reduced from 18% to 17%, and the random coil reduced from 8% to 1%. In amide II region HSA free consists of (25%)  $\beta$ -Sheet, (7%) random coil, (53%)  $\alpha$ -helical structure, and (15%) turn structure. After

cholesterol- HSA interaction, see Fig.(4.22) and Table (4.3),  $\alpha$ -helical structure reduced from 53% to 43%,  $\beta$ -sheet increased from 25% to 30%, turn structure increased from 15% to 16%, and the random coil increased from 7% to 11%. And in amide III region HSA free consists of (40%)  $\beta$ -Sheet, (8%) random coil, (46%)  $\alpha$ -helical structure, and (6%) turn structure. After cholesterol- HSA interaction, see Fig.(4.23) and Table (4.3),  $\alpha$ -helical structure reduced from 46% to 38%,  $\beta$ -sheet increased from 40% to 46%, turn structure remained the same without changes, and the random coil increased from 8% to 10%.

The reduction of  $\alpha$ -helix intensity percentage in favor of the increase of  $\beta$ -sheets are believed to be due to the unfolding of the protein in the presence of progesterone or cholesterol as a result of the formation of H bonding between HSA and the hormone or hormone parent compound. The newly formed H-bonding result in the C–N bond assuming partial double bond character due to a flow of electrons from the C=O to the C–N bond which decreases the intensity of the original vibrations (Jackson, et al., 1991). as discussed in chapter two the hydrogen bonds in  $\alpha$ -helix are formed inside the helix and parallel to the helix axis, while for  $\beta$ -sheet the hydrogen bonds take position in the planes of  $\beta$ -sheets as the preferred orientations especially in the anti-parallel sheets, so the restrictions on the formation of hydrogen bonds in  $\beta$ -sheet relative to the case in  $\alpha$ -helix explains the larger effect on reducing the intensity percentage of  $\alpha$ -helix to that of  $\beta$ -sheet. Similar conformational transitions from an  $\alpha$ -helix to  $\beta$ -sheet structure were observed for the protein unfolding upon protonation and heat denaturatio (Surewicz, et al., 1987; Holzbour, et al., 1996).

**Table 4.3:** Secondary structure determination for Amide I, amide II, and amide III regions in HSA and its Progesterone complexes.

<b>2<sup>nd</sup> Structure</b>	HSA	HSA-Prog	HSA-Prog	HSA-Prog	HSA-Prog	HSA-Prog
	free(%)	2:10(%)	6:10(%)	10:10(%)	14:10(%)	18:10(%)
<b>Amide I</b>						
$\beta$ -sheets (cm <sup>-2</sup> ) (1610-1624) (1689-1700)	17	31	31	30	30	34
Random(cm <sup>-2</sup> ) (1625-1640)	8	3	4	4	3	2
$\alpha$ -hilex (cm <sup>-2</sup> ) (1646-1669)	57	51	49	52	53	49
Turn (cm <sup>-2</sup> ) (1672-1687)	18	15	15	14	16	15
<b>Amide II</b>						
$\beta$ -sheets (cm <sup>-2</sup> ) (1488-1504) (1585-1598)	25	30	33	32	33	33
Random(cm <sup>-2</sup> ) (1508-1523)	7	10	11	10	10	10
$\alpha$ -hilex (cm <sup>-2</sup> ) (1528-1560)	53	46	43	45	43	43
Turn (cm <sup>-2</sup> ) (1562-1585)	15	14	13	13	14	14
<b>Amide III</b>						
$\beta$ -sheets (cm <sup>-2</sup> ) (1220-1256)	40	41	41	46	44	45
Random(cm <sup>-2</sup> ) (1257-1285)	8	9	13	7	11	10
Turn (cm <sup>-2</sup> ) (1287-1301)	6	6	3	4	4	4
$\alpha$ -hilex (cm <sup>-2</sup> ) (1302-1329)	46	44	43	43	41	41

**Table 4.4:** Secondary structure determination for Amide I, amide II, and amide III regions in HSA and its Cholesterol complexes.

<b>2<sup>nd</sup> Structure</b>	HSA free(%)	chol -HSA 2:10(%)	chol -HSA 6:10(%)	chol -HSA 10:10(%)	chol -HSA 14:10(%)	chol -HSA 18:10(%)
<b>Amide I</b>						
$\beta$ -sheets (cm <sup>-2</sup> ) (1610-1624) (1687-1700)	17	23	23	25	26	29
Random(cm <sup>-2</sup> ) (1625-1640)	8	4	3	2	1	1
$\alpha$ -hilex (cm <sup>-2</sup> ) (1643-1671)	57	57	57	56	55	53
Turn (cm <sup>-2</sup> ) (1672-1687)	18	16	17	17	18	17
<b>Amide II</b>						
$\beta$ -sheets (cm <sup>-2</sup> ) (1488-1504) (1585-1598)	25	29	28	29	32	30
Random(cm <sup>-2</sup> ) (1508-1523)	7	12	13	12	9	11
$\alpha$ -hilex (cm <sup>-2</sup> ) (1525-1560)	53	42	42	42	41	43
Turn (cm <sup>-2</sup> ) (1562-1585)	15	17	17	17	18	16
<b>Amide III</b>						
$\beta$ -sheets (cm <sup>-2</sup> ) (1220-1256)	40	45	47	46	45	46
Random(cm <sup>-2</sup> ) (1257-1285)	8	8	7	8	11	10
Turn (cm <sup>-2</sup> ) (1287-1301)	6	6	6	6	5	6
$\alpha$ -hilex (cm <sup>-2</sup> ) (1302-1329)	46	41	40	40	39	38

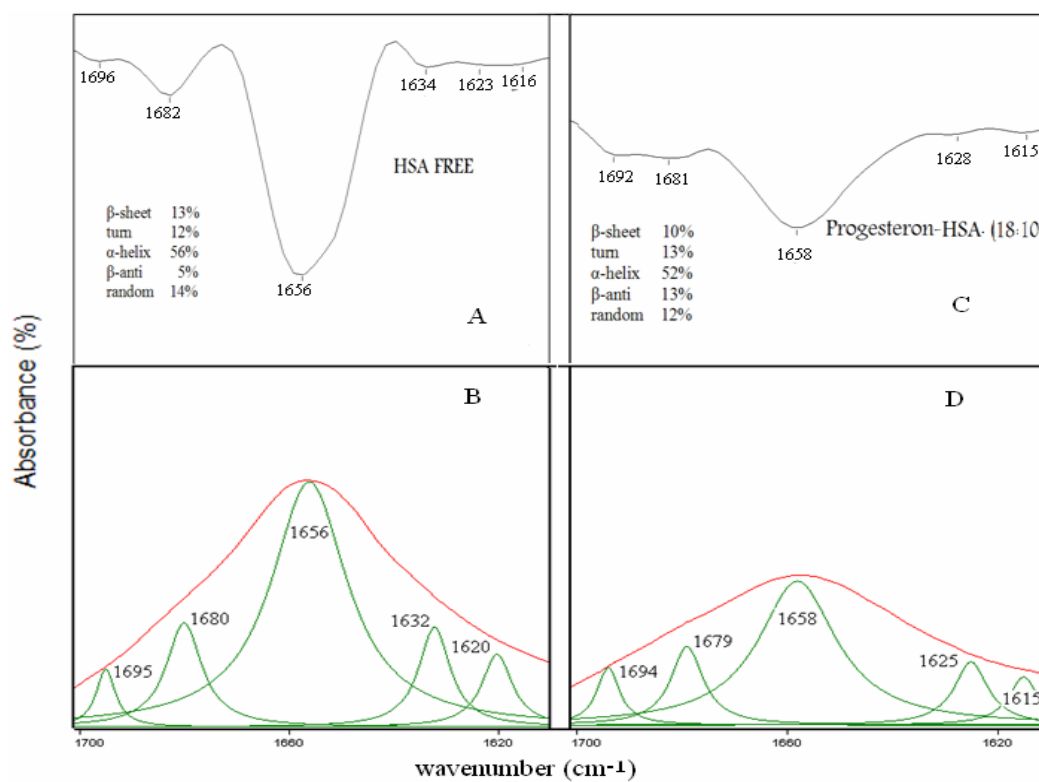


**Figure 4.18:** Second-derivative enhancement and curve-fitted Amide I region (1610-1700  $\text{cm}^{-1}$ ) and secondary structure determination of the free human serum albumin ( A and B) and it progesterone complexes ( C and D) with 18:10 progesterone: HSA ratios.

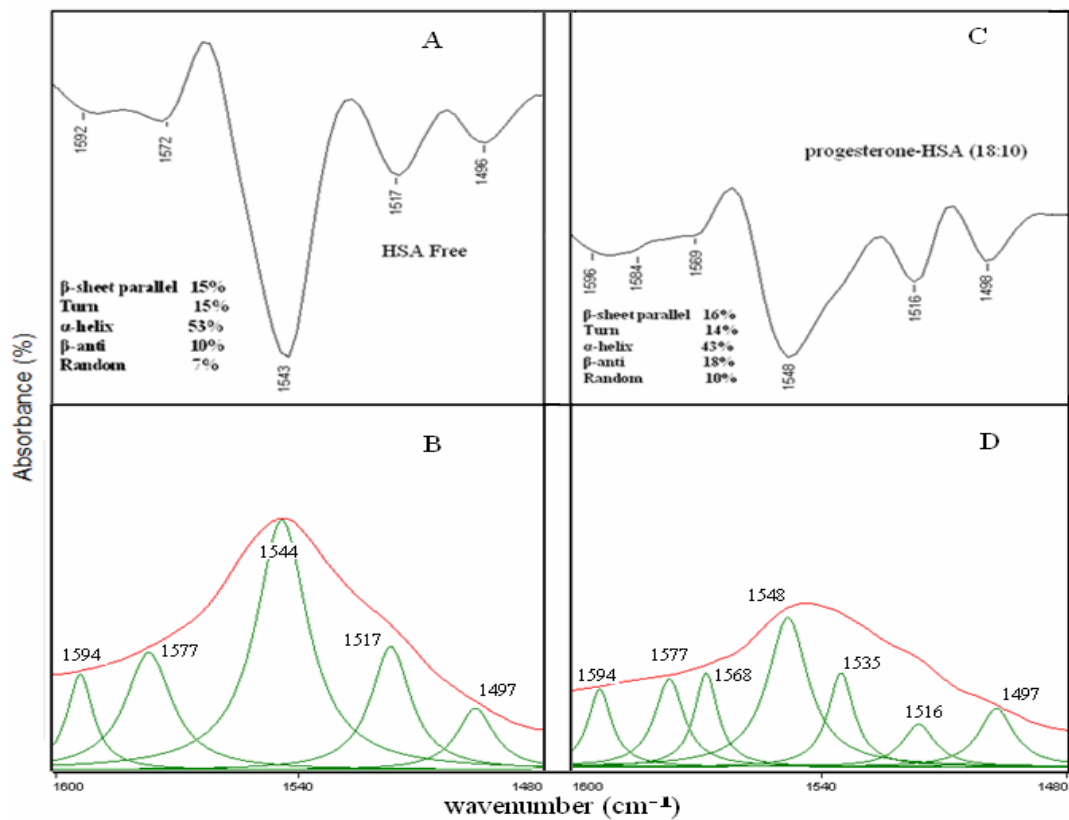


**Figure 4.19:** Second-derivative resolution enhancement and curve fitted amide II region (1600-1480  $\text{cm}^{-1}$ ) and secondary structure determination of the free human serum albumin (A,B) and its progesterone complexes (C,D) with 18:10 hormone: protein ratio.

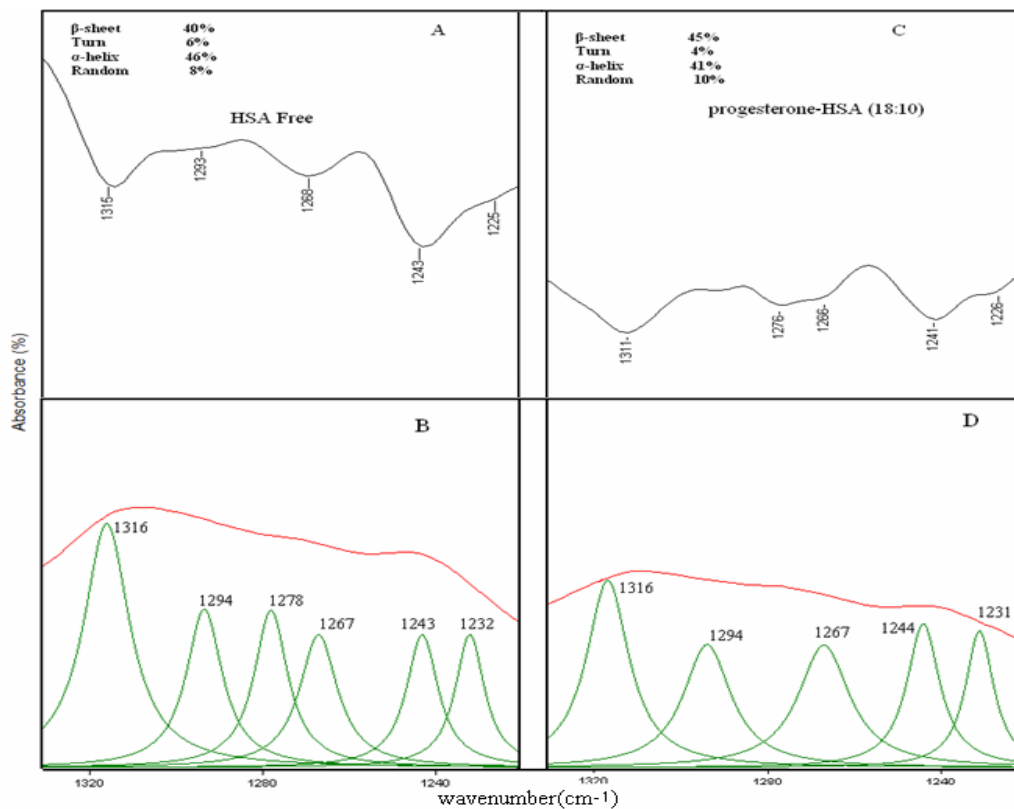


**Figure 4.20:** Second-derivative resolution enhancement and curve fitted amide III region ( $1330\text{-}1220\text{ cm}^{-1}$ ) and secondary structure determination of the free human serum albumin (A,B) and its progesterone complexes (C,D) with 18:10 hormone: protein ratio.

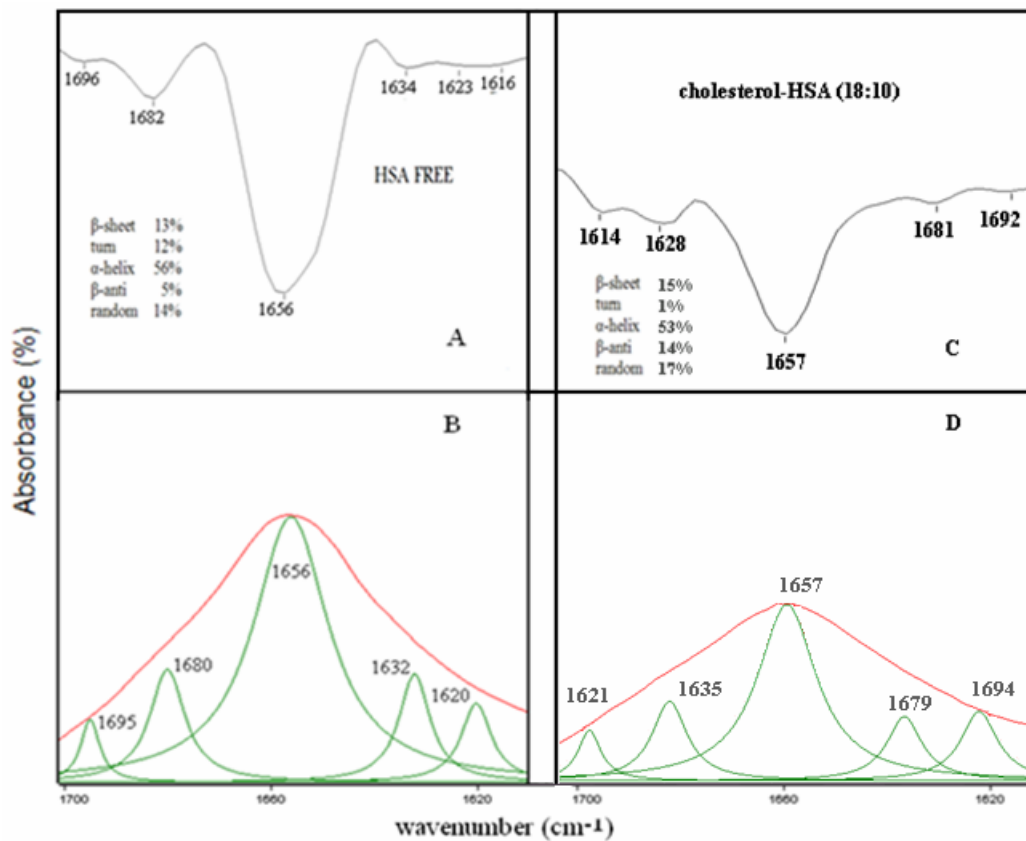


**Figure 4.21:** Second-derivative enhancement and curve-fitted Amide I region ( $1610\text{-}1700\text{ cm}^{-1}$ ) and secondary structure determination of the free human serum albumin ( A and B) and its cholesterol complexes ( C and D) with 18:10 cholesterol: HSA ratios.

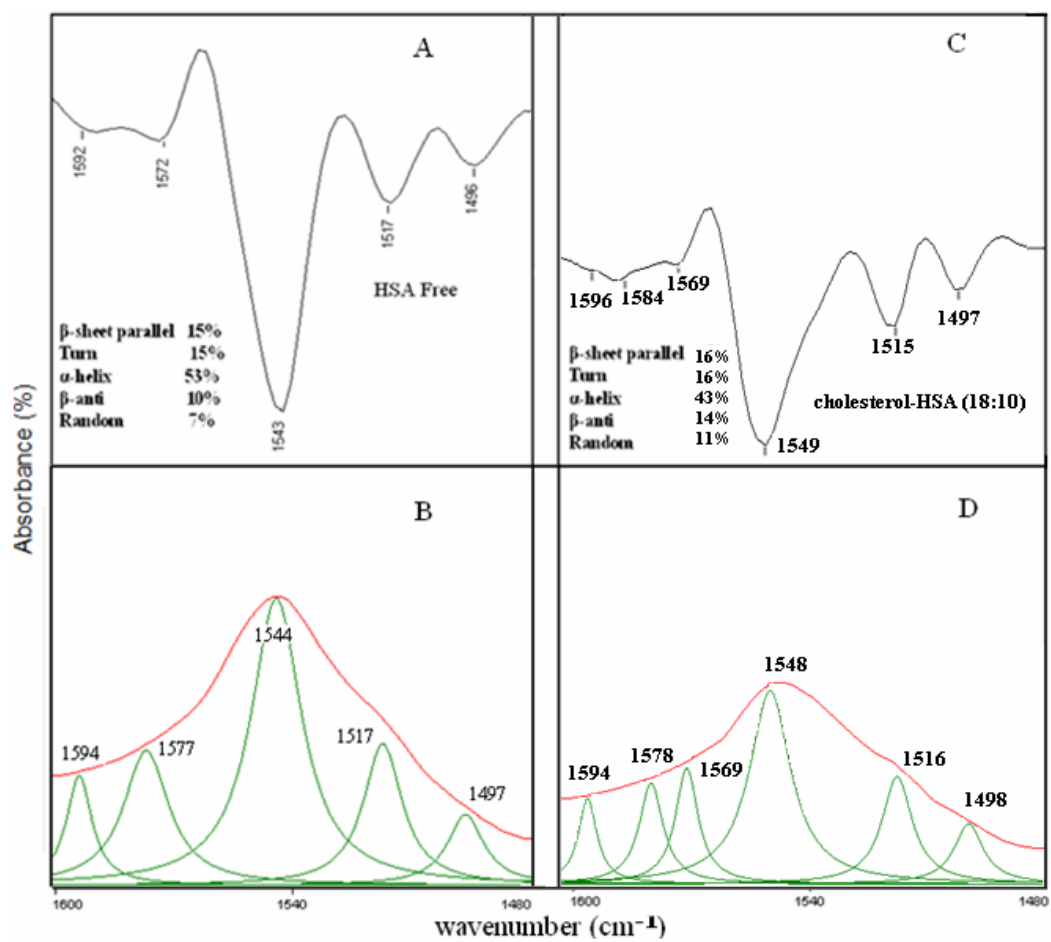


**Figure 4.22:** Second-derivative enhancement and curve-fitted Amide II region (1600-1480 cm<sup>-1</sup>) and secondary structure determination of the free human serum albumin ( A and B) and it cholesterol complexes ( C and D) with 18:10 cholesterol: HSA ratios.

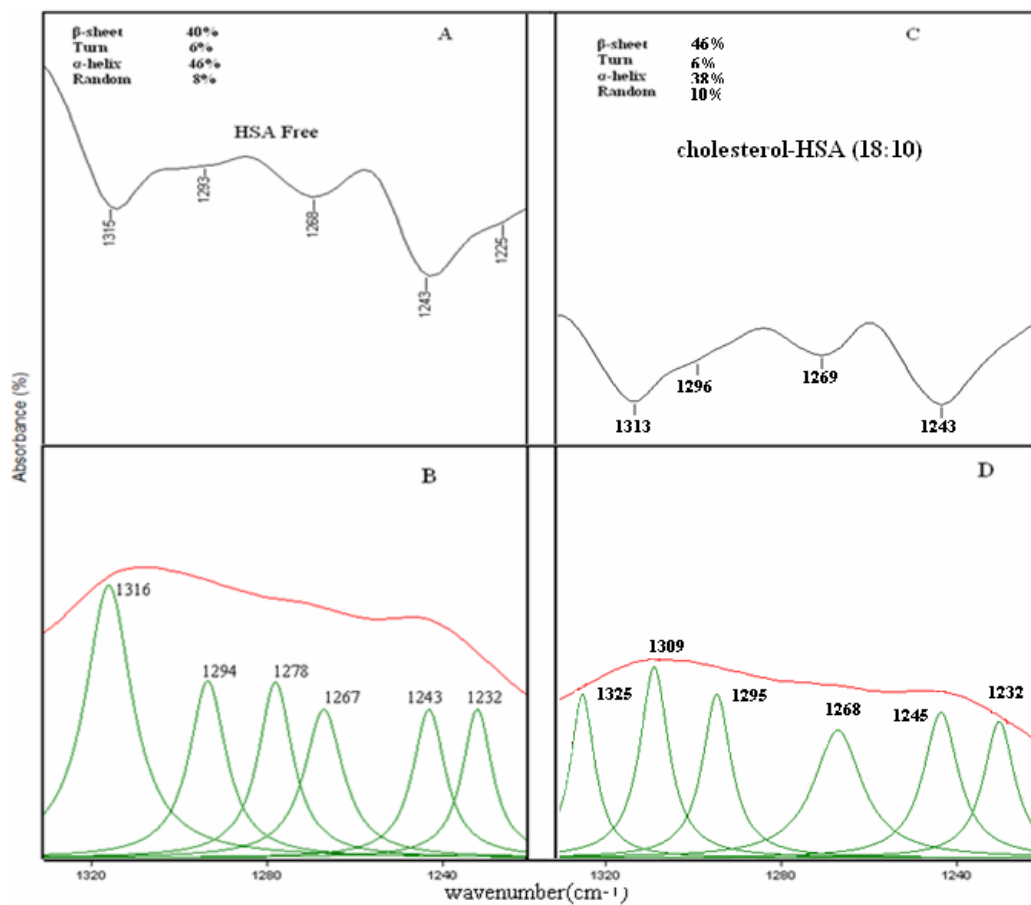


**Figure 4.23:** Second-derivative resolution enhancement and curve fitted amide III region (1330-1220 cm<sup>-1</sup>) and secondary structure determination of the free human serum albumin (A,B) and its cholesterol complexes (C,D) with 18:10 cholesterol: protein ratio.

Progesterone or cholesterol interaction with HSA mainly induce changes in HSA secondary structure, reducing  $\alpha$ -helical structure in favor of  $\beta$ -sheets, which indicates partial unfolding of HSA upon progesterone and cholesterol interaction.

Cholesterol interaction with HSA is similar to the interaction of steroid hormones to HSA (Ha, et al., 2003), and the affinity of steroid hormones to HSA is low (L. K. Amundsen et al., 2007); which is obviously seen in our results with a low binding constants we got between progesterone or cholesterol interaction with HSA. Relatively cholesterol interaction with HSA was stronger than progesterone HSA interaction. This may be due to the chemical structure of progesterone and cholesterol; there are more side interaction in presence of cholesterol to interact with HSA. While in the presence of progesterone there is less side interaction, this is line with the reported results that cholesterol binds to HSA in subdomains IIA and IIIA (Ha et al., 2003), and progesterone have one binding site located in domain II (Kragh-Hansen, U.1981).

*Chapter Five:*

**Conclusions and future  
work**

## Chapter five

---

### Conclusions and future work

The interaction between steroid hormones and albumin is of great interest from both the endocrinological and pharmaceutical point of view. In our work the interaction of progesterone and its parent compound cholesterol with HSA was investigated by means of UV-VIS spectrophotometer, Fluorescence spectrophotometer, and FT-IR spectroscopy. The experimental results indicates a low binding affinity between progesterone or cholesterol with HSA. From analysis of the UV spectrum, the binding constants for progesterone-HSA and cholesterol- HSA are ( $K=6.354 \times 10^2 \text{ M}^{-1}$ ,  $K=0.2641 \times 10^4 \text{ M}^{-1}$ ), respectively. The analysis of the fluorescence spectrum yield binding constants for progesterone-HSA and cholesterol-HSA interactions, that have been measured to be ( $K=6.56 \times 10^2 \text{ M}^{-1}$ ,  $K=0.214 \times 10^4 \text{ M}^{-1}$ ), respectively. The binding constants obtained by different methods have very close values. Comparing the binding constants of progesterone and cholesterol, one can conclude, that progesterone interactions with albumins were substantially weaker than cholesterol-HSA interaction. In addition, the values of Stern-Volmer quenching constants and quenching rate constants for both progesterone and cholesterol were measured to be ( $K_{sv}=6.26 \times 10^2 \text{ L mol}^{-1}$ ,  $K_q=6.2 \times 10^{10} \text{ L mol}^{-1}\text{s}^{-1}$ ) and ( $K_{sv}=6.21 \times 10^2 \text{ L mol}^{-1}$ ,  $K_q=6.21 \times 10^{10} \text{ L mol}^{-1}\text{s}^{-1}$ ), respectively. As a result, it was found that the decrease in fluorescence intensity can be considered as the result of static quenching, which is indicative of a complex formation between the protein with the hormone and cholesterol molecules.

Analysis of FT-IR spectrum indicated that increasing the concentration of progesterone or cholesterol lead to the unfolding of protein, decreasing the percentage of the  $\alpha$ -helical structure in favor of  $\beta$ -sheet structure. Beside that it can be inferred that the binding forces which are involved in the binding process includes hydrophobic interactions. The newly

formed H-bonding result in the C–N bond assuming partial double bond character due to a flow of electrons from the C=O to the C–N bond which decreases the intensity of the original vibrations.

These experimental results may be useful for drug design, and provides some important information for clinical study of steroid hormones. And since body temperature changes during inflammatory processes, therefore, this research need further studies such as thermodynamic parameters (enthalpy, free energy, entropy) at different temperature to investigate the changes in the binding characteristics of steroid hormones with HSA.

Furthermore, it has been reported that progesterone caused appreciably more cholesterol accumulation than other steroid hormones such as testosterone (Butler et al., 1992). So a comparison study for cholesterol- HSA complexes with different concentrations of progesterone or testosterone on the binding constants, will be a useful guide for synthesis of efficient drugs, since existence of steroid hormones may influence the binding force of cholesterol with protein.

## References

---

Abou-Zied, O. K., and Al-Shishi, O. I. K. (2009). *Journal of the American Chemical Society*, 130, p10793.

Amundsen, L. K. and Sirén, H. (2007). *Electrophoresis*, 28, p3737.

André, C., Thomassin, M., Truong, T. T, Robert, J. F., Guillaume, Y. C. (2003). *Journal of Chromatograph. B, Analytical Technologies in the Biomedical and Life Science*, 796, p267.

Arrondo, J.L., Muga, A. (1993). *Prog. Biophys. Mol. Biol.*, 59, p23.

Artali, R., Bombieri, G., Calabi, L., Del Pra, A. (2005). *Il Farmaco*, 60, p485.

Banwell, C. N. (1972): *Fundamentals of Molecular Spectroscopy*, 2<sup>nd</sup>, MCGRAW-Hill Book Company, UK.

Bellamy, L. J. (1975); *The Infrared Spectra of Complex Molecules*, 3<sup>rd</sup>, John Wiley, New York.

Bhattacharya, A., Gruene, T., Curry, S. (2000). *J. Mol. Biol.* 303, p721.

Bian, Q. Q., Liu, J. Q., Tian, J. N., Hu, Z. D. (2004). *International Journal of Biological Macromolecules*, 34, p333.

Bi, S. Y., Song, D. Q., Yian, Y., Liu, X. Y., Zhang, H. Q. (2005). *Spectrochim. Acta. Part A*, 61, p629.

Brittain, E. F. H., George, W. O., Wells, C. H. J. (1970): *Introduction to Molecular Spectroscopy*, Academic Press, London.

Butler, J. D., Blanchette-Mackie, J., Goldin, E., O'Neill, R. R., Carstea, G., Roff, C. F., Patterson, M. C., Patel, S., Comly, M. E., Cooney, A., Vanier, M. T., Brady, P. O., Pentchev, P. G. (2001). *The Journal of Biological Chemistry*, 276, p23797.

Byler, M. and Susi, H. (1986). *Biopolymers*, 25, p469.

- Chalmers, J. M. and Griffiths, P. R. (Eds). (2002): Handbook of Vibrational Spectroscopy Theory and Instrumentation, Vol. 1, John Wiley & Sons Ltd, UK.
- Cheng, F. Q., Wang, Y. P., Li, Z. P., Chuan, D. (2006). Spectrochimica Acta Part A, 65, p1144.
- Chirgadze, Y. N., Fedorov, V., Trushina, P. P. (1975). Biopolymers, 14, p679.
- Coleman, P. B. (Eds). (1993): Practical Sampling Techniques for Infrared Analysis, CRC Press LLC, USA.
- Cooper, A. (2004); Biophysical Chemistry, The Royal Society of Chemistry, UK.
- Cui, F., Wang, J., Cui, Y., Yao, X., Qu, G., Lu, Y. (2007). Luminescence, 22, p546.
- Cui, F., Wang, J., Li, F., Fan, J., Qu, G., Yao, X., Lei, B. (2008). Chinese Journal of Chemistry, 26, p661.
- Cui, F., Qin, L., Zhang, G., Liu, X., Yao, X., Lei, B. (2008). Bioorganic and Medical Chemistry, 16, p7615.
- Curry, S., Brick, P., Franks, N. P. (1999). Biochim. Biophys. Acta, 1441, p131.
- Darwish, S. M., Abu sharkh, S. E., Abu Teir, M. M., Makharza, S. A., Abu-hadid, M. M. (2010). Journal of Molecular Structure, 963, p122.
- Dukor, R.K., Chalmers, J.M., Griffiths, P.R. (2001): Vibrational Spectroscopy in the Detection of Cancer, Handbook of Vibrational Spectroscopy, Vol. 5, John Wiley and Sons, Chichester.
- Eftink, M.R. (1991): Fluorescence Quenching Reactions: Probing Biological Macromolecular structures. In Biophysical and Biochemical Aspects of Fluorescence Spectroscopy, Plenum, New York.
- Fabian, H., Schultz, C., Backmann, J., Hahn, U., Saenger, W., Mantsch, H. H., Naumann, D. (1994). Biochemistry, 33, p10725.
- Fengling, C., Yanrui, C., Hongxia, L., Xiaojun, F., Jing, F., Yan, L. (2006). Chinese Science Bulletin, 51, p2201.
- Ganim, Z. and Tokmakoff, A. (2006). Biophysical Journal, 91, p2636.

- Gerbanowski, A., Malabat, C., Rabiller, C., Gueguen, J. (1999). *J. Agric. Food Chem.* 47 p. 5218.
- Goormaghtigh, E., Cabiaux, V., Ruyschaert, J.M. (1990). *European Journal of Biochemistry*, 193, p409.
- Goormaghtigh, E., Ruyschaert, J.M., Raussens, V. (2006). *Biophysical Journal*, 90. p2946.
- Griffiths, P. R., and de Haseth, J. A. (2007): *Fourier Transform Infrared Spectrometry*, 2<sup>nd</sup>, John Wiley & Sons, New Jersey.
- Gruenwedel, D. W. and Whitaker, J. R. (Eds). (1987): *Food Analysis Principles and Techniques, Separation Techniques*, Vol. 4, Merce Dekker, New York.
- Ha, J.S., Theriault, A., Bhagavan, N. V., Ha, C.E. (2006). *Biochimica et Biophysica Acta*. 1761. p717.
- Ha, J.S., Ha, C.E., Chaob, J.T., Petersena, C. E., Theriault, A., Bhagavana, N. V. (2003). *Biochimica et Biophysica Acta*, 1640, p119.
- Hardie, D.G. (1991): *Biochemical Messengers, Hormones, Neurotransmitters And Growth Factors*, 1<sup>st</sup>, university press, Cambridge.
- Haris, P. I., and Severcan, F. (1999). *Journal of Molecular Catalysis B: Enzymatic*, 7, p207.
- He, X. M. and Carter, D. C. (1992). *Nature*, 358, p209.
- Hollas, J. M. (2004): *Modern Spectroscopy*, 4<sup>th</sup>, John Wiley & Sons Ltd, UK.
- Holzbaaur, I.E., English, A.M., Ismail, A.A. (1996). *Biochemistry*, 35, p5488.
- Il'ichev, Y.V., Perry, J.L., Simon, J.D. (2002). *J. Phys. Chem. B*, 106, p460.
- Jackson, M. and Mantsch, H. H. (1991). *J. Chem.*, 69, p1639.
- Jackson, M. and Mantsch, H. H. (1995). *Critical Reviews in Biochemistry and Molecular Biology*, 30, p95.
- Jiang, M., Xie, M. X., Zheng, D., Liu, Y., Li, X. Y., Chen, X. (2004). *Journal of Molecular Structure*, 692, p71.

- Jue, T. (Ed). (2009): Handbook of Modern Biophysics; Fundamental Concepts in Biophysics, Vol.1, Humana Press a part of Springer Science+Business Media, LLC, New York.
- Jürgens, G., Müller, M., Garidel, P., Koch, M. H. J., Nakakubo, H., Blume, A., Brandenburg, K. (2002). Journal of Endotoxin Research, 8, p115.
- Kandagal, P.B., Shaikh, S. M. T., Manjunatha, D.H., Seetharamappa, J., Nagaralli, B.S. (2007). J. Photochem. Photobiol. A, 189, p121.
- Kang, J., Liu, Y., Xie, M.X., Li, S., Jiang, M., Wang, Y.D. (2004). Biochimica et Biophysica Acta, 1674, p205.
- Kauppinen, J. K., Moffatt, D. J., Mantsch, H. H., Cameron, D. G. (1981). Applied Spectroscopy, 18, p35.
- Kauppinen, J. K., Moffatt, D.J., Mantsch, H. H., Cameron, D. G. (1981). Appl. Spectrosc., 35, P271.
- Kauppinen, J., Partanen, J. (2001): Fourier Transforms in Spectroscopy, Wiley-VCH Verlag GmbH, Germany.
- Klotz, M.I. and Hunston, L.D. (1971). Biochemistry, 10, p3065.
- Korkmaz, F. and Severcan, F. (2005). Archives of Biochemistry and Biophysics, 440, p141.
- Kragh-Hansen, U. (1981). Pharmacol. Rev., 33, p17.
- Krimm, S. and Bandekar, J.(1986). Adv. Protein Chem., 38, p181.
- Krishnakumar, S.S. and Panda, D. (2002). Biochemistry, 41, p7443.
- Lakowicz, J. R. (2006): Principles of Fluorescence Spectroscopy, 3<sup>rd</sup>, Springer Science+Business Media, USA.
- Lakowica, J. R., Weber G. (1973).Biochem, 12, p4161.
- Li, Y., He, W. Y., Dong, Y. M., Sheng, F., Hu, Z. D. (2006). Bioorganic & Medicinal Chemistry, 14, p1431.

- Li, Y., He, W. Y., Liu, H., Yao, X., Hu, Z. (2007). *Journal of Molecular Structure*, 831, p144.
- Li, J., Ren, C., Zhang, Y., Liu, X., Yao, X., Hu, Z. (2008). *Journal of Molecular Structure*, 881, p 90.
- Liu, Y., Xie, M.X., Kang, J., Zheng, D. (2003). *Spectrochim. Acta, Part A*, 59, p2747.
- Maiti, T. K., Ghosh, K. S., Samanta, A., Dasgupta, S. (2008). *Journal of Photochemistry and Photobiology A*, 194 , p297.
- Matsuura, H., Hasegawa, K., Miyazawa, T. (1986). *Spectrochim. Acta*, 42, p1181.
- Mirabeela, F. M. (Ed) (1998): *Modern Techniques in Applied Molecular Spectroscopy*, John Wiley and Sons, USA.
- Morly, J. E., Kaiser, F., Raum, W. J., Perry, H., Flood, J. F., Jensen, J., Sliver, A. J., Roberts, E. (1997). *Proc. Nati. Acad. Sci.*, 94, p7537.
- NanoDrop 3300 Fluorospectrometer V2.7 User's Manual, (2008), Thermo Fisher Scientific.
- NanoDrop 1000 Spectrophotometer V3.7 User's Manual, (2008), Thermo Fisher Scientific.
- Neault, J.F., and Tajmir-Riahi, H.A.(1998). *Biochimica et Biophysica Acta*, 1384, p153.
- Oberg, K. A., Ruysschaert, J. M., Goormaghtigh, E. (2004). *Eur. J. Biochem.*, 271, p2937.
- OPUS Bruker manual version 5.5, (2004): BRUKER OPTIK GmbH.
- Ouameur, A. A., Mangier, E., Diamantoglou, S., Carpentier, R., Tajmir-Riahi, H. A. (2004). *Biopolymers*, 73, p503.
- Pani, A., and Dessi, S. (2003): *Cell Growth and Cholesterol Esters*, Eureka.com and Kluwer Academic / Plenum Publishers, USA.
- Pavia, D. L., Lampman, G. M., Kriz, G. S., Vyvyan, J. R. (2009): *Introduction to Spectroscopy*, 4<sup>th</sup>, Brooks/Cole, Cengage Learning, USA.

- Peng, L., Minboa, H., Fang, C., Xi, L., Chaocan, Z. (2008). *Protein & Peptide Letters*, 15, p360.
- Peters, T. (1985). *Adv. Protein Chem.*, 37, p161.
- Petitpas, I., Bhattacharya, A. A., Twine, S., East, M., Curry, S. (2001). *Journal of Biological Chemistry*, 276, p22804.
- Purcell, M., Neault J. F., Tajmir-Riahi, H. A. (2000). *Biochimica et Biophysica Acta*, 1478, p61.
- Rondeau, P., Armenta, S., Caillens, H., Chesne, S., Bourdon, E. (2007). *Archives of Biochemistry and Biophysics*, 460, p 141.
- Royer, C. A. (1995). *Biophysical Journal*, 68, p1191.
- Schermann, J.P. (2008): *Spectroscopy and Modelling of Biomolecular Building Blocks*, 1<sup>st</sup>, Elsevier, UK.
- Schrader, B. (1995): *Infrared and Raman Spectroscopy Methods and Applications*, VCH Verlag mbH, Germany.
- Serdyuk, I. N., Zaccai, N. R., Zaccai, J. (2007): *Methods in Molecular Biophysics Structure, Dynamics, Function*, Cambridge University Press, New York.
- Settle, F. A. (Ed). (1997): *Handbook of Instrumental Techniques for Analytical Chemistry*, Prentice Hall PTR, New Jersey.
- Siebert, F. and Hildebrandt, P. (2008): *Vibrational Spectroscopy in Life Science*, WILEY-VCH Verlag GmbH & Co. KGaA, Weinheim.
- Simard, J. R., Zunszain, P. A., Hamilton, J. A., Curry, S. (2006). *J. Mol. Biol.*, 361, p336.
- Sirotkin, V. A., Zinatullin, A. N., Solomonov, B. N., Faizullin, D. A., Fedotov, V. D. (2001). *Biochimica et Biophysica Acta*, 1547, p359.
- Stephanos, J.J., and Inorg, J. (1996). *Biochem.* ,62, p155.
- Stuart, B. H. (2004): *Infrared Spectroscopy: Fundamentals and Applications*, John Wiley & Sons Ltd, UK.

- Sulkowska A. (2002). *J. Mol. Struct.* ,614, p227.
- Surewicz, W. K., Mantsch, H. H., Chapman, D. (1993). *Biochemistry*, 32, p389.
- Surewicz, W.K., Moscarello, M.A., Mantsch, H.H. (1987). *J. Biol. Chem.*, 262, p8598.
- Tang, J., Luan, F., Chen, X. (2006). *Bioorg. Med Chem*, 14, p3210.
- Yang, M.M., Yang, P., Zhang, L.W. (1994). *Chin. Sci. Bull.*, 39, p734.
- Tian, J. N., Liu, J. Q., Zhang, J. Y., Hu, Z. D., Chen, X. G.(2003). *Chem. Pharm. Bull.*, 51, p579.
- Tsai, C., S. (2007): *Biomacromolecules: Introduction to Structure, Function and Informatics*, John Wiley & Sons, New Jersey.
- Ulrich, K. H., Hiroshi, W., Keisuke, N., Yasunori, I., Masaki, O. (2006). *J. Mol. Biol.* 363, p702.
- Uversky, V. N. and Permykov, A. E. (Eds). (2007): *Methods in Protein Structure and Stability Analysis; Vibrational spectroscopy*, Nova Science Publishers, Inc, Hauppauge, New York.
- Valeur, B. (2001): *Molecular Fluorescence Principles and Applications*, 1<sup>st</sup>, WILEY-VCH Verlagsgesellschaft mbH, Germany.
- Vandenbussche, G., Clercx, A., Curstedt, T., Johansson, J., Jornvall, H., Ruyschaert, J. M. (1992). *European Journal of Biochemistry*, 203, p201.
- Vass, E., Holly, S., Majer, Zs., Samu, J., Laczko, I. Hollosi,M. (1997). *Journal of Molecular Structure*, 47, p408.
- Vij, D. R. (2006): *Handbook of Applied Solid State Spectroscopy*, Springer Science+Business Media, LLC, USA.
- Vonhoff, S., Condliffe, J., Schiffter, H. (2010). *Journal of Pharmaceutical and Biomedical Analysis*, 51, p39.
- Wang, C., Wu, Q., Li, C., Wang, Z., Ma, J., Zang, X., Qin, N. (2007). *Analytical Sciences*, 23, p429.

Wang, T., Xiang, B., Wang, Y., Chen, C., Dong, Y., Fang, H., Wang, M. (2008). *Colloids Surf. B*, 65, p113.

Workman, J. R. (1998): *Applied Spectroscopy: Optical Spectrometers*, Academic Press, San Diego.

Wybranowski, T., Cyrankiewicz, M., Ziomkowska, B., Kruszewski, S. (2008). *BioSystems.*, 94, p258.

Xie, M.X. and Liu, Y. (2003). *Chem. J. Chin. Univ.*, 24, p226.

Yamamoto, T. and Tasumi, M. (1991). *J. Mol. Struct.*, 242, p235.

Zhang, G., Que, Q., Pan, J., Guo, J. (2008). *Journal of Molecular Structure*, 881, p132.

(HSA)

(Human Serum Albumin)

(Fluorescence Spectrophotometer)

(UV-VIS Spectrophotometer)

(FT-IR Spectrophotometer)

(Binding Constant)

(0.2641 × 10<sup>4</sup> M<sup>-1</sup>) (6.354 × 10<sup>2</sup> M<sup>-1</sup>)

(Stern-Volmer) (Static quenching)

(6.21 × 10<sup>2</sup> Lmol<sup>-1</sup>) (6.26 × 10<sup>2</sup> Lmol<sup>-1</sup>)

(6.65 × 10<sup>2</sup> M<sup>-1</sup>)

(0.214 × 10<sup>4</sup> M<sup>-1</sup>)

(Fourier Self-deconvolution)

(Curve fitting)

(Second derivative resolution)

(Secondary Structure)

(Peaks)

(Absorption Bands)

( $\beta$ -sheets)

( $\alpha$ -helix)

(H-bonding)

( $\beta$ -sheets) ( $\alpha$ -helix)